Dissertation

Role of lysosomal acid lipase in thermogenesis and energy homeostasis

submitted by

Madalina-Cristina DUTA-MARE

for the Academic Degree of

Doctor of Philosophy

(PhD)

at the

Medical University of Graz

Gottfried Schatz Research Center for Cell Signaling, Metabolism and Aging
Molecular Biology and Biochemistry

Under the Supervision of

Prof. Dr. Dagmar Kratky

2018

"Per aspera ad astra"

~To my beloved parents~

Acknowledgement

Most sincere thanks are dedicated to my supervisor Dagmar Kratky, who trusted and guided me unconditionally in this journey. I am always grateful for your dedication, patience, professionalism and support. You are an example both as a person and as a professional and the role model I will look up to in my career.

I'm grateful to you, Vinay for all the love, support and motivation, for giving me the strength I never knew I have. You brightened my world with your optimism, something what I learn from you every day.

Hearty thanks to my family and close friends from home and from Austria for your love, support, phone calls, messages, company and jokes. You made these three years so much colorful.

Thank you, Anton for your outstanding technical support and all the great words at the right time. Many thanks to Silvia and my colleagues for your help, the great laughs and the supply of chocolate, it was very welcome lately. I am grateful to my thesis committee members and advisors: Achim Lass, Günter Hammerle, and Juliane Bogner-Strauss and to all our collaborators for sharing their expertise and adding value to our research.

I would like to thank the funding institutions FWF, Medical University of Graz and DK-Program "Metabolic and Cardiovascular Disease" and to Karin Osibow for all her great help and outstanding administration of student affairs.

Table of contents

Declaration

I hereby declare that this thesis is my own original work and that I have fully acknowledged by name all of those individuals and organizations that have contributed to the research for this thesis. Due acknowledgement has been made in the text to all other material used. Throughout this thesis and in all related publications I followed the “Standards of Good Scientific Practice and Ombuds Committee at the Medical University of Graz”

Graz, 19.05.2018

…….

Madalina-Cristina DUTA-MARE

Please note that parts of this thesis have been published and/or are under preparation for future publications.

Lysosomal acid lipase regulates fatty acid channeling in brown adipose tissue to maintain thermogenesis

Duta-Mare M, Sachdev V, Leopold C, Kolb D, Vujic N, Korbelius M, Hofer CD, Xia W, Huber K, Auer M, Gottschalk B, Magnes C, Graier WF, Prokesch A, Radovic B, Bogner-Strauss JG, Kratky D; Biochimica et biophysica acta. 2018 Jan 31;1863(4):467-78.

Zusammenfassung

Adipositas, Diabetes mellitus, Atherosklerose und nichtalkoholische Fettlebererkrankungen sowie die damit assoziierten Erkrankungen zählen zu den häufigsten Todesursachen in der modernen Gesellschaft. Während sich Gewichtsverlust und sportliche Betätigung positive auf Prävention und Verlauf dieser Krankheiten auswirken können, mangelt es an effektiven therapeutischen Möglichkeiten zur Behandlung von Patienten. Folglich werden pharmakologische Angriffspunkte bei den verschiedenen klinischen Manifestationen des metabolischen Syndroms, wie beispielsweise Dyslipidämie, erhöhter Fettgehalt, Hypertonie und Hyperglykämie, gesucht. Die lysosomale saure Lipase (LAL) ist eine wichtige Hydrolase von Cholesterinestern (CE) und Triglyzeriden (TG) und wird in den meisten Zelltypen exprimiert. In Menschen und Mäusen führt der Mangel an LAL (LAL-D) zu einer Vielzahl an Komplikationen und zum frühzeitigen Tod. Der Mangel an LAL führt zur übermäßigen Ansammlung an Neutralfetten in der Leber, dem Darmtrakt und der Lunge, was zu Dyslipidämie und schweren Störungen des Immunsystems führt. Viele Studien untersuchten die Akkumulation von Cholesterin in der Leber und die Auswirkungen auf entzündliche Prozesse, während über den Energiestoffwechsel bei Fehlen dieser Lipase wenig bekannt ist. LAL-D wird oft fehldiagnostiziert. Besonders bei Erwachsenen wird LAL-D aufgrund der damit verbundenen Fettleber und Atherosklerose in das Krankheitsbild des metabolischen Syndroms eingeordnet, obwohl diese Patienten kaum an Übergewicht leiden. In an LAL-D leidenden Säuglingen/Kinder sowie in LAL-D Tiermodellen zeigt sich sogar eine Kachexie.

In dieser Dissertation wurde die physiologische und pathophysiologische Rolle der LAL in der Thermogenese sowie im Energiestoffwechsel untersucht, um potentielle therapeutische Angriffspunkte zur Behandlung von Adipositas und kardiovaskulären Krankheiten zu finden. Im ersten Teil der Dissertation verwendete ich LAL-defiziente (Lal-/-) Mäuse um die Rolle der LAL in der Thermogenese sowie den Beitrag der lysosomalen Lipolyse im braunen Fettgewebe (BAT) zu untersuchen. Dabei konnten wir zeigen, dass der Mangel an LAL zum metabolischen Ungleichgewicht in Mäusen und damit zu Veränderungen im Gesamtmetabolismus sowie in der Thermogenese führt.

Im zweiten und dritten Teil untersuchten wir die Auswirkungen von LAL Defizienz im Gesamtorganismus mit gewebsspezifischer Defizienz (Fettgewebe, atLal-/- und Makrophagen, macLal-/-). Wir konnten zeigen, dass die LAL im Fettgewebe bei Hungerphasen wichtig zur Pufferung des Bedarfs an Fettsäuren ist. Minimale Effekte ausgenommen, wirkt sich der gewebespezifische LAL Mangel (atLal-/- and macLal-/-) nicht entscheidend auf den Energiestoffwechsel in Mäusen, welche mit fett- oder cholesterinreicher Diät ernährt wurden, aus. Die molekularen Aspekte dieser metabolischen Anpassung in LAL-defizienten Zellen muss noch weiterführend untersucht werden.

Die Resultate dieser Dissertation zeigen, dass die LAL einen essentiellen Beitrag zum Energiehaushalt (zumindest in Mäusen) leistet. Die wichtige Rolle der LAL in der Thermogenese bei LAL-D Patienten ist derzeit unbekannt und die möglichen Auswirkungen auf die Erkrankung sollten in Zukunft untersucht werden.

Abstract

Obesity, diabetes mellitus, atherosclerosis, non-alcoholic fatty liver disease (NAFLD) and their downstream morbidities are the most common causes of mortality in the modern society. Although weight loss and exercise have a beneficial impact on the prevention and cure of these diseases, very little is done in this direction by and for the patients. Thus, many efforts are directed toward pharmacological targeting of different components of the metabolic syndrome, such as dyslipidemia, fat mass, hypertension, hyperglycemia, etc.

Lysosomal acid lipase (LAL) is a critical cholesteryl ester (CE) and triglyceride (TG) hydrolase and it is widely expressed in most cell types. LAL deficiency (LAL-D) in humans and mice produces a bulk of complications, which converge to premature demise. Hallmarks of LAL-D are excessive accumulation of neutral lipids in liver, intestine and lungs, resulting in dyslipidemia and severe immune imbalance. To date, the most studied aspects are cholesterol accumulation in liver and the inflammatory angle, but still little is known about energy metabolism in the absence of the main lipase involved in lipoprotein catabolism and lipid autophagy.

LAL-D is often misdiagnosed and is categorized as a morbidity of the metabolic syndrome in adults, due to fatty liver and atherosclerosis, but these patients are rarely overweight. Moreover, LAL-D infants/children and animal models of the disease are cachectic. This thesis targets mainly the physio/pathological role of LAL in thermogenesis and energy metabolism with the aim of revealing potential therapeutic targets in the battle against obesity and cardiovascular disease.

In the first part of the thesis, we focused on investigating the role of LAL in thermogenesis, using the LAL-deficient (Lal-/-) mouse model with the aim of dissecting the relationship between acid and neutral lipid hydrolysis in fueling brown adipose tissue (BAT). We provide evidence that LAL deficiency produces a metabolic imbalance in mice and thus affects whole body energy metabolism and overall thermogenesis.

In the second and third part, comparing mice with total and tissue-targeted LAL deletion (adipose tissue, atLal-/- and macrophages, macLal-/-), we studied the distinct role of LAL in different cell types in connection to its global contribution to lipid and carbohydrate metabolism. We found that adipose tissue LAL is important for buffering fatty acids (FA) demand during fasting, but not during cold exposure.

Except for minimal effects, tissue-specific LAL deficiency does not fundamentally affect energy metabolism in mice challenged with diet rich in fat and cholesterol.
Our data help to understand the distinct roles of LAL in pathological conditions. While the molecular aspects of these metabolic adaptations in cells lacking LAL remain to be addressed, this study revealed the critical impact of LAL on energy metabolism and thermogenesis**.** Since BAT activity in humans is positively correlated with metabolic health, it is plausible that defective BAT function additionally aggravates dyslipidemia in LAL-D patients.

1. General introduction and outline

1.1 Lysosomal acid lipase

1.1.1 LAL molecular biology

LAL is the only known enzyme to mediate the hydrolysis of CE and TG in lysosomes (1, 2). Receptor-mediated endocytosis of low-density lipoproteins (LDL) (3) and lysosomal degradation of CE by LAL was described more than 4 decades ago (4, 5). LDL binds its receptor on the plasma membrane and it is internalized in clathrin-coated vesicles. The cargo loses the clathrin coat and fuses with endosomes and lysosomes. While the receptor is recycled and returns to the cell membrane, LDL is completely degraded by lysosomal enzymes (6, 7). More recent research connected lysosomal lipid degradation via autophagy to a physiological significant extent (8, 9). An interesting crosstalk of acid and neutral lipolysis has been described. Contrary to canonical believes where neutral lipolysis is the sole lipid droplet (LD)-derived fatty acid provider, acid lipolysis can as well degrade lipid droplets. This process is currently known as (macro) lipophagy (10). Autophagy was connected to neutral lipolysis through degradation of LD-associated membrane proteins to enhance lipolysis (11) or via direct interaction of autophagy-mediating proteins and the main cytosolic TG hydrolase, adipose triglyceride lipase (ATGL) (12). Additionally, macrophages, as professional recyclers, internalize modified lipoproteins and extracellular material for lysosomal degradation by acidic hydrolases. CE are broken down by LAL and the resulting free cholesterol is effluxed to high-density lipoproteins (HDL) for reverse cholesterol transport (RCT) to the liver (Fig. 1). RCT is crucial for cholesterol and bile acids homeostasis and its malfunction is correlated to accelerated atherosclerosis development (13-15).

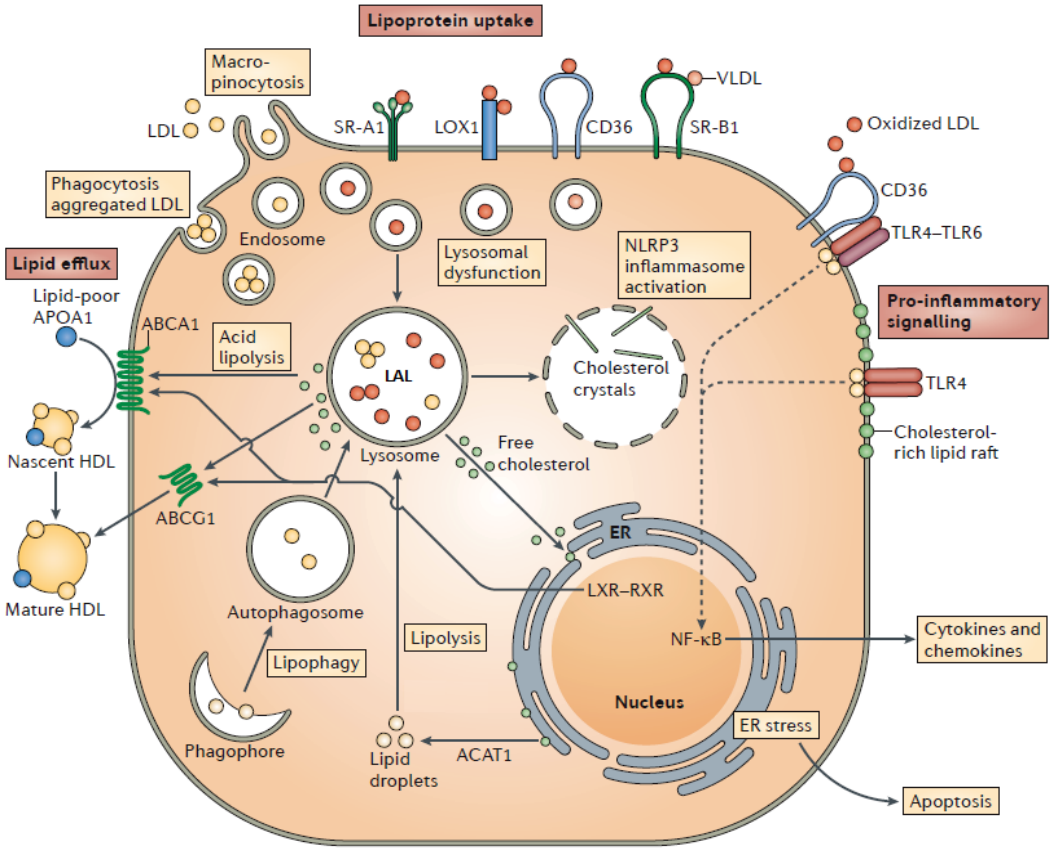

Figure 1: Lysosomal acid lipase-mediated hydrolysis and cholesterol processing in macrophages. Intact or modified lipoproteins are internalized into the cytosol via various receptors or though phago/pinocytosis and cholesteryl esters and triglycerides are hydrolyzed by LAL. LAL products are fatty acids (FA) and free cholesterol (FC). FC can be directly effluxed from the cell via ABCA1/ABCG1 or can be esterified in the ER membrane and budded into lipid droplets. The stored cholesterol can be mobilized for efflux either via neutral lipolysis or through lipophagy. If free cholesterol excessively accumulates in the lysosomes, it can induce formation of cholesterol crystals and consequently activate the NLRP3 inflammasome. Alternatively, excessive cytosolic free cholesterol induces ER stress and cell apoptosis. Lysosomal acid lipase (LAL); low-density lipoprotein (LDL); very low-density lipoprotein (VLDL); high-density lipoprotein (HDL); scavenger receptor (SR); lectin-like oxidized LDL receptor 1 (LOX1); cluster of differentiation 36 (CD36); endoplasmic reticulum (ER); acetyl-coenzyme A:cholesterol acetyltransferase 1 (ACAT1); liver X receptor (LXR); retinoid X receptor (RXR); ATP-binding cassette (ABC); apolipoprotein A1 (APOA1); NOD-, LRR- and pyrin domain-containing 3 (NLRP3); toll-like receptor (TLR); nuclear factor-κB (NF-κB) (14). Requisite permission to use this figure was obtained (Appendix).

Besides CE and TG, other known substrates for LAL hydrolysis are retinyl esters, di- and mono-acylglycerols (16-18).

Lysosomal acid lipase (LAL) is encoded by the LIPA gene mapped to the human chromosome locus 10q23.2-23.3, has a size of approximately 36.5 kb, and contains 10 exons (19-21). Although the full length cDNA encoding hepatic human LAL predicts a 399 amino acid protein, due to post-translational modifications, the mature protein consists of 323 amino acids with a molecular weight of 37 kDa, active as a monomer (22). The molecular weight of the LAL protein varies due to its diverse glycosylation grades between cell types and localization, i.e. intracellular LAL is smaller (~41 kDa) compared to the highly glycosylated secreted LAL of ~47 kDa (23-25). LAL glycosylation is crucial for recognition of phosphomannosyl residues on the lysosomal proteins by the mannose-6-phosphate receptor (26). Correction of enzyme activity and lysosomal lipid accumulation in LAL-deficient (Lal-/-) fibroblasts by co-culture with healthy fibroblasts or LAL-enriched medium provided the proof of concept that LAL is a secreted protein (27, 28). In addition, different glycosylation patterns lead to different specificity of human LAL (hLAL) uptake in Lal-/- mice. These receptor-mediated effects led to recovered activity mostly in the liver (high mannosylation-hLAL expressed in *Pichia pastoris*) or broader enzyme distribution (low mannosylation-hLAL expressed in CHO cells) (29).

Mouse Lal gene is located on chromosome 19 (30), contains 10 exons and has a similar exon-intron organization to the human gene (31). Human and mouse LAL protein share high amino acid sequence identity (75%) and similarity (95%) (24) with ubiquitous expression in human (22) and mouse (24) cells and organs. In the mouse, LAL is highest expressed in the kidney (cortical tubes), adrenal glands (zona fasciculata and reticularis), and pancreas (acinar cells). High mRNA expression was detected in liver (hepatocytes and sinusoidal cells) and small intestine (enterocytes). Other organs as well had abundant LAL gene expression, though this was mainly due to tissue-resident macrophages (spleen, thymus and uterus). LAL gene transcript was low in heart, tongue, ovary, and testis (24).

1.1.2 LAL regulatory pathways

Lysosomes are exclusively recycling organelles and have no storage function, which implies that the entire lysosomal machinery is constitutively active.

Accordingly, there is little post-translational activity modulation of hydrolytic enzymes and therefore these proteins are mostly regulated at transcriptional level (1). Nutrient restriction triggers autophagy and, thus, delivery of combusting material to lysosomes. In the absence of nutrients, the mechanistic target of rapamycin kinase complex 1 (mTORC1)-dependent phosphorylation of transcription factor EB (TFEB) is reduced. Hence TFEB translocates to the nucleus and promotes lysosomal biogenesis (32-34). TFEB also positively regulates LAL expression and activity indirectly via PPAR-PGC1α signaling cascade (35-37). Alternatively, starvation induces SIRT1-dependent deacetylation and translocation to the nucleus of forkhead box protein O1 (FOXO1). Consequently, this signaling cascade increases both LAL and ATGL expression to mobilize FA release following acid and neutral lipolysis (38, 39).

Post-transcriptionally, LAL activity can be pathologically decreased by oxidized and aggregated LDL. These modified lipoproteins alter LAL function due to an increase in lysosomal pH, which leads to accumulation of CE in the lysosomal compartment (40-42).

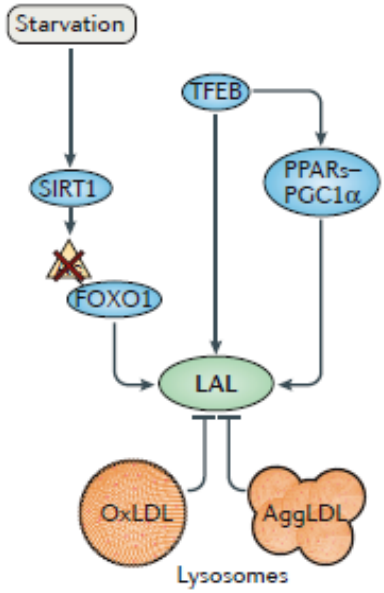

Figure 2: LAL gene regulation. LAL expression is positively regulated by transcription factor EB (TFEB), PGC1α and SIRT1-dependent deacetylation of FOXO1. Oxidized (Ox) or aggregated (Agg) low-density lipoproteins (LDL) inhibit LAL activity by changing the lysosomal pH. (1) Requisite permission to use this figure was obtained (Appendix).

1.1.3 Modulators of LAL enzymatic activity

LAL has optimal activity at pH ranges from 4-5 and can be measured using radioactively labeled CE and TG or artificial substrates like 4-methylumbelliferone esters of palmitic (4MUP) or oleic acid (4MUO). In the latter experimental setup,

the quantifiable product of LAL hydrolysis is the fluorescent lactone 4-methylumbelliferone. Although using 4MUP as substrate gives a global readout of the enzyme activity and cannot discriminate between separate esterified species, it is widely used in clinical diagnosis of LAL-D and in research (22, 23, 43, 44).

The hydrolytic profile of LAL has been investigated in detail in a variety of conditions and experimental settings. LAL protein is associated with lysosomal membranes with limited solubility (18, 45). *In vitro*, LAL activity and optimal hydrolysis pH are largely depending on the reaction conditions, like detergent, substrate, and salts concentration. For example, LAL activity is enhanced by TritonX-100, taurocholate, and phospholipids (23, 46, 47). Conversely, high salt concentration, divalent cations, and acidic phospholipids are known to decrease LAL-dependent hydrolysis (23, 45, 48).Several drugs have strong LAL inhibitiory action through direct or indirect effects. Due to their chemical properties, weak bases like chloroquine and chlorpromazine have an excessive affinity for acidic pH and accumulate in the lysosomes through a process known as lysosomotropism. Accordingly, lysosomotropic agents cause an increase in the lysosomal pH, hence altering the enzymatic activity of acidic hydrolases (5, 8, 49). In the last decade, the specific and potent LAL inhibitor Lalistat was developed (50, 51). Lalistat treatment induces lysosomal accumulation of neutral lipids (CE, TG) (52, 53). Therefore, lalistat has been proposed as adjuvant therapy to prevent the neurotoxic effects of excessive free cholesterol accumulation found in Niemann-Pick disease (54). Other known drugs like progesterone (55) and the antifungal agent esterasin (56) have as well been described to have an inhibitory effect on LAL activity.

1.1.4 LAL deficiency in humans

Autosomal recessive mutations in the LIPA gene result in impaired enzyme activity and consequential accumulation of TG and CE in the lysosomes. The exon 8 splice junction mutation (E8SJM) is the most common inherited defect found in more than half of all children and adults affected by LAL-D. LAL-D has a highly variable phenotype in humans and, depending on the residual amount of functional enzyme, was categorized as Wolman disease (WD) or cholesteryl ester storage disease (CESD) (Table 1). Generically named as LAL-D, it is classified as

a rare disease with a prevalence ranging from one in 40,000 to 300,000 due to ethnic origin and geographic location. However, because of its overlapping phenotype with other metabolic diseases, LAL-D might be substantially underdiagnosed (57, 58).

Table 1: Comparative clinical signs in Wolman Disease and Cholesteryl Ester Storage Disease (58). Requisite permission to use this figure was obtained (Appendix)

Disease Symptoms/ Characteristics	***Wolman Disease***	***Cholesteryl Ester Storage Disease***
Lipid Profile	Elevated LDL-cholesterol, triglycerides. Reduced levels of HDL.	Elevated LDL-cholesterol, triglycerides, serum total cholesterol. Reduced levels of HDL.
Liver Function	Elevated ALT + AST.	Elevated ALT + AST.
Hepatic Pathology	Yellow and greasy. Infiltration by lipid-filled Kupffer cells. Fibrosis.	Microvesicular steatosis of the hepatocytes. Cirrhosis. Infiltration by lipid-filled Kupffer cells and macrophages.
Splenic Pathology	Enlarged spleen.	Enlarged spleen.
Adrenal Pathology	Calcification of the adrenal glands.	Very rare calcification of the adrenal glands.
Intestinal Pathology	Massive CE and TG accumulation in the small intestine. Infiltration of the lamina propria by foamy macrophages.	CE accumulation, but to a much lesser degree than WD.
Biochemical Features	No functioning levels of LAL.	1-12% of functioning LAL relative to healthy patients.
Age of Onset	First few months of birth.	Childhood to adulthood.
Life Expectancy	<1 year.	Patients live into adulthood.
Causes of Death	Malnutrition, malabsorption, liver failure.	Liver failure.

WD was first described in 1956 in a post-mortem case report of a two months-old infant with multiple organ pathology, exhibiting adrenal calcification and severe lipid accumulation with hyperplastic foamy (macrophages) cells infiltrations in the liver, intestine, lungs, thymus, bone marrow, and spleen. Other organs like brain, kidneys or heart did not seem to be affected. A hallmark in WD is the enlargement

and calcification of the adrenal glands confirmed by abdominal radiographs or histological examination (Fig. 3A). Additionally, cholesterol crystals accumulate in liver macrophages (Kupffer cells) (59, 60), a process which contributes to the inflammatory profile of LAL-D (Fig. 3B).

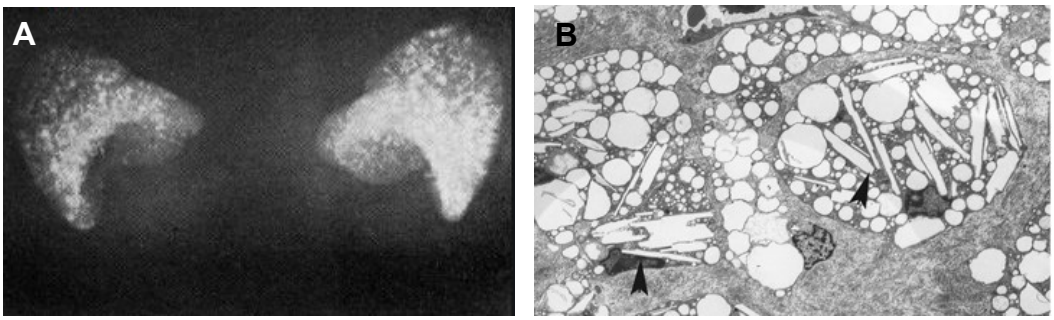

Figure 3: Wolman disease. (A) Radiography of abnormal adrenal glands calcification. (B) Electron micrograph of Kupffer cells in the liver; arrowheads show cholesterol crystals in lysosomes (61). Requisite permission to use this figure was obtained (Appendix).

The cause of WD was revealed 13 years later as LAL-D, leading to extensive TG and CE accumulation in the liver, intestine, adrenal glands, lymph nodes, spleen, and other tissues. The rapid disease evolution and severity revealed an important function of the LAL in TG and CE hydrolysis (62). Consistent with first reports, WD has an early onset with extremely severe progression being lethal in the first year after birth due to multiple organ dysfunction and failure to thrive. The disease's fulminant progression is caused by complete loss of LAL activity (less than 1% residual activity) (63). Due to its acute manifestation, WD is characterized by a relatively uniform clinical course, with abdominal distension due to hepatomegaly, vomiting, diarrhea, malabsorption and overall failure to thrive, which eventually causes the premature demise of affected infants.

Compared to WD, CESD patients present more heterogeneous evolution and clinical severity due to variations in LAL residual enzymatic activity, ranging from 1% to 12%. Overall, CESD has a longer life expectancy and patients survive through adulthood. Due to its later onset, CESD is often diagnosed due to hepatomegaly. The problem of miss/underdiagnosis is most frequent in these patients due to overlapping clinical signs with pathologies like NAFLD, non-alcoholic steatohepatitis (NASH), cryptogenic cirrhosis, hereditary dyslipidemia, Niemann-Pick, and even Gaucher disease (64-68). The complications arising in CESD are caused by the chronic progression of the pathology, which affect mainly

the liver and blood vessels leading to atherosclerotic plaques. Affected patients present enlarged fibrotic livers with microvesicular steatosis and portal hypertension which evolves to cirrhosis with esophageal varices and in some cases to hepatocarcinoma (69). A schematic description of the compensatory mechanisms triggered by LAL-D in the liver is illustrated in Fig. 4.

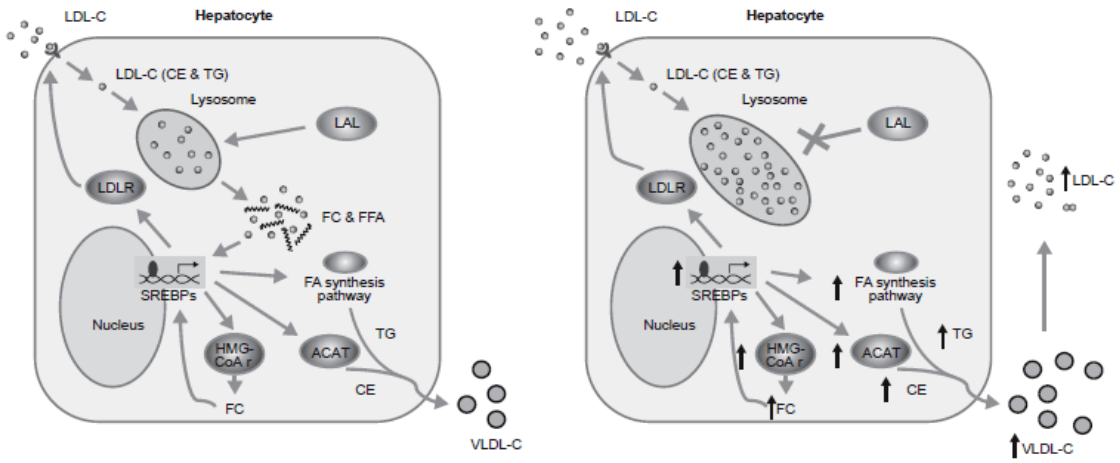

Figure 4: Cholesterol metabolism in hepatocytes of heathy (left) versus LAL-D patients (right). In healthy individuals lysosome-derived FC and FFA negatively regulate their *de novo* synthesis to maintain metabolic homeostasis (left). In LAL-D patients, TG and CE accumulate in lysosomes, triggering FA and cholesterol *de novo* synthesis and increased circulating LDL-C concentrations. Acyl-cholesterol acyltransferase (ACAT); cholesteryl esters (CE); fatty acid (FA); free cholesterol (FC); free fatty acid (FFA); hydroxymethylglutaryl-coenzyme A reductase (HMG-CoA r); lysosomal acid lipase LAL; LAL deficiency (LAL-D); low-density lipoprotein cholesterol (LDL-C); low-density lipoprotein receptor (LDLR); sterol regulatory element binding proteins (SREBPs); triglyceride (TG); very-low-density lipoprotein cholesterol (VLDL-C) (69). Requisite permission to use this figure was obtained (Appendix).

Cholesterol entrapment in the lysosomal compartment creates a negative feedback loop and thus extensive *de novo* cholesterol synthesis is triggered leading to dyslipidemia. This decompensation causes accelerated atherosclerosis in patients starting already at young age and eventually life threatening cardiovascular events (70).

1.1.5 Diagnosis and treatment of LAL-D

LAL-D can be easily misdiagnosed due to overlapping features to various and more frequent metabolic diseases, which may seriously delay diagnosis (68). Usually, young patients are diagnosed more easily than older patients with slower

disease evolution. One of the first indications of the disease is the non-obese profile of the patients and a combination of multi-organ clinical signs often at young age: hepatosplenomegaly, hepatomegaly with microvesicular steatosis and elevated concentrations of circulating transaminases; micronodular cirrhosis with portal hypertension and esophageal varices; dyslipidemia, advanced atherosclerosis, and cardiovascular diseases; little responsiveness to classical cholesterol-lowering treatment (57, 71, 72). Other relatively frequent symptoms are gastro-intestinal manifestations as diarrhea, malabsorption, emesis, gallbladder dysfunction, and steatorrhea (69).

Although clinical investigation is critical to narrow down the possible causal disease, final confirmative diagnosis is based on LAL activity and/or LIPA mutation analyses. Nevertheless, several patients have been as well diagnosed by microscopic analysis of liver biopsies (58, 60).

To facilitate the diagnosis of LAL-D patients, a very precise and non-invasive diagnostic fluorescent enzyme activity assay has been standardized using dried blood spots (DBS) from patients as source for blood leukocytes (43, 73).

Until recently, therapeutic approaches in LAL-D patients mainly targeted the hypercholesterolemia through the administration of statins, cholestyramine and ezetimibe (69). While improving circulating cholesterol concentrations in some patients, statin treatment rather aggravated the liver pathology, which necessitated hepatic transplantation. Liver and bone marrow transplantations were performed with relative poor prognosis in LAL-D patients and numerous procedure-related complications as organ rejection were frequently reported (74, 75). Nevertheless, the above therapeutic strategies were either supportive and insufficient or highly invasive and not suitable/available for LAL-D patients as routine interventions (57, 61, 75). Recent advances brought hope for treating LAL-D patients through enzyme replacement therapy (ERT) by intravenous administration of human recombinant LAL (hLAL) (76). The proof of concept that secreted LAL is taken up by deficient cells was first shown *in vitro* using co-culture experiments with LAL-D fibroblasts (27, 28). *In vivo,* ERT was for the first time successful in reverting the pathological phenotype of Lal-/- mice and rats (77-79). In humans, several clinical trials deemed great success for ERT in LAL-D patients of all ages (80-84) and led to its rapid approval by Drug Agencies in the USA, Europe, and Japan (76, 85-87). The hLAL used for the treatment of LAL-D patients is produced in eggs from

genetically engineered chickens (*Gallus gallus*). The enzyme is then purified from the egg white and formulated as concentrate for solution for infusion. ERT is indicated by European Medicines Agency for long-term treatment in patients of all ages with LAL-D (87). However, ERT is not covered by the state medical insurance in the UK, due to its unjustified high treatment price (500,000 £, according to guidance from National Institute for Health and Care Excellence) (88).

1.1.6 LAL deficient animal models

An animal model of LAL-D was first reported in 1990 and originated from a spontaneous mutation in a colony of Donryu rats (89). Lack of acid lipase activity confirmed the etiology of the disease. These animals have severe accumulation of unhydrolyzed lipids in liver, intestine, lymph nodes, and spleen and were described as a model for WD because of premature death by 120 days of age due to cachexia (90). Later, in 1998, a Lal-/- mouse model was developed by targeted LAL gene disruption. Despite total lack of LAL mRNA and protein expression as well as activity, these mice had a life span of approx. one year and were classified as a phenotypical CESD and a biochemical WD model (91).

Similarly to CESD patients, Lal-/- mice excessively accumulate CE and TG in the liver which reached 35% of the body weight (BW) by the age of 8 months. This was equivalent with 7 fold increase compared to WT mice Lal-/- mice develop hypertrophy of a single mesenteric lymph node and progressively lose their white adipose tissue (WAT) depots as shown in Fig. 5 (92).

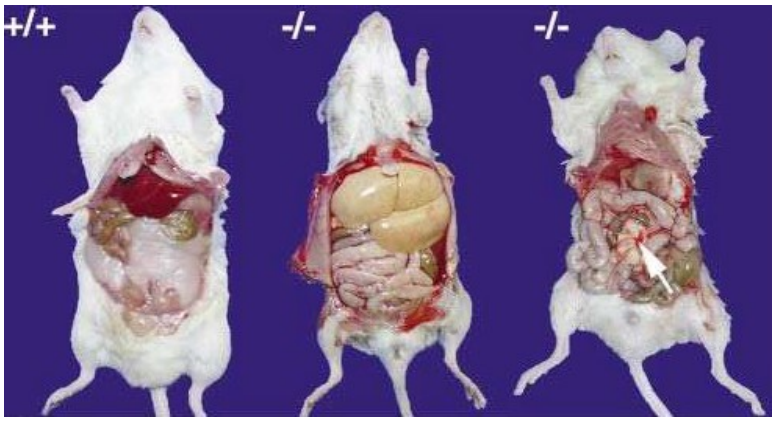

Figure 5: Photographs of WT (+/+) and Lal-/- mice aged 6 months. An example of a Lal-/- mouse with enlarged fatty liver and absence of WAT (middle) compared with the wild-type mouse. A unique large lymph node is a hallmark of the phenotype (right, white arrow) (92). Requisite permission to use this figure was obtained (Appendix).

The liver enlargement and WAT atrophy phenotype cause complex molecular adaptations in the Lal-/- mice which have decreased hepatic VLDL production. These mice present improved increased insulin sensitive and glucose tolerance compared to WT controls (93). Another organ affected by the disease is the small intestine which progressively accumulates lipids, and develops engorged macroscopic villi especially in the proximal part. Interestingly these lipids are predominantly TG, as shown in Fig. 6 (61, 92, 94).

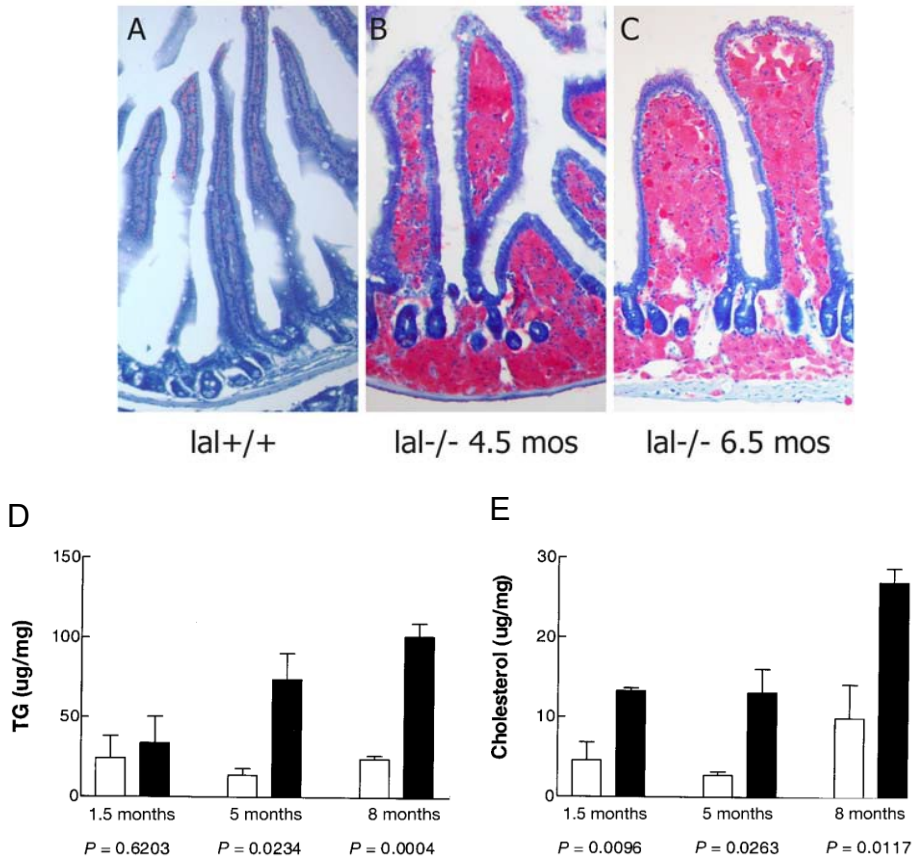

Figure 6: Intestinal phenotype of Lal-/- mice. Oil red O staining of intestinal villi in (A) WT and (B, C) Lal-/- mice. (D) Triglycerides (TG) and (E) total cholesterol concentrations in the intestine of WT (white bars) and lal-/- (Black bars) mice at different ages (61, 92). Requisite permission to use this figure was obtained (Appendix).

Detailed studies in Lal-/- mice were carried out over the years, exploring various aspects like inflammation, lipid and energy metabolism in the pursuit of understanding the molecular complexity and the physiological role of LAL in health and disease. Lal-/- mice have increased pro-inflammatory cytokines and eicosanoids production caused by severe lipid laden macrophages infiltration in key organs like liver, intestine, lungs, lymph nodes, and spleen (53, 92, 93, 95,

96). Interestingly, these macrophages stimulate tumor growth directly and indirectly, by suppression of peripheral T cell proliferation and lymphokine release (97). *In vivo* and *in vitro* LAL inhibition and deficiency causes macrophage impaired efferocytosis, and reduced capacity to promote RCT (98, 99).

1.2 Brown adipose tissue

1.2.1 Brown adipose tissue in energy metabolism regulation

The metabolic syndrome (MS) comprehends a wide palette of clinical abnormalities closely connected through their relationship and downstream co-morbidities, narrowing down to cardiovascular disease and diabetes mellitus (100). Beyond its conceptual meaning, the need to define MS comes from a practical point of view, i.e. to predict the risk factors of a major cardiovascular event and/or diabetes mellitus complications (101) as summarized according to the WHO in Table 2.

Table 2: Definition of the metabolic syndrome (102).

At least one of	***and at least two of***
• *Type 2 diabetes* • *Impaired glucose tolerance* • *Insulin resistance*	• *Hypertension (BP ≥ 140/90 mmHg)* • *Obesity (BMI ≥ 30 kg/m^2, or waist–hip ratio > 0.90 for men, > 0.85 for women)* • *Hypertriglyceridemia (≥150 mg/dL) or low serum HDL concentrations: <35 mg/dL in men and <39 mg/dL in women* • *Microalbuminuria*

Beyond genetics, MS is a consequence of disturbed energy balance and builds up onto complex inflammatory processes resulting in large number of morbidities and mortalities world-wide (103, 104). While state of the art therapeutics are currently quite successful in targeting dyslipidemia, hyperglycemia, insulin resistance, and hypertension, there is no miracle treatment available to date. Thus these branches of MS, including obesity, are pharmacologically incurable (105). Lipid lowering, hypoglycemiant, antihypertensive, classic anorexigenic molecules etc., sum up dozens of drug classes (106-108), for which patients (un)knowingly pay in the failed attempt to compensate for an imbalanced lifestyle. By far the most successful intervention to correct MS and even revert diabetes mellitus in encouraging number of patients is bariatric surgery, which drastically reduces disease-related mortality, independently of surgical risk (109-111). On the other hand, the free of charge cure of at least early to moderate metabolic morbidities, which is weight loss through improving eating habits and increasing physical activity (112-116), is not an option for the majority of affected individuals.

Obviously, the increasing number of supporting studies does not increase patient adherence to healthy lifestyle, frequently due to poor education on targeted alimentation and exercise plans to achieve and maintain weight loss. Adding up to the misfortune, resistance to weight loss in many patients and prolonged plateau periods can lead to little responsiveness to diet and exercise (100, 108). An ideal situation would thus imply discovering the holy grail of metabolic health and make MS a historical notion.

A decade ago, light in the dark arose by promising the much desired metabolic health at no dessert sacrifice: increasing energy expenditure by activating brown adipose tissue (BAT) (117). Historically, BAT was known as a thermogenic organ which prevents hypothermia in small mammals and newborn children (118, 119). Although BAT and its heat generating protein, UCP1, were as well documented in adults, their role (if any) in energy metabolism, was elusive. Nevertheless, decades later, research in animals proved extremely beneficial effects of BAT activation and its presence in adult humans was published as a major breakthrough (120, 121). With the (re)discovery and quantitative evidence of brown fat in human adults via positron emission tomography (PET) (Fig. 7), BAT was seen as a therapeutic target against metabolic syndrome (122).

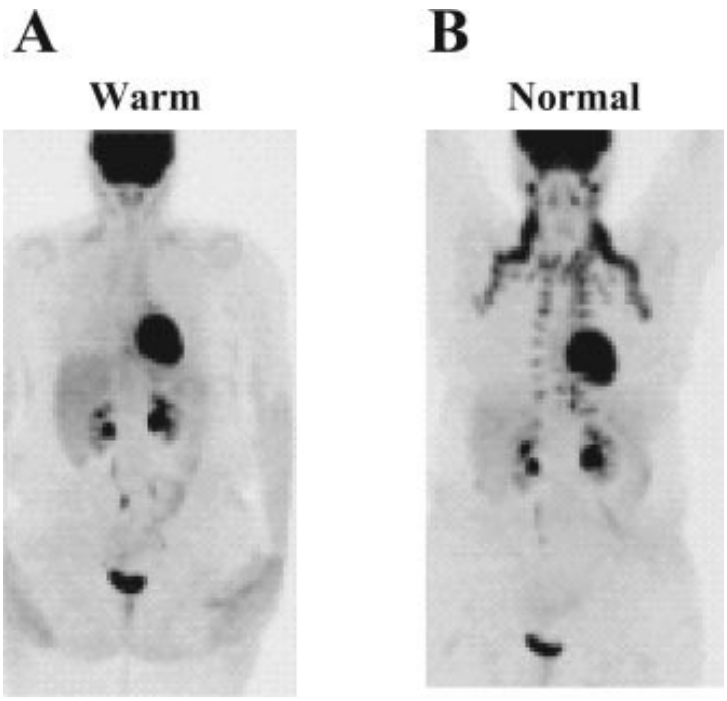

Figure 7: Cold-induced brown adipose tissue activation in adult man visualized by PET, routinely performed to visualize tumors in patients. Patient kept under (A) warm conditions

before fluorodeoxyglucose (FDG) injection and (B) under comparatively colder temperature under routine conditions (117). Requisite permission to use this figure was obtained (Appendix).

Humans have a particular physiological location pattern of the BAT depots, which are mostly found in the supraclavicular and the neck regions and additionally in paravertebral, mediastinal, para-aortic, and suprarenal localizations (117, 123). Importantly, BAT presence and activity in humans is inversely correlated with features of the metabolic syndrome, such as obesity, insulin resistance, and dyslipidemia. Thus, exploring brown adipocyte expenditure potential may help establish better prediction and disease-related risks and discover novel, more efficient therapeutic approaches (124-126). Whereas WAT has low metabolic rate and ideally stores excessive calories in the form of TGs, BAT presents a multilocular morphological structure, abundant with mitochondria and high expenditure potential (1, 127). BAT can be activated pharmacologically or by cold exposure and extensively burns lipid and glucose substrates (128). Etiologic and metabolic characteristics of brown adipocytes relate closely to SM cells as both cell types share common precursors (129). BAT is abundantly vascularized and innervated by sympathetic networks, which activate beta3-adrenergic receptors (β3-AR) (130). Altogether, these features put BAT into the center of non-shivering thermogenesis (NST) which is dependent on a brown adipocyte-specific protein UCP1 to uncouple mitochondrial respiration and generate heat instead of ATP (131, 132). Additionally, under β-AR stimulation, white adipocytes or their precursors can (trans)differentiate into brown-like adipocytes known as beige or brite cells. Stimulating NST triggers energy expenditure (EE) via utilization of diet and WAT-derived substrates as FA and glucose by brown or beige adipocytes (133, 134). Moreover, ectopic fat deposition can be reduced in organs such as liver, skeletal muscle (SM), and heart when FA from WAT are appropriately partitioned into activated brown and beige adipocytes (Fig. 8) (135, 136).

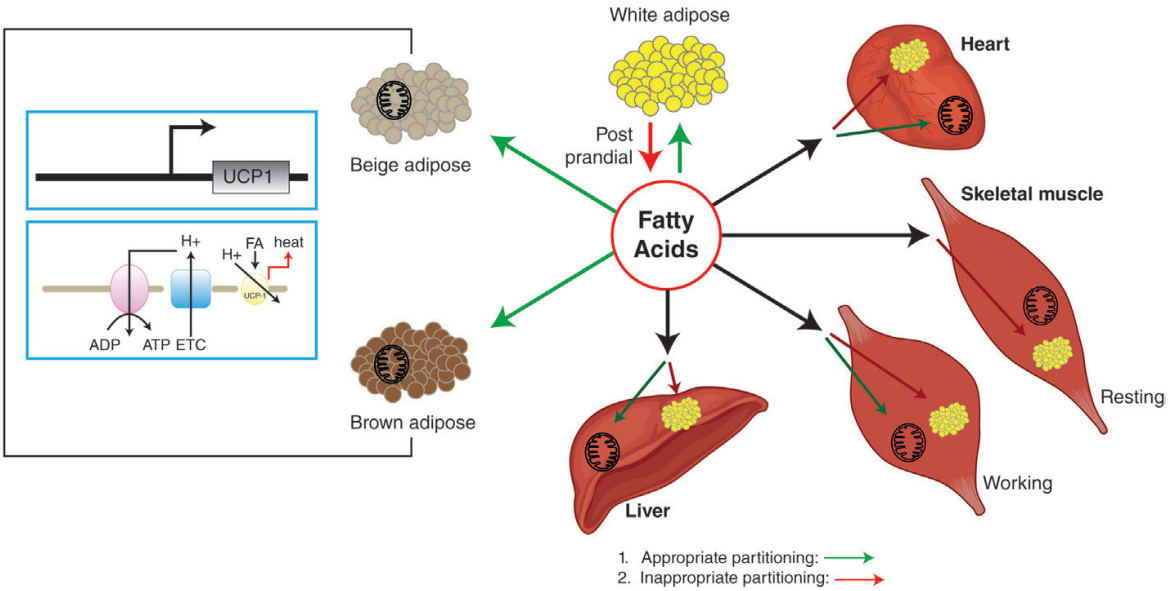

Figure 8: Triglyceride distribution from WAT to metabolically active tissues. WAT stores excess energy as triglycerides that can be mobilized by lipolysis to generate FFA for use by other tissues: brown and beige adipocytes, liver, heart and SM. Brown and beige cells perform non-shivering thermogenesis, regulated by uncoupling protein 1 (UCP1) (136). Requisite permission to use this figure was obtained (Appendix).

1.2.2 Substrate utilization in brown adipose tissue

Research conducted to investigate the benefits of BAT activation in mice by cold exposure or β-AR agonists revealed impressive improvements of different metabolic parameters. Activated BAT following cold exposure or β-AR agonist treatment corrected severe dyslipidemia, protected from diet-induced weight gain, and reduced atherosclerosis in mice (137, 138). Additionally, BAT mass increase by transplantation improved glucose tolerance and insulin sensitivity by boosting energy expenditure in obese, insulin-resistant mice (139). It is well established that BAT utilizes glucose and FA to fuel thermogenesis. Cold exposure triggers norepinephrine (NE) secretion via the sympathetic nervous system and activates the β3-AR on brown adipocytes (140). This results in adenylyl cyclase-dependent increases of cyclic adenosine monophosphate (cAMP) concentrations. cAMP activates protein kinase A (PKA) and triggers gene transcription of uncoupling protein-1 (Ucp-1) and peroxisome proliferator-activated receptor-gamma co-activator (Pgc-1α) via cAMP response element-binding protein (CREB) (141-143). In addition, PKA activates hydrolysis of TG stored in cytosolic LD and releases FA for mitochondrial β-oxidation. Acetyl-CoA is produced and acts as a substrate for

the citric acid cycle where intermediates generate electrons to maintain the electron transport chain. UCP-1, a characteristic proton transporter, uncouples the respiratory chain from producing ATP and, instead, generates heat, which is thereafter dissipated through the body via the blood stream (144, 145). The continuous flux of FA into the mitochondria depletes intracellular TG stores in the BAT, which are continuously replenished by enhanced uptake of FA from the circulation. These FA result from intravascular hydrolysis of TG-rich lipoproteins (TRLs) by LPL. The uptake of FAs is facilitated by specific membrane transporters and converted to TG. Additionally, BAT takes up glucose via glucose transporter (GLUT) 1 and 4 and is either used as thermogenesis fuel in the mitochondria or undergoes *de novo* lipogenesis (146, 147) (Fig. 9).

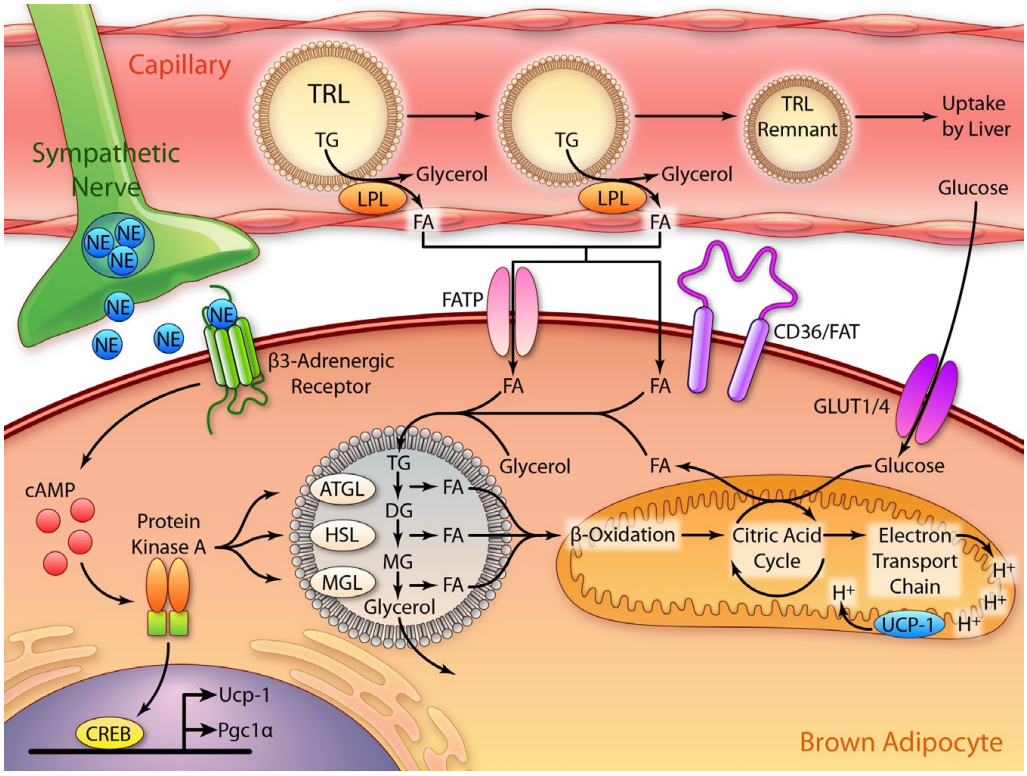

Figure 9: Fuel utilization in activated brown adipose tissue. BAT is activated via the sympathetic nerves which concomitantly activate cytosolic lipolysis and mitochondrial biogenesis and UCP1 synthesis. Fatty acids derived from TG hydrolysis are oxidized in the mitochondria. UCP1 shifts the electron transport chain from ATP synthesis, process which leads to heat production. Cytosolic lipid droplets are replenished with TG from circulating TRL via LPL mediated lipolysis. Additionally, glucose serves as substrate for beta oxidation or *de novo* lipogenesis. NE, norepinephrine; cAMP, cyclic adenosine monophosphate; CREB, cAMP response element-binding protein; FA, fatty acids; UCP-1, uncoupling protein 1; TRL, triglyceride-rich lipoprotein; LPL, lipoprotein lipase; CD36, cluster of differentiation 36 ; FAT, FA transport protein; GLUT, glucose transporter; TG, triglyceride; ATGL, adipose triglyceride lipase; DG, diacylglycerol; HSL, hormone-

sensitive lipase; MG, monoacylglycerol; MGL, monoglyceride lipase; Pgc-1α , peroxisome proliferator-activated receptor-gamma co-activator; (146). Requisite permission to use this figure as obtained (Appendix).

2. Materials and methods

2.1 Equipment

Table 3: Equipment used for various procedures

Equipment	Company
Centrifuge (5471R)	Eppendorf, Wien, Austria
ß-counter	Packard, Dayton, UK
Power supply (Power Pac 300)	Bio-Rad, Hercules, CA
Lightcycler 480	Roche, Palo Alto, CA
Sonicator	B.Braun, Hessen, Germany
Lyophilisator	Virtis, Warminster, PA
Nano Drop Spectrophotometer	Peqlab, Darmstadt, Germany
Thermal cycler C1000	Bio-Rad, Hercules, CA
Microwave	Whirlpool, Benton Harbor, MI
Precellys	Peqlab, Darmstadt, Germany
Anthos 2000	Anthos, Toulouse, France
Viktor 1420 Multilabel counter	Wallac, Saskatchewan, Canada

2.2 Animals and diets

Lal-/- mice were available in our laboratory and the line founder animals were kindly provided by Hong Du and Cong Yan (Indiana University School of Medicine, IN); these mice were backcrossed to a C57BL6 background. Tissue-specific Lal-deficient mice were generated by crossing Lal-floxed mice ($Lipa^{tm1a(EUCOMM)Hmgu}$) with transgenic mice expressing the Cre-recombinase under the control of the lysozyme M promoter for specific deletion of LAL in myeloid cells including macrophages (macLal-/-). For adipose tissue-specific LAL deficiency (atLal-/-), Lal-floxed mice were crossed with adiponectin-Cre mice.

All experiments were performed using female and male Lal-/-, atLal-/- and macLal-/- mice and their corresponding wild-type (WT) littermates. The mice were maintained in a clean environment with unlimited access to food and water in a regular light-dark cycle (12 h light, 12 h dark).

For all the experiments, age-matched mice were used. Mice were fed either regular chow diet (4% fat and 9% protein; Altromin 1324, Lage, Germany) or were

switched to a high-fat/high-cholesterol diet (HF/HCD; 30% fat plus 1% cholesterol; Ssniff, Soest, Germany) or western type diet (WTD, 21% fat, 0.2% cholesterol; Ssniff Spezialdiaeten GmbH, Soest, Germany).

For cold exposure experiments, mice were housed at 4°C with or without access to food, as described in the Results section. Core body temperature was measured using a rectal probe thermometer (Physitemp Instruments, Inc., Clifton, NJ). Blood glucose was determined using Accu-Chek® Active glucometer and glucose strips (Roche Diagnostics GmbH, Mannheim, Germany).

All animal experiments were performed in compliance with national laws and were approved by the Austrian Federal Ministry of Education, Science, and Research, Vienna, Austria, in accordance with the European Directive 2010/63/EU.

2.3 Energy metabolism *in vivo*

Assessment of energy intake and energy expenditure was performed using an indirect calorimetry system (TSE PhenoMaster, TSE Systems, Bad Homburg, Germany). Weight-matched Lal-/- and WT mice were housed in fully automatic metabolic cages, with free access to food and water in a regular light-dark cycle (12 h light, 12 h dark) and acclimatized for 48 h before the experiments. The same system was used to gradually decrease the ambient temperature from 22°C to 5°C and for thermoneutrality (30°C) housing conditions. The detailed conditions are enclosed in the Results section. O_2 consumption, CO_2 production and locomotor activity (using infrared sensor frames) were measured every 15 min. Carbohydrate and lipid oxidation rates were determined as described (148) and converted from mg/hour into kcal/hour (149). In some experiments, to stimulate NST, 1 mg/kg i.p. injection of the β3 adrenergic agonist CL316,243 (CL) was administered as single dose.

2.4 Fat mass quantification using micro-computed tomography (µCT)

WT and atLal-/- mice were anesthetized with isoflurane (Abbvie GmbH, Vienna, Austria) and transferred to a Siemens Inveon µCT scanner (Siemens, Erlangen, Germany), under continuous anesthetic inhalation during scanning. Obtained data for body and fat volume were calculated using Materialise Mimics 20.0 software (Materialise HQ, Leuven, Belgium).

2.5 [$_3$H]2-deoxy-D-glucose uptake

Weight-matched mice aged 12 weeks were housed at 4°C with access to food for 3 h. Thereafter, food was removed and the mice were injected intraperitoneally with 2 g/kg BW of glucose in PBS containing 2 µCi [^{3}H]2-deoxy-D-glucose. Mice were sacrificed 60 min post injection and radioactivity in tissue lysates was determined by β-counting using Packard ß-counter (Packard, Dayton, UK) (149).

2.6 Fatty acid uptake

Sixteen weeks old WT and Lal-/- female mice were kept at 5°C for 4 h with *ad libitum* access to food and water. Thereafter, food was removed and the mice were gavaged with 100 µl corn oil containing 8 µCi [^{3}H]triolein. Three h post gavage, mice were sacrificed and BAT was harvested. Radioactivity in BAT lysates was determined by liquid scintillation counting (Packard, Dayton, UK) (149).

2.7 Intra-peritoneal glucose tolerance test (IPGTT)

Mice were fasted for 6 h in the morning without access to drinking water. Blood was taken from the tail vein before and 15, 30, 60, 120, and 180 min after an intraperitoneal injection of D-glucose (2 g/kg BW). Glucose concentrations from tail vein blood were determined using glucometer AccuCheck-active (Roche Diagnostics, Palo Alto, CA).

2.8 Very low density lipoprotein (VLDL) secretion

Twelve h fasted mice were injected intraperitoneally with 500 mg/kg BW of tyloxapol in PBS. Blood was drawn from *v. facialis* every hour post-injection and plasma was separated by centrifugation at 7,000 rpm for 7 min at 4°C. TG and free glycerol content were determined enzymatically as described before (93).

2.9 Plasma lipid, ALT, AST and creatine phosphokinase activity analysis

Blood was collected by facial vein puncture and prepared within 20 minutes. TG, total cholesterol (TC), and free cholesterol (FC) concentrations were measured in plasma from mice using enzymatic kits (DiaSys, Holzheim, Germany). Plasma free glycerol (FG) and free fatty acid (FFA) concentrations were determined using Free Glycerol Reagent (Sigma-Aldrich, St. Louis, MO) and NEFA-HR kit (Wako Life Sciences, Mountain View, CA), respectively. Lipoprotein fractions were separated from 200 µl pooled plasma from each group using fast protein liquid

chromatography (Pharmacia P-500) as previously described (150). ALT, AST, and creatine phosphokinase activity in plasma samples were measured using a Spotchem EZ analyzer and test strips (A. Menarini GmbH, Vienna, Austria) (149).

2.10 Mitochondrial respiration measurement

Lal-/- and WT mice were housed at 5°C for 3 h. Oxygen consumption rate of freshly isolated BAT was determined using a Clark electrode (Strathkelvin Instruments, Glasgow, Scotland) as previously described (151) with some modifications. Approximately 20 mg of tissue were minced and subsequently transferred into the MT200A measurement chamber containing 1 ml of 100% air saturated respiration buffer (2% BSA, 0.45% or 0.1% D-glucose, 6 mg pyruvate). For measurement of maximal respiration, 25 µM carbonyl cyanide-4-(trifluoromethoxy)phenylhydrazone (FCCP) was added to the respiration buffer. Oxygen consumption rates were normalized to tissue weight and calculated as µg O_2/min/tissue (149). This experiment was performed together with Dina C. Hofer (Graz University of Technology).

2.11 Lipase activity assays

Lipase activity measurements were performed as described (53) with minor modifications. BAT was lysed in lysis buffer (100 mM potassium phosphate, 250 mM sucrose, 1 mM EDTA, 1 mM DTT, pH 7) and centrifuged at 10,000 x g and 4°C for 30 min. The protein content of the clear infranatant was determined by a Lowry assay (Bio-Rad Laboratories, Hercules, CA). To measure neutral TG hydrolase activity, 50 µg of protein from tissue lysates were mixed with 100 µl of TG substrate [0.3 mmol triolein/sample, 0.5 µCi/sample [9,10 3H(N)]triolein (Perkin Elmer, Waltham, MA), 3.5 µg mixed micelles of phosphatidylcholine and phosphatidylinositol (3:1, w:w)]. The substrate contained FFA-free BSA at a final concentration of 2% in 100 mM phosphate buffer. After incubation in a water bath for 1 h at 37°C, the reaction was stopped by the addition of 3.25 ml stop solution (methanol:chloroform:n-heptane, 10:9:7, v:v:v) and 1 ml of 0.1 M potassium carbonate (pH 10.5, adjusted with boric acid). The tubes were vortexed for 10-15 s and centrifuged at 1,700 x g for 15 min at 4°C. The radioactivity in 1 ml of the upper phase was determined by liquid scintillation counting, and the release of FA was calculated (149).

LAL activity was estimated using the fluorogenic substrate 4-methyl-umbelliferyl-palmitate (4-MUP) as described (53). Briefly, iBACs were lysed in lysis buffer (100 mM NAH_2PO_4, pH 6.8, 1 mmol/l EDTA, 1 mmol/l dithiothreitol, 0.5% NP-40, 0.02% sodium azid, protease inhibitors) and centrifuged for 10 min at 10000 rpm. The clear infranatant was used for protein concentrations estimation by a Lowry assay. Per sample, 2 µl of 4-MUP (10 mM) were mixed with 2 µl phosphatidylcholine (16 mM) in hexane, evaporated under a stream of nitrogen, and resuspended in 50 µl sodium taurocholate (2.4 mM) by sonication. Fifty microliters of 4-MUP substrate, 125 µl assay buffer (200 mM sodium acetate pH 4.5), and 25 µl cell lysate were incubated for 30 min at 37°C. The reaction was stopped by the addition of 100 µl of 0.75 M Tris (pH 11). Relative fluorescence units (RFU) were determined at 360 nm excitation/460 nm emission on a Victor 1420 multilabel counter (PerkinElmer, Waltham, MA) using 4-MU as standard. LAL activity is expressed as nmol MU/h*mg protein (149).

2.12 Determination of acyl-CoA and acyl-carnitine concentrations

Acyl-CoA concentrations were measured by on-line solid phase extraction liquid chromatography-mass spectrometry as described previously (93). The same method was used for separation and semi-quantitative analysis of carnitine esters (152). Acyl-CoA (internal standards 0.5 nmol/ml C17:0-CoA, 0.6 nmol/ml $^{13}C_2$-acetyl-CoA, 0.6 nmol/ml $^{13}C_3$-malonyl-CoA), and acyl-carnitines (internal standard 0.5 nmol/ml C17:0-CoA) were extracted from tissue lysates using 500 µl ice-cold buffer containing 0.1 M KH_2PO_4 and 2-propanol in a 1:1 ratio (v:v). Samples were homogenized for 2x30s using a tissue homogenizer (Precellys 24, Bertin Technologies, Montigny-le-Bretonneux, France). Subsequently, 30 µl of saturated aqueous $(NH_4)_2SO_4$ and 500 µl ml of acetonitrile were added (ice-cold). The homogenate was vigorously mixed and centrifuged at 2,500 x g for 10 min at 4°C, and the supernatant was transferred to autosampler vials. Extracts were stored at -80°C. Analyses were performed on an Ultimate 3000 System (Dionex, LC Packings, Sunnyvale, CA) consisting of an autosampler with cooled tray and a column oven with a switching unit coupled to an LTQ Orbitrap XL (Thermo Scientific, Waltham, MA). A Phenomenex Strata X 2.0 × 20-mm cartridge (Torrance, CA) and a Waters XBridge column (2.1 × 50 mm, 2.5 µm) (Milford, MA) were used for on-line solid phase extraction and as analytical column,

respectively. Positive electrospray ionization-mass spectrometry was performed by high resolution mass spectrometry (scan range 150–2000 m/z, resolution 60,000). Compound identities were confirmed using accurate mass, tandem mass spectrometry, and retention time. Peak area ratios of acyl-carnitines were compared with C17:0-CoA for semi-quantitative analysis (93, 152). This experiment was performed in collaboration with Christoph Magnes (Joanneum Research, Graz).

2.13 Tissue lipid content

WT and macLal-/- mice were fed HF/HCD for 10 weeks. The animals were fasted for 12 h, livers were collected and snap frozen in liquid nitrogen. Liver samples were homogenized in lysis buffer. Lysates containing 500 µg protein were normalized with the appropriate amount of lysis buffer to the same volume. A hexane:isopropanol (3:2) solution was added to the tissue lysates in 20-fold excess and rotated for 2 h at room temperature (RT). Thereafter, extracts were centrifuged at 4000 rpm for 15 min at 4 °C and the organic phase was decanted to the fresh vial. Two hundred 2% Triton X-100 in chloroform was added to the extracts, vortexed, and dried under a stream of nitrogen. Thereafter, the samples were redissolved in 100 µl of ddH_2O and TG, TC, and FC concentrations were measured enzymatically according to manufacturers' instructions. CE concentrations were calculated by subtracting FC from TC concentrations (153).

2.14 Electron microscopy

Tissues were fixed in phosphate buffer/2.5% glutaraldehyde for 2 h, washed, post-fixed in phosphate buffer/OsO_4 for 2 h and 4x10 min in phosphate buffer. After dehydration, tissues were infiltrated (acetone and agar 100 epoxy resin, pure agar 100 epoxy resin) for 4 h, placed in agar 100 epoxy resin (8 h), transferred into embedding molds, and polymerized (48 h, 60°C). Sections stained with lead citrate and platine blue were imaged at 120 kV with a Tecnai G 2 FEI microscope (FEI, Eindhoven, Netherlands) equipped with a Gatan ultrascan 1000 CCD camera.

For BAT morphology assessment, LD and mitochondria from 97 electron micrographs (each having a surface of 142.09 µm²) per genotype were counted and analyzed by open source ImageJ software image processing and analysis in

Java (149). This experiment was performed in collaboration with Dagmar Kolb (Medical University of Graz).

2.15 Toluidine blue staining

Twelve weeks old female WT and Lal-/- mice were exposed to cold for 4 h in the fed state with or without an additional corn oil gavage (100 µl). BAT was collected and prepared as described in “Electron microscopy”. Thereafter, 2.5 µm-thick sections were stained with toluidine blue by transfer to a drop of distilled water on a glass slide. The slide was placed on a hot plate at approximately 60°C until the drop of water was evaporated. Thereafter 1% toluidine blue staining solution was added to cover the sections. When the edge of the stain drop just began to tum to a metallic gold color the slide was removed from the hot plate and the stain was washed from the slide with distilled water and dried by open air (149). This experiment was performed in collaboration with Dagmar Kolb (Medical University of Graz).

2.16 Hematoxylin and eosin staining

Mouse tissues were fixed in 4% neutral-buffered formaldehyde for 24 h and stored in PBS at 4°C until embedded in paraffin. Sections (5 µm) were deparaffinized and stained with Mayer’s haematoxylin and eosin (149). This experiment was performed in collaboration with Martina Auer (Medical University of Graz).

2.17 Immunofluorescence staining

BAT from 2 h cold-exposed mice aged 20 weeks was dissected from interscapular regions, washed in PBS, and immediately fixed in 4% paraformaldehyde for 24 h. Fixed samples were transferred to PBS for storage. The tissue was embedded in paraffin, cut in 5 µm-thick sections, and mounted on Superfrost Plus slides (Menzel-Glaeser, Braunschweig, Germany). Standard de-paraffinization was followed by boiling sections in 10 mM sodium citrate buffer (pH 6.0) for 7 min for antigen retrieval. Protein blocking was performed with UltraVision Protein Block (Thermo Fisher Scientific, Waltham, MA) and M.O.M.™-Blocking reagent (Vector Laboratories, Burlingam, CA). Slides were incubated with anti-cathepsin D (1:200, ab6313, Abcam , Cambridge, UK) and anti-perilipin 1 antibodies (1:200, 9349, Cell Signaling Technology, Danvers, MA) for 30 min. Subsequently, slides were washed and incubated with a mixture of Alexa Fluor 488 goat anti-rabbit and Alexa

Fluor 594 goat anti-mouse antibodies (both 1:500; Thermo Fisher Scientific) for 30 min at RT. Negative control for rabbit IgG (Dako, Glostrup, Denmark) and negative control mouse IgG2a (Dako) generated non-specific staining. After staining, tissue sections were mounted with ProLong Gold antifade reagent (Thermo Fisher Scientific). Confocal images of samples were acquired with a Zeiss Observer Z.1 inverted microscope equipped with a Yokogawa CSU-X1 Nipkow spinning disk system, a piezoelectric z-axis motorized stage (CRWG3-200; Nippon Thompson Co., Ltd., Tokyo, Japan), and a CoolSNAP HQ2 CCD Camera (Photometrics, Tucson, AZ). Cells were excited with 488 nm and 568 nm laser lines (Visitron Systems, Puchheim, Germania) with exposure times of 500 to 1,000 ms using an alpha Plan-Fluar 100x/1.45 Oil M27 (Zeiss, Jena, Germany) (149). This experiment was performed in collaboration with Martina Auer and Benjamin Gottschalk (Medical University of Graz).

2.18 RNA isolation, cDNA generation, and real-time PCR

a) cDNA preparation and reverse transcription

Total RNA from tissues was extracted using TriFast (Peqlab, Erlangen, Germany) following the manufacturer's protocol. RNA concentration was measured using a Nano Drop Spectrophotometer (Peqlab, Darmstadt, Germany). Two µg RNA in a final volume of 10 µl were reverse transcribed by using High-Capacity cDNA Reverse transcription kit (Applied Biosystems, Carlsbad, CA). High-Capacity cDNA Reverse transcription kit's master mix composition is shown in Table 4.

Table 4: Master mix for cDNA Reverse transcription kit

Component	**Volume (µl)/reaction**
10 X Buffer	2
25 X dNTP Mix (100 mM)	0.8
10 X RT Random Primers	2
Multiscribe reverse transcriptase	1
RNase inhibitor	0.7
Nuclease-free water	3.5
2 µg RNA/10 µl water	10

Total volume / reaction	20

The reverse transcription reaction of the samples took place in a thermocylcer C-1000 (Bio-Rad, Hercules, CA) using the program shown in Table 5.

Table 5: Reverse transcription conditions in the thermocycler

Step	**Step 1**	**Step 2**	**Step 3**	**Step 4**
Temperature	25°C	37°C	85°C	4°C
Time	10 min	120 min	5 s	∞

b) Quantitative real-time PCR

Three µl of diluted cDNA (1:50 in ddH_2O) and 1 µl of each forward and reverse primer (see below) were mixed with 5 µl QuantiFastTM SYBR® Green PCR Kit (Qiagen, Valencia, CA). Quantitative real-time PCR was performed on a Roche LightCycler 480 (Roche Diagnostics, Palo Alto, CA) using the program shown in Table 6. Samples were analyzed in duplicate and normalized to the expression of cyclophilin A. Expression profiles and associated statistical parameters were calculated using the $2^{-\Delta\Delta CT}$ method (154).

Table 6: PCR program for real time PCR

Step	**Temperature**	**Time**	**No of cycles**
Denaturation and Amplification	95°C 60°C	10 s 30 s	40
Melting curve	95°C 60°C 95°C	10 s 20 s continuous	1 1
Cool down	4°C	20 s	1

Table 7: Primer sequences used for qPCR

Gene	**Forward primer**	**Reverse primer**
Angptl4	CTTTGGCTATGGGCTTCCAGTC	GCAAGGAGGACAGAGTTTATCGTG
Atg7	CAGCAGCACATCAACAAGAG	GTCACACACCAGCAGGTTAT

Atgl	CCACCACGCTCTTCTGTCTAC	AGGGTCTGGGCCATAGAACT
Atrogin1	ACTGCCACACCTCCAGTCATT	CTTTGCCTCACTCAGGATTGG
Cact	TGCTGACGGATACAGAGGTGT	CCACGCAGAACTTCTCGCTAC
Cd36	CCCTGCCATTGTTAAGACC	TGCTGCTGTTCTTGTTT
Cpt1β	AGAGTGGAGGCGCATGCT	GGCATCTAGGAGGAAGCTGTTC
Cpt2	CTGTCCACACTATGAAGAC	AGGTTCTTCATGAGGCCTGT
Crtc2	TGGCTGCTACTTCTGCAATGATGT	AGGACAGAGACCATCAGCTCCAC
Cyclophilin	AAGGTTCGGGAGTATCTGTCTG	GGGTTGGAGCTGATATGTAGCA
Dio2	CAGCACTCTTTGAGGTGAAAAAC	CCATTCGCAGTCTCGTAGGTG
Emr1	TGTATTTGGCTAATGGCTCAGC	TATGGGCACAAGGAAGTTGTC
Fabp4	GCTGGGTTACTCTGATGGGTC	CCACCACGGACATAGGCATAC
Glut-1	ATGAACCCTAACCCCCAAGAC	CGTTCTCCTCAATAGCAGGGA
Glut-4	GCCACTCACATCTACGGAGC	GACAGCCACGGATGGTGTTC
Hsl	GCTGGTGACACTCGCAGAAG	TGGCTGGTGTCTCTGTGTCC
Il-1β	AAGGTGAAGAGCATCATAACCCT	TCACGCCTTTCATAACACATTCC
Lamp1	GCAGGTCTATCTACGCTGTG	GGTTGTCTGGATTCTGGAGG
Lamp2	TTCAACACTACACGCATCCC	GCCCTCATAGAGCCAGACC
Lcad	TCTTTTCCTCGGAGCATGACA	GACCTCTCTACTCACTTCTCCAG
Lpl	CAGCACAGCATCGTACCCA	TCCCAATGCCGTTCTCAAAAT
Mcoln1	CTACTGTGCTTCAGGGACAAC	CAAAGGACTTCGATTCTGCCC
Murf1	CGTGGCCATCTTCTCTGTCG	AGGCCGCAGTACACACCGAT
Pgc1α	GTGACTGGAACACTGGTCCTA	CCAGCCACGTTGCATTGTAG
Pparγ	TGGGATGTTATCTGGTGTGTTCAC	AAGCCTGAATCTGCAGTAAGCAT
Prdm16	GCTGGTGGAAAACATCATTGACAT	CATCGGGTGGCTGCCTTT
Tfeb	CTTTCAACAGACTGGACTTCTCGA	CAGCTCCAACAGCCTTACTACGT
Tnfα	ACATTCCCGTTACCGTCCATC	GGACCCCTGAAGACACAG
Ucp1	GCATCCTGGGACGAGATGAAC	CATGGCCGAGCTGTAGCAG
Vlcad	CCATCCAGCCATTCAGTCTT	TTCCAGGATTCATGTGCCAG

2.19 Western blotting analysis

Tissues were lysed in RIPA buffer and protein concentrations were determined by modified Lowry assay (DC™ Protein assay, BioRad, Hercules, CA). Tissue lysates were separated by SDS-PAGE and transferred onto nitrocellulose or PVDF membranes. Non-specific binding sites of the membranes were blocked using a 5% solution of milk powder or 1% BSA in washing buffer for 1 h. For detection of the proteins of interest, anti-rabbit polyclonal antibodies against LAL (Genetex, Hsinchu City, Taiwan), UCP1 (Abcam), LC3B, AKT, and anti-mouse polyclonal antibody against p-AKT (Cell Signaling Technology) were used at a dilution of

1:1,000. Polyclonal anti-rabbit calnexin (Santa Cruz, Heidelberg, Germany) or GAPDH (Cell Signaling Technology), diluted 1:1,000 were used as loading control. HRP-conjugated goat anti-rabbit (1:2,500) and rabbit anti-mouse antibodies (1:500) (Dako) were visualized by enhanced chemiluminescence detection (ClarityTM Western ECL substrate; Bio-Rad) using a ChemiDoc^{TM} MP imaging system (Bio-Rad, Hercules, CA) (149).

Western blotting buffers

a) RIPA lysis buffer:

Fifty mM Tris HCl, 150 mM NaCl, 1% Triton X-100, 0.5% deoxycholate, and 1:2,000 protease cocktail inhibitor cocktail were mixed and pH 7 was adjusted with KOH.

b) Sample buffer:

In 25 ml H_2O, 2.3 g SDS, 0.6 g Tris, pH was adjusted to 6.8 with HCl, thereafter 10 ml glycerol was added and volume adjusted up to 45 ml. One drop of bromphenolblue and mercaptoethanol (3%) was added followed by incubation for 10 min in hot water.

c) Separating gel buffer:

1.5 M Tris and 0.4% SDS were mixed in 80 ml H_2O, pH 8.8 was adjusted with HCl, and volume adjusted up to 100 ml.

d) Stacking gel buffer:

Six g Tris was dissolved in 90 ml ddH_2O. pH was adjusted to 6.8 with HCl, and volume was ajusted up to 100 ml with ddH_2O.

e) Separating gel

Ingredients were mixed in the order shown in Table 8.

Table 8: Separating gel

Reagents	**10% SDS gel**
Acrylamide	2866.25 µl
Seperating gel buffer	2712.5 µl
ddH_2O	5171.25 µl
10 % SDS	100µl

TEMED	4.4 µl
10% APS	7.6 µl
Final volume	87804.4 µl

f) Stacking gel

Stacking gel was prepared according to Table 9.

Table 9: Stacking gel

Reagents	**4% SDS gel**
Acrylamide	326 µl
Buffer 2	500 µl
ddH_2O	1650 µl
10 % SDS	21.5µl
TEMED	1.25 µl
10% APS	19 µl
Final volume	2517.75 µl

2.20 iBACs cell culture, differentiation, lipid staining and quantification

Immortalized brown adipocytes (iBACs) were obtained from Patrick Seal (University of Pennsylvania, PA) and cultured in DMEM (high glucose) supplemented with 10 % FBS (Invitrogen, Carlsbad, CA) µg/ml streptomycin, 50 units/ml penicillin, 2 mM l-glutamine, and 20 mM Hepes at 37°C in 5% CO_2 atmosphere. Adipocyte differentiation was induced by culturing cells in differentiation medium supplemented with 0.5 mM 3-isobutyl-1-methylxanthine, 0.5 µM dexamethasone, 20 nM insulin, 1 nM triiodthyronine, and 125 µM indomethacin. After a two days induction period, the medium was replaced by maintenance medium supplemented with 20 nM insulin and 1 nM triiodothyronine. Thereafter, medium was changed every day. Full differentiation was achieved after 7 days. For the entire differentiation period, we treated one set of cells with 30 µM Lalistat2 (gift from Paul Helquist, University of Notre Dame, IN) from a 10 mM stock in DMSO, whereas control cells were treated with DMSO. To stimulate lipolysis, cells were incubated with 10 µM isoproterenol for 2 h. Free FA content was determined using NEFA-HR(2) Kit (Wako Life Sciences, Mountain View, CA).

Cellular TG concentration was determined using Infinity Triglyceride Reagent (Thermo Scientific, Waltham, MA). Values were normalized to total protein content (BCA reagent, Pierce, Rockford, IL). Lipid staining was performed with fixed cells (10% formalin in PBS, 30 min) using Oil red O (ORO; 0.25% in 60% isopropyl alcohol stock solution diluted 3:2 with dH_2O) for 45 min (149). This experiment was performed in collaboration with Katharina Huber (Graz University of Technology).

2.21 Adipocytes and stromal vascular cell isolation

The isolation of adipose stromal vascular cells (SVC) was described previously (155) with some modifications. Subcutaneous WAT from 8-10 weeks old mice was dissected, washed, minced, and digested in 1 ml PBS containing 0.125 U/ml collagenase D (Roche Diagnostics), 2.4 U/ml dispase II (Sigma), 10 mM $CaCl_2$ (Sigma, added just before tissue digestion) at 37°C with constant agitation at 180 rpm for 25-30 min. Complete DMEM/F12 containing Glutamax (Life Technologies, Carlsbad, CA), 10% FBS, and 1% Penicillin/Streptomycin was added to stop the digestion. After centrifuging at 200 x g for 10 min, the pellet was resuspended in fresh complete medium and filtered through a 70-µm cell strainer. After centrifugation for 10 min at 700 x g, the cell pellet containing the SVC was resuspended in complete DMEM/F12 and seeded on a 10-cm cell culture dish. At a confluency of ~80%, SVC were seeded on 12-well plates and grown to confluency for differentiation. Differentiation was induced by using complete DMEM/F12 supplemented with 1 µM dexamethasone, 0.5 mM isobutylmethylxanthine (IBMX), 5 µg/ml insulin with/without additional 1 uM rosiglitazone. Three days after induction, medium was changed to complete DMEM/F12 supplemented with 5 µg/mL insulin for two days and afterwards cells were maintained in complete DMEM/F12. On day 7, the fully differentiated cells were stained with ORO for neutral lipid visualization (149). This experiment was performed in collaboration with Wenmin Xia (Graz University of Technology).

2.22 Mouse peritoneal macrophages (MPMs)

MPMs were collected by injecting 3 ml of 3 % thioglycollate intraperitoneally. Seventy-two hours postinjection, MPMs were collected by flushing the peritoneum with 9 ml EDTA-PBS (1 mM EDTA in PBS). Cells were centrifuged at 850 rpm at 4 °C for 5min after which they were resuspended in the appropriate amount of

Dulbecco's Modified Eagle Medium (DMEM) containing high-glucose (25 mM), 4 mM glutamine, 1 mM pyruvate, 10 % lipoprotein-deficient serum (LPDS) and 1 % penicillin/1 % streptomycin (1 % P/S) and cultured for at least 2 h. Thereafter, the cells were washed three times with pre-warmed PBS and cultured for additional 6, 24, 48 or 72 h.

2.23 Statistics

Statistical analyses were performed using GraphPad Prism 5.0 software, (San Diego, CA). Data are presented as mean ± SEM. Comparisons between 2 groups were performed using unpaired 2-tailed Student's t test. Comparisons of multiple groups were analyzed by 2-way ANOVA followed by Bonferroni post-tests. Significance levels were set at $p < 0.05$ (*), $p \leq 0.01$ (**), and $p \leq 0.001$ (***).

3. Impact of global LAL deficiency on thermogenesis in mice

3.1 Introduction

LAL hydrolyzes exogenous (via lipoproteins) or endogenous (via autophagy) CE and TG within lysosomes (2, 4). Mutations in the LIPA gene, which encodes LAL, lead to severe intra-lysosomal lipid accumulations, caused by the lack or dysfunction of the only known enzyme involved in the acid hydrolysis of CE and TG (20). Both in humans and mice, the hallmark of LAL deficiency is severe hepatomegaly, together with ectopic lipid accumulations in multiple organs and tissues (91, 156). Interestingly, it was reported that Lal-/- mice present progressive loss of WAT and BAT with aging (92). LAL deficiency causes reduced BW (96) and circulating leptin levels in the fed state, persistent hypercholesterolemia and hypoglycemia. Nevertheless, Lal-/- mice have improved glucose tolerance and insulin sensitivity (93).

In mammals, BAT is responsible for nonshivering thermogenesis and thereby has an important role in maintaining temperature homeostasis, particularly during cold exposure. Compared to WAT, BAT is functionally and morphologically different by its multilocular appearance, abundance in mitochondria, high metabolic rate, and the presence of UCP1 (157, 158). UCP1 has a unique role by uncoupling mitochondrial respiration to produce heat instead of ATP and thereby supports thermogenesis in times of cold stress (159). Cold activates BAT via β3-AR triggering the utilization of FA and glucose as substrates for thermogenesis. To fuel this process, TG resources, stored in BAT cytosolic LD, are initially used via ATGL-, HSL- and MGL-mediated lipolysis (146, 160). As brown adipocytes have limited fat storage capacity, LD are continuously replenished by the supply of FA from the blood stream (146) through several inter-dependent processes. In a cold environment, food intake is robustly increased and delivers sufficient lipids in form of chylomicrons into the circulation (157). On the other hand, WAT serves as TG depot ready to release necessary FA in times of need, like nutrient restriction or high metabolic demand via ATGL-coordinated hydrolysis (161). Similarly, cold triggers WAT lipolysis (162, 163) resulting in release of FA, which are delivered to the liver, assembled in VLDL in form of TG and CE, and systemically secreted

(164, 165) to supply activated BAT with lipid substrates. In summary, three main sources supply the liver with FA: WAT, chylomicron remnants, and portal vein import from the intestine (166).

Excessive TRL concentrations in the blood cause dyslipidemia, a risk factor for atherosclerosis and a read-out of the metabolic syndrome (144, 163). New hope for hyperlipidemia treatment arose when it was shown that TRL are massively cleared by activated BAT (138). Intensive research in the last decade has revealed multiple benefits of BAT activation in correcting not only increases in blood TG but also cholesterol concentrations, improving glucose tolerance, insulin sensitivity, and decreasing fat depots (134, 137). Furthermore, enhancing BAT activity was reported to protect from atherosclerosis development by accelerating blood cholesterol clearance in mice expressing functional apolipoprotein E (ApoE) and LDL receptor (137). Interestingly, besides the canonical LPL-mediated lipolysis of TRL, Bartelt et al. could prove an alternative uptake of entire lipoproteins by BAT. This process is dependent on LPL-CD36 tandem actions and possibly mediated by increased endothelial permeability or transcytosis (138). The quantitative contribution of holoparticle uptake energy homeostasis and thermogenesis of BAT is still unclear (147). Moreover, this type of substrate processing would require lysosomal hydrolysis and, in terms of lipid breakdown, LAL.

Since LAL deficiency in mice causes WAT loss but intra-lysosomal lipid accumulation, we investigated in more detail the role of this enzyme with regard to BAT thermogenesis and its consequences on metabolic homeostasis. We provide evidence that LAL deficiency in mice leads to modified BAT morphology and defective thermogenesis. Lal-/- mice have abolished UCP1 protein expression and consequent hypothermia when housed at RT. Moreover, cold leads to severe hypothermia and exacerbates dyslipidemia in Lal-/- mice, suggesting that restoring blood lipoprotein balance depends on functional LAL both in normal and cold housing conditions (149).

3.2 Results

Lal-/- mice exhibit transient drops in energy expenditure correlated with hypothermic events in mice housed at RT

To investigate the effects of LAL deficiency on energy metabolism, we housed Lal-/- and WT mice in metabolic cages at RT and observed regular decreases in energy expenditure, which were most pronounced by fasting (Fig. 10A). Respiratory exchange rate (RER) was as well occasionally decreased (Fig. 10B). As energy expenditure is positively correlated with BAT oxygen consumption and therefore thermogenesis, we measured core body temperature at different time points of the day. In accordance with reduced energy expenditure, we found decreased body temperature in Lal-/- mice at the end of the active phase (Fig. 10C), hinting to altered BAT metabolism in Lal-/- mice. These mice exhibit reduced locomotor activity (Fig. 10D) and comparable food intake (Fig. 10E) indicative of a coordinated decrease in energy expenditure. These results imply that Lal-/- mice store their excess energy as fat and therefore would have increased BW. However, this is not the case since Lal-/- mice have reduced BW (Fig. 10F) and increased BW loss after fasting (Fig. 10G) (149).

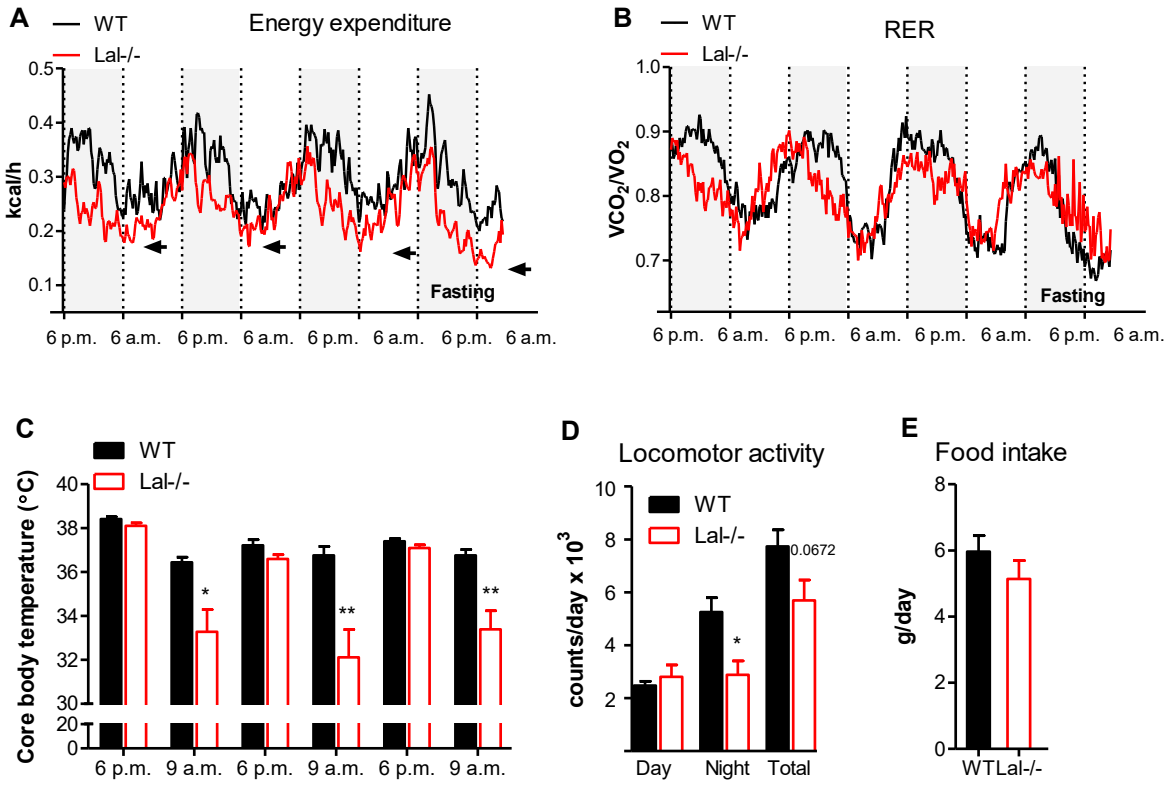

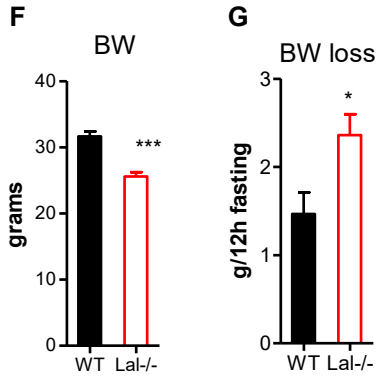

0: Decreased body temperature after the active phase in Lal-/- mice housed at RT. (A) Energy expenditure and (B) RER measured by indirect gas calorimetry in chow diet-fed male WT (black line) and Lal-/- mice (red line), housed at RT. Gray-shaded areas represent dark phase (6 p.m. - 6 a.m.); non-shaded, light phase (6 a.m. - 6 p.m.). Arrows represent transient drops of energy expenditure in Lal-/- mice. (C) Body temperature of WT and Lal-/- mice, measured in the fed state. (D) Daily locomotor activity, (E) daily food intake, (F) BW, and (G) BW loss after overnight fasting (n=5-9). Data represent means + SEM; $p < 0.05$ (*), $p \leq 0.01$ (**), $p \leq 0.001$ (***).–Student's unpaired t test (149). Requisite permission to use this figure was obtained (Appendix)

.

Altered brown adipocyte morphology but intact BAT mass in Lal-/- mice

It was previously reported that LAL deficiency in mice leads to progressive loss of BAT (92). However, we found no difference in BAT mass between Lal-/- mice and controls (Fig. 11A). We then performed electron microscopy imaging in BAT from 20 weeks old mice. Interestingly, Lal-/- BAT morphology was altered compared to the WT mice, with numerous small LD, abundant in mitochondria, and apparent accumulation of lysosomes (Fig. 11B). The mitochondria in BAT of Lal-/- mice were markedly increased in number and seemed to be in close contact to each other (Fig. 11B, C). Size distribution analysis revealed that small LD are predominant in the BAT of Lal-/- mice (Fig. 11D) with reduced total LD area (Fig. 11E) (149).

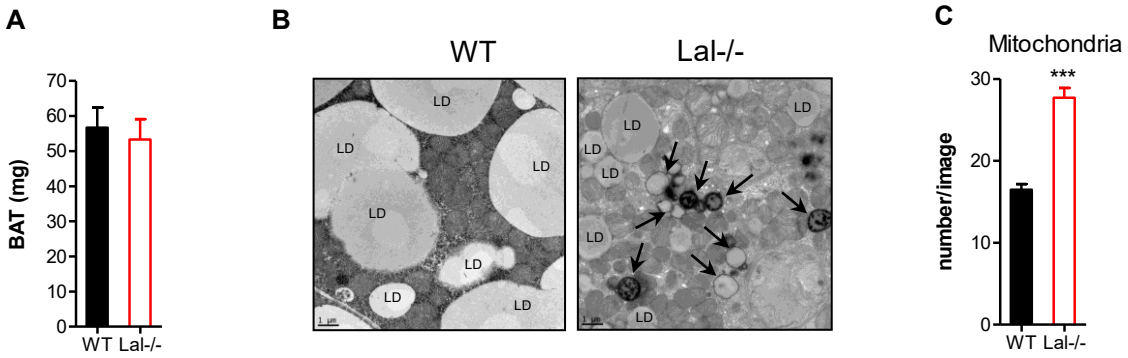

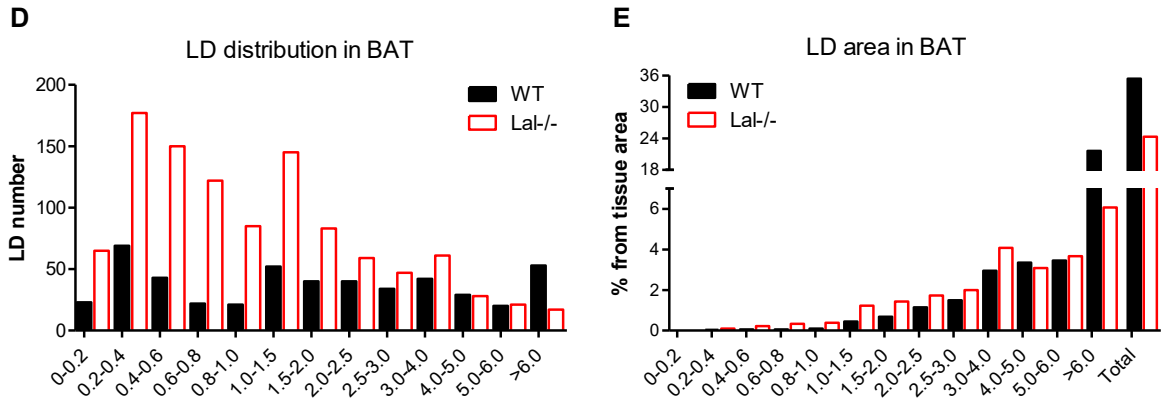

Figure 11: LAL deficiency causes modified BAT morphology in mice kept at RT

(A) BAT weights (n=3) and (B) representative electron micrographs of BAT from WT and Lal-/- mice housed at RT; scale bar, 1 µm; LD indicate cytosolic lipid droplets, arrows indicate lysosomes. (C) Average number of mitochondria from 97 electron micrographs of BAT, each measuring 142.09 μm^2. Cytosolic lipid droplet (D) distribution and (E) area in BAT of mice. Data represent means + SEM; $p \leq 0.001$ (***). Student's unpaired t test (149). Requisite permission to use this figure was obtained (Appendix).

We further investigated the *in vitro* effects on differentiation of iBACs following LAL pharmacological inhibition using Lalistat2, a potent and specific LAL inhibitor (51, 53). During 7 days of differentiation, we found no difference in intracellular neutral lipids when stained by ORO (Fig. 12A). In line, TG accumulation was similar in Lalistat2-treated and control cells in presence and absence of isoproterenol-stimulated lipolysis (Fig. 12B). Interestingly, in the basal state, LAL inhibition decreased release of FA (Fig. 12C). LAL inhibition and Lalistat2 specificity in cells were confirmed by reduced acid (Fig. 12D) and unchanged neutral lipolysis (Fig. 12E) activity in Lalistat2-treated cells compared to controls (149).

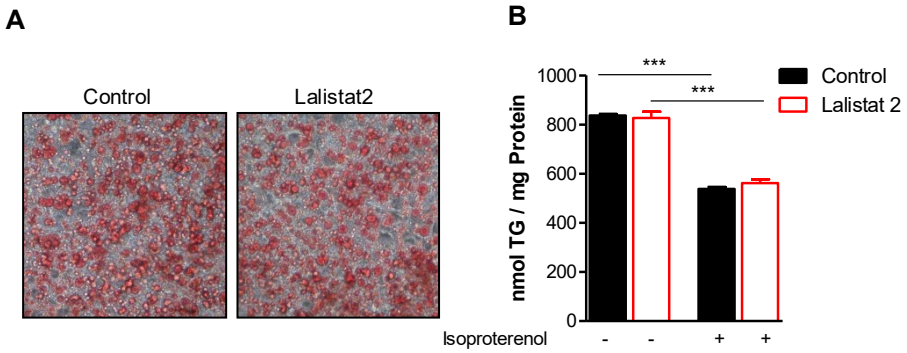

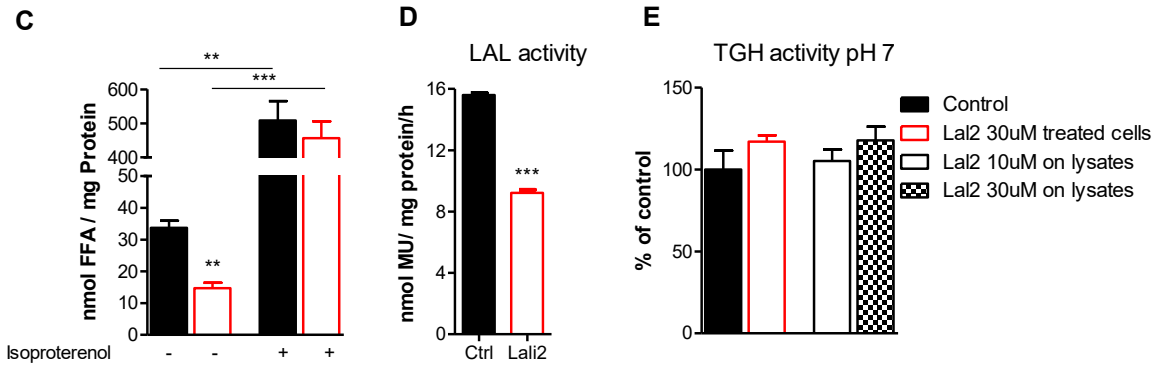

Figure 12: LAL inhibition *in vitro* does not affect differentiation into brown adipocyte

(A) Oil red O staining of mature iBACs (day 7 of differentiation) to visualize neutral lipids (200x). (B) TG content and (C) FFA release measured in mature iBACs in the basal state or after isoproterenol treatment. (D) LAL activity and (E) neutral TG hydrolase activity assays (n=3). Data represent means + SEM; $p \leq 0.01$ (**), $p \leq 0.001$ (***) (149). Requisite permission to use this figure was obtained (Appendix).

We and others published that Lal-/- mice progressively loose WAT depots (92, 93). Reduced WAT in Lal-/- mice may be a result of poor differentiation of precursor cells into white adipocytes. To test this hypothesis, we isolated SVC from Lal-/- and WT mice and differentiated them into white adipocytes. We observed that Lal-/- SVC cells differentiated similarly to the WT cells (Fig. 13A). Moreover, when analyzing Lal mRNA expression in WT cells, Lal gene was evenly expressed during all the differentiation days (Fig. 13B). These findings indicate that LAL is not required for neither brown nor white adipocyte differentiation (149).

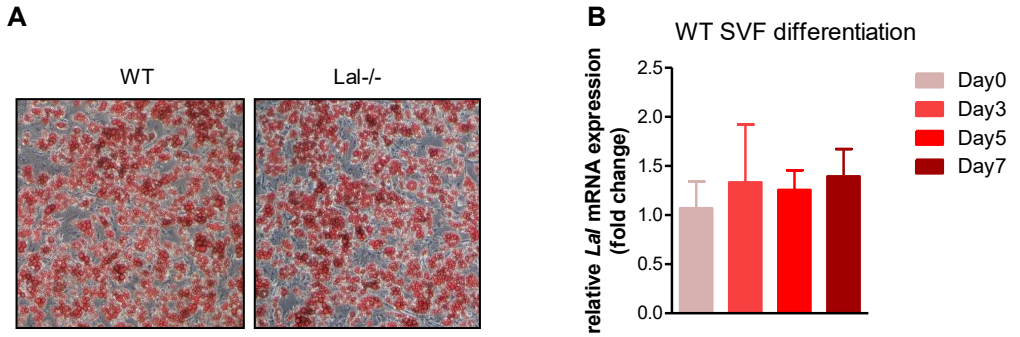

Fig. 13: LAL deficiency does not affect SVF differentiation into white adipocytes

(A) Oil red O staining of differentiated adipocytes to visualize neutral lipids (200x). (B) mRNA expression of LAL during SVF differentiation to white adipocytes relative to cyclophilin A expression as reference gene. Expression profiles were determined using the $2^{-\Delta\Delta Ct}$ method (n=3). Data represent means + SEM. Student's unpaired t test (149). Requisite permission to use this figure was obtained (Appendix).

UCP1 protein expression is reduced in the BAT of Lal-/- mice housed at RT

The ability of BAT to sustain thermogenesis is dependent on UCP1 protein expression and activity. Beside β3-AR stimulation, FA are important activators of UCP1-mediated heat generation in BAT (131). Lal-/- mice demonstrated decreased core body temperature events at RT and, correspondingly, UCP1 protein expression was markedly decreased in the BAT of Lal-/- mice (Fig. 14A). TG hydrolase activity at neutral pH was decreased by 70% in BAT of Lal-/- mice (Fig. 14B), suggesting poor hydrolysis of LD-originated TG. Furthermore, in the randomly fed state, Lal-/- mice have decreased plasma free FA (Fig. 14C), free glycerol (Fig. 14D), and blood glucose (Fig. 14E) concentrations. Additionally, circulating TG tended to be as well reduced (Fig. 14F). These data suggest that decreased BAT thermogenesis and hypothermia in Lal-/- mice might be due to abolished UCP1 protein expression and substrate mobilization. By correlating the previously published data reporting that UCP1 expression is negatively affected by inflammation (167, 168) with the well described pro-inflammatory phenotype of Lal-/- mice (94, 95, 169) we analyzed mRNA expression of inflammatory markers in BAT. In agreement, we found increased expression of macrophage (Emr1) and inflammatory markers (Il-1β, Tnf-α) in BAT of Lal-/- mice already at the age of 7 weeks (Fig. 14G) (149).

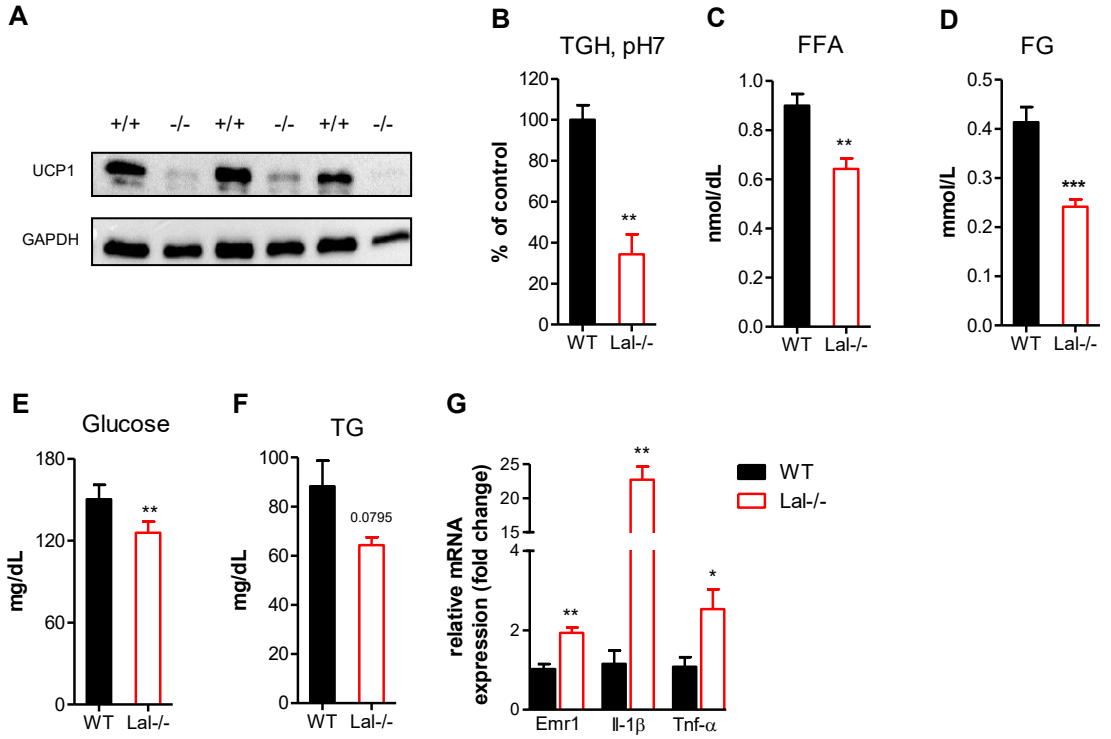

Figure 14: Lal-/- mice housed at RT have reduced UCP1 protein expression and neutral triglyceride hydrolase activity in BAT

(A) Immunoblotting against UCP1 and (B) neutral TG hydrolase activity in BAT of 20 weeks old mice (n=3). (C) Plasma free fatty acids, (D) free glycerol, (E) blood glucose and (F) TG concentrations in the fed state (n=6). (G) mRNA expression of inflammation markers in BAT from 7 weeks old mice, relative to cyclophilin A expression as reference gene. Expression profiles were determined using the $2^{-\Delta\Delta Ct}$ method (n=4). Data represent means + SEM; $p < 0.05$ (*), $p \leq 0.01$ (**), $p \leq 0.001$ (***). Student's unpaired t test (149). Requisite permission to use this figure was obtained (Appendix).

Lal-/- mice suffer from severe hypothermia under cold conditions

We then housed the mice at 4°C (food and water ad libitum) and observed a striking drop in core body temperature in Lal-/- mice after only 4 h of cold-exposure (Fig. 15A). Next, we checked the mRNA expression of several genes involved in BAT activation upon a cold stimulus. BAT from Lal-/- mice revealed upregulation of Pparγ and its coactivator Pgc1α and a trend to increased Prdm16 gene expression. Despite unchanged Ucp1 mRNA expression (Fig. 15B) these results suggest rather an accelerated activation signal in the brown adipocytes of Lal-/- mice. As fuel replenishment in form of lipids is critical for maintaining optimal BAT function (146), we checked genes involved in autophagy, lysosomal activity, and LD hydrolysis. We found upregulated Atg7 mRNA, indicating increased autophagy. In addition, the lysosomal master regulator Tfeb, the lysosomal membrane associated proteins (Lamp1, Lamp2), and the cytosolic TG lipases Atgl and Hsl were also upregulated in BAT of Lal-/- mice (Fig. 15C). UCP1 protein expression was unchanged between the genotypes, whereas LC3I-II protein was markedly increased in Lal-/- mice (Fig. 15D). In line, increased TG hydrolase activity at neutral pH indicates that cold-exposed BAT of Lal-/- mice strives to utilize lipid substrates to sustain thermoregulation (Fig. 15E). Plasma FFA as well as mRNA expression of the main FA transporters in BAT were comparable between both groups (Fig. 15F, G), suggesting that FA transport into BAT is not impaired and should provide sufficient FA to fuel thermogenesis and activate UCP1 (170). Despite upregulation of the processes to generate more lipid substrates for heat production, Lal-/- mice cannot survive cold challenge, pointing out a critical role for LAL in providing FA for BAT thermogenesis (149).

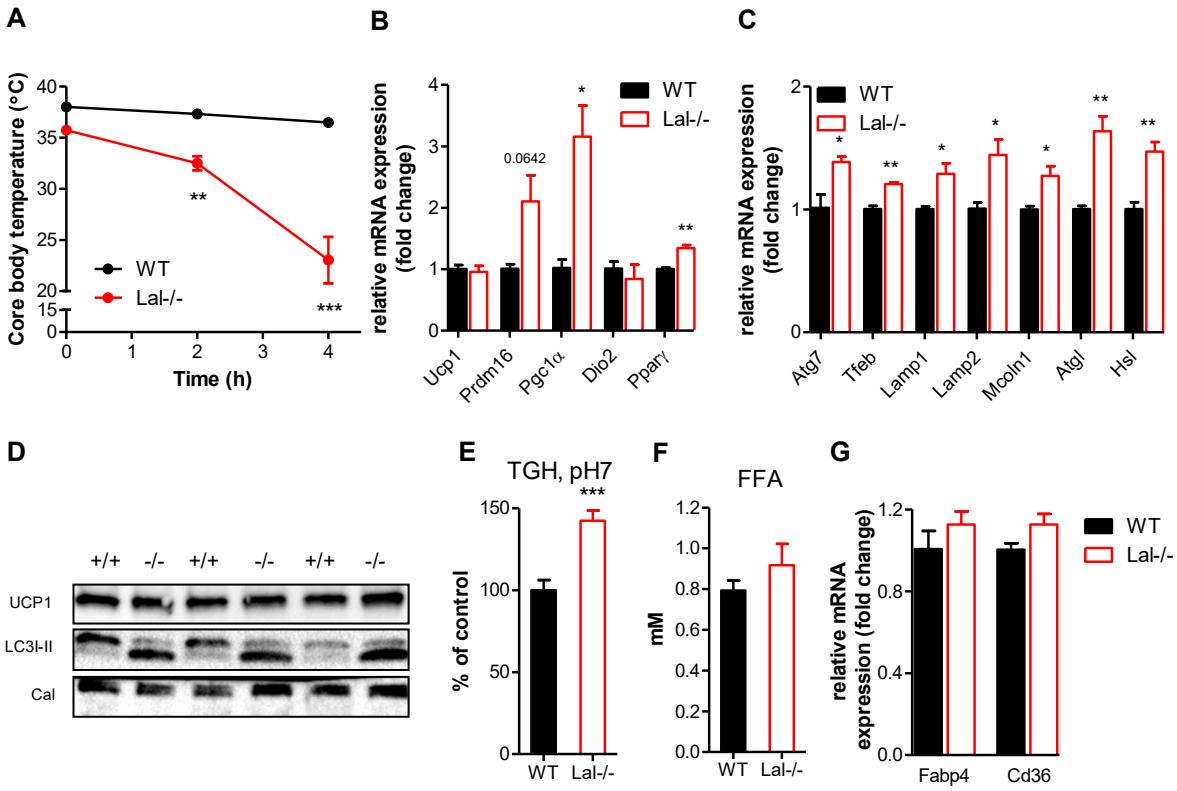

Figure 15: Lal-/- mice are cold intolerant despite comparable UCP1 expression and increased neutral lipolysis and autophagy in BAT. Lal-/- and WT mice on chow diet were acutely exposed to 5°C with free access to food and water. (A) Body temperature curves of WT and Lal-/- mice acutely exposed to 5°C (n=6). mRNA expression of genes involved in (B) thermoregulation and (C) autophagy/lysosomal activity and neutral lipolysis in BAT, relative to cyclophilin A expression as reference gene. Expression profiles were determined using the $2^{-\Delta\Delta Ct}$ method (n=3). (D) Immunoblotting against UCP1 and LC3-I/II in BAT using calnexin as loading control. (E) Neutral TG hydrolase activity in BAT (n=5-7). (F) Plasma free fatty acid concentrations (n=6). (G) mRNA expression of genes involved in FA uptake relative to cyclophilin A expression as reference gene. Expression profiles were determined using the $2^{-\Delta\Delta Ct}$ method (n=3-4). Data represent means ± SEM; $p < 0.05$ (*), $p \leq 0.01$ (**), $p \leq 0.001$ (***). (A) ANOVA; (B, C, E, F, G) Student's unpaired t test (149). Requisite permission to use this figure was obtained (Appendix).

To support heat production in a cold environment, heart function is important for providing BAT with necessary nutrients and oxygen via increased blood flow (120). Lipid accumulation due to loss of neutral TG hydrolase activity affects the contractility and plasticity of the cardiac muscle in mice (171). Visually, Lal-/- mice have normal heart phenotype , but we did not exclude the possibility of major modifications at cellular levels, which may lead to cardiac dysfunction. We therefore analyzed cardiac muscle morphology of mice kept at RT using electron microscopy. The heart muscle histomorphology was grossly unchanged in Lal -/-

mice, with no accumulation of LD and normal size and structure of mitochondria. The sarcomere structure looked similar in both genotypes. In some areas, cadiomyocytes from Lal-/- mice had sporadic clusters of lysosomes, which was not the case in WT mice. We observed few lipid-laden macrophages in the cardiac muscle of Lal-/- mice. These lipids appear to be entrapped in lysosomes (Fig. 16).

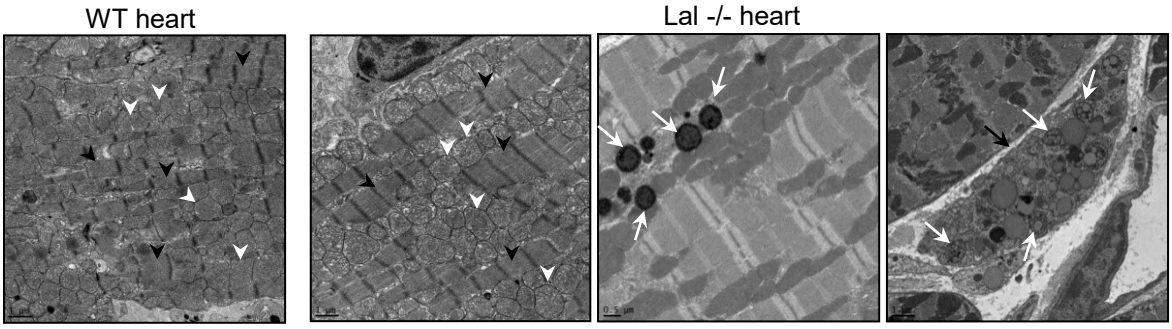

Figure 16: LAL deficiency does not cause lipid accumulation in cardiac muscle. Transmission electron micrographs of cardiac muscle sections from WT and Lal-/- mice housed at RT. White arrow heads indicate mitochondria; black arrow heads indicate sarcomere; white arrows indicate lysosomes; black arrow indicates a lipid laden macrophage in the cardiac muscle of Lal-/- mice.

LAL deficiency in cold-exposed mice leads to decreased acetyl-CoA and increased acyl-carnitine concentrations in BAT

During cold challenge, Lal-/- mice activate both energetic and thermogenic machineries yet facing severe hypothermia. To visualize LD and lysosomes in BAT, we performed immunofluorescence staining using perilipin 1 (LD membrane protein) as LD marker and cathepsin D (a lysosomal protease) to track lysosomes. In sharp contrast to controls, BAT of cold-exposed Lal-/- mice had reduced cytosolic LD size. Unlike in BAT from WT mice, where cathepsin D signals were diffused and less pronounced, the presence of abundant ring-like structures positive for cathepsin D in the Lal-/- mice indicated lipid-laden lysosomes in BAT (Fig. 17A) (149).

To determine if FA from intracellular TG hydrolysis or taken up by external lipoprotein lipolysis are effectively shuttled to the mitochondria, we analyzed acyl-CoA and acyl-carnitine levels in BAT from cold-exposed mice. Interestingly, acetyl-CoA concentrations were decreased in Lal-/- mice, indicating an energy deficiency in BAT. Individual acyl-CoAs were either decreased or increased in BAT from Lal-/- mice, whereas total acyl-CoA species were similar between both genotypes (Fig.

17B). Conversely, acyl-carnitines were overall increased (Fig. 17C) in BAT from cold-exposed Lal-/- mice. To decipher if this is a result of accelerated binding to carnitine or an accumulation of carnitine esters due to impaired mitochondrial transport/processing, we analyzed the mRNA expression of several genes involved in these pathways. Increased Cpt1b gene, responsible for transferring the CoA-bound FA to carnitine, indicates increased trafficking of acyl-carnitines. Furthermore, no defect in carnitine esters processing was detected in Lal-/- mice (Fig. 17D), as mRNA expression levels of Cpt2, Cact, Lcad, and Vlcad were unchanged. Overall these findings suggest that the decrease in acetyl-CoA concentration is not due to poor mitochondrial FA shuttling, but rather due to increased energy demand and/or defective respiration (149).

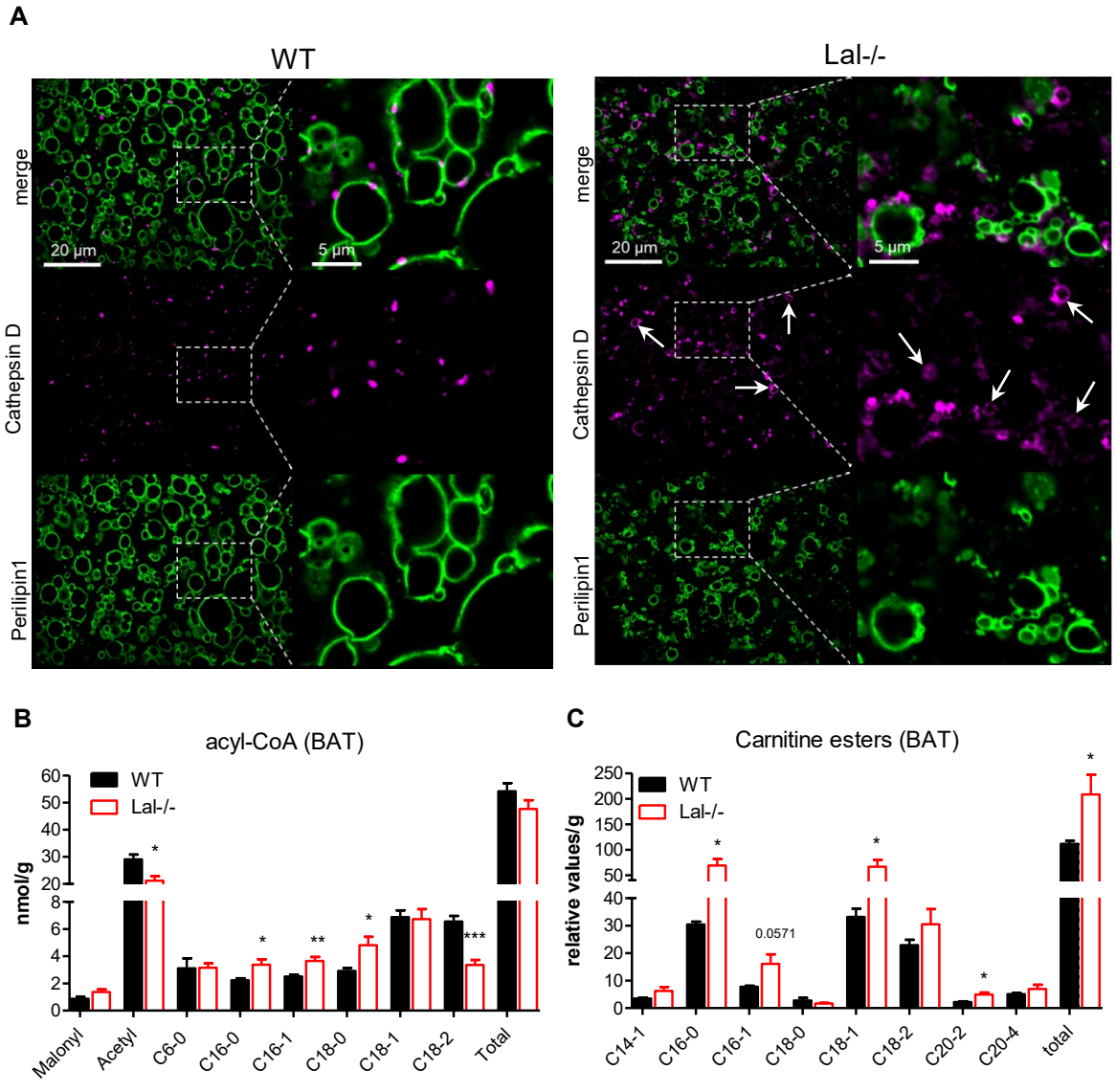

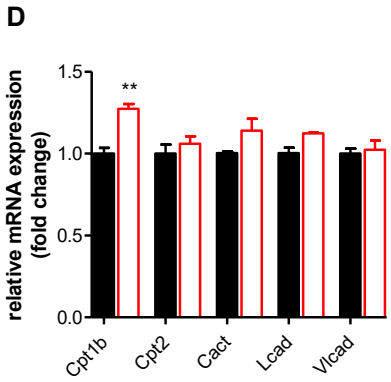

Figure 17: Acute cold exposure triggers increased acyl-carnitine generation in the BAT of Lal-/- mice. (A) Representative immunofluorescence micrographs of BAT using perilipin 1 as LD marker and cathepsin D as lysosomal marker. (B) Long-chain acyl-CoA and (C) carnitine ester concentrations were determined in BAT of Lal-/- and WT mice (n=4-5). (D) mRNA expression of genes involved in FA mitochondrial trafficking and oxidation, relative to cyclophilin A expression as reference gene. Expression profiles were determined using the $2^{-\Delta\Delta Ct}$ method (n=3). Data represent means + SEM; $p < 0.05$ (*), $p \leq 0.01$ (**), $p \leq 0.001$ (***). Student's unpaired t test (149). Requisite permission to use this figure was obtained (Appendix).

Lal-/- mice have decreased oxygen consumption in BAT upon cold exposure

Besides lipids, glucose serves as important substrate for heat generation, and cold exposure triggers massive glucose uptake in BAT (139). Cold exposure did not but lead to severe decrease in blood glucose (Fig. 18A) in Lal-/- mice. Therefore, we hypothesized that glucose may be crucial in maintaining temperature homeostasis in Lal-/- mice. Indeed, both basal and uncoupled (FCCP) BAT oxygen consumption rates were decreased in the presence of respiration medium with low glucose concentration (100 mg/ml) only in the Lal-/- mice, but not in their WT controls (Fig. 18B). Furthermore, high glucose respiration medium normalized oxygen consumption in the BAT of Lal-/- mice (Fig. 18C). To assess if glucose supplementation has the same effects *in vivo*, we injected the mice with a single dose of 2 g/kg glucose i.p. before the cold exposure, still providing unlimited access to food. Surprisingly, Lal-/- mice entered hypothermia within 4 h of cold exposure (Fig. 18D). Blood glucose levels, measured after 2 h in cold, were increased compared to the basal state and slightly decreased compared to WT mice, reaching 170 mg/ml (Fig. 18E). Since the concentrations we used for the high glucose respiration conditions are supra-physiological (450 mg/ml), we conclude that normal glucose levels cannot support the deficit in energy demand of cold-exposed Lal-/- mice (149).

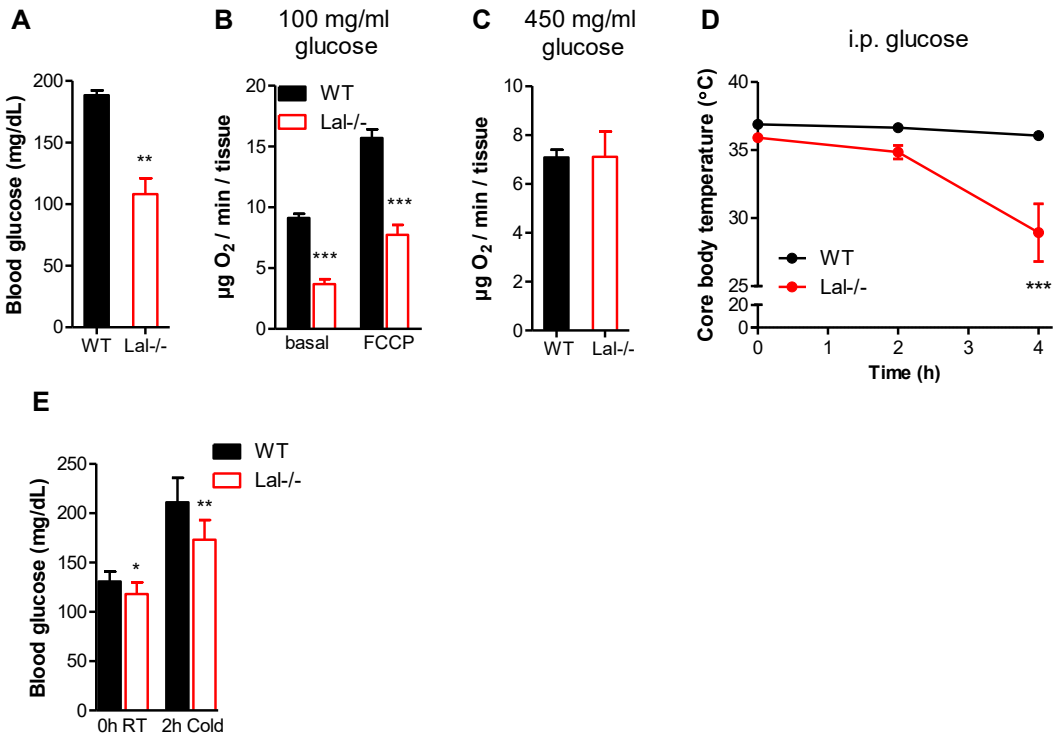

Figure 18: Cold exposure causes hypoglycemia and decreased oxygen consumption in the BAT of Lal-/- mice. (A) Blood glucose concentrations after 4 h of cold exposure. BAT oxygen consumption in respiration buffer containing (B) 100 mg/ml or (C) 450 mg/ml glucose. (D) Core body temperature curve of cold exposed mice pre-injected i.p. with glucose 2 g/kg. (E) Glycemia at RT before i.p glucose injection and 2 h after glucose injection in mice housed at 4°C (cold) (n=5-6). Data represent means + SEM; $p < 0.05$ (*), $p \leq 0.01$ (**), $p \leq 0.001$ (***). Student's unpaired t test (149). Requisite permission to use this figure was obtained (Appendix).

Cold triggers increased glucose uptake in the BAT of Lal-/- mice

The inability of Lal-/- mice to improve cold tolerance in the presence of glucose may be caused by the defective uptake of glucose in target organs as BAT and muscle. To clarify this, we performed [^{3}H]2-deoxy-D-glucose uptake in cold-exposed mice. As expected, radioactivity accumulation was increased in BAT of Lal-/- mice and SM (gastrocnemius, GN) showed the same trend. Glucose uptake by inguinal WAT (ingWAT), liver and small intestine (SI) was similar between genotypes (Fig. 19A). Plasma glucose clearance was comparable to WT mice (Fig. 19B). Cold exposure-mediated glucose uptake in BAT is mainly executed by GLUT 1 transporter (140). In line with increased glucose incorporation by the BAT of Lal-/- mice, we found increased mRNA expression of Glut1 (Fig. 19C) and increased AKT phosphorylation (Fig. 19D), hinting toward an additive regulation of glucose uptake mechanisms. Moreover, these findings demonstrated that glucose

plays a secondary role in BAT and glucose supplementation in a lipid-defective metabolism cannot fully support thermogenesis in Lal-/- mice (149).

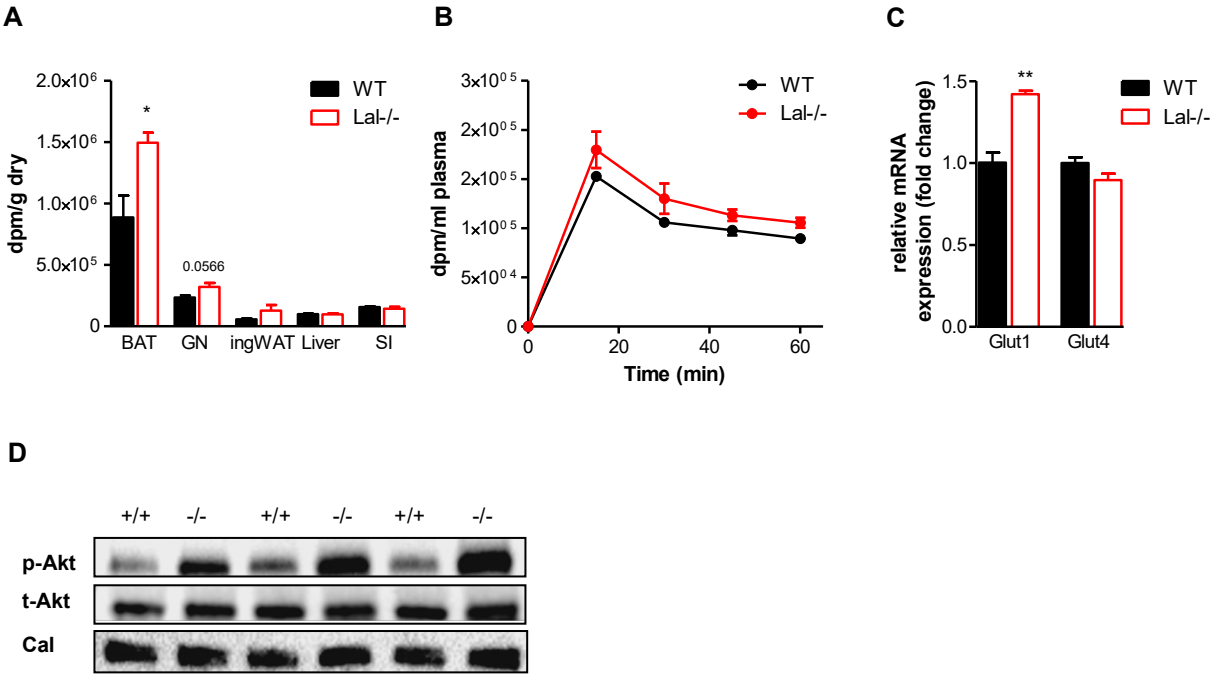

Figure 19: Increased glucose uptake in BAT of Lal-/- mice during cold exposure. (A) Radioactivity in tissues and (B) plasma of mice (n=4) after i.p. injection of [^{3}H]2-deoxy-D-glucose. (C) mRNA expression of glucose transporters in BAT, relative to cyclophilin A expression as reference gene. Expression profiles were determined using the $2^{-\Delta\Delta Ct}$ method (n=3). (D) Immunoblotting against phosphorylated AKT and total AKT in BAT with calnexin as loading control. Data represent means ± SEM; $p < 0.05$ (*), $p \leq 0.01$ (**). Student's unpaired t test (149). Requisite permission to use this figure was obtained (Appendix).

Increased shivering in Lal-/- mice during cold exposure

The increase in glucose uptake in SM of cold-exposed Lal-/- mice indicated increased metabolic activity. To investigate FA-originated fuel, we measured acyl-CoA and carnitine esters in SM. We observed a major reduction in individual and total CoA-bound FA (Fig. 20A), which implies an intensified usage of lipids to support shivering. Carnitine esters followed the opposite direction, with increases in sole and total species (Fig. 20B). The genes involved in regulating acyl-carnitines transport and processing were unaltered at mRNA level. Furthermore, the mRNA expression of muscle proteolysis markers revealed upregulated Murf1 and Atrogin1 in Lal-/- mice (Fig. 20C). Plasma creatine phosphokinase activity was markedly increased by cold in Lal-/- mice (Fig. 20D). These data confirm that, during cold exposure, Lal-/- mice use SM for two purposes: i) additional source of

energy in the form of amino acids from proteolysis and ii) shivering to maintain temperature homeostasis (149).

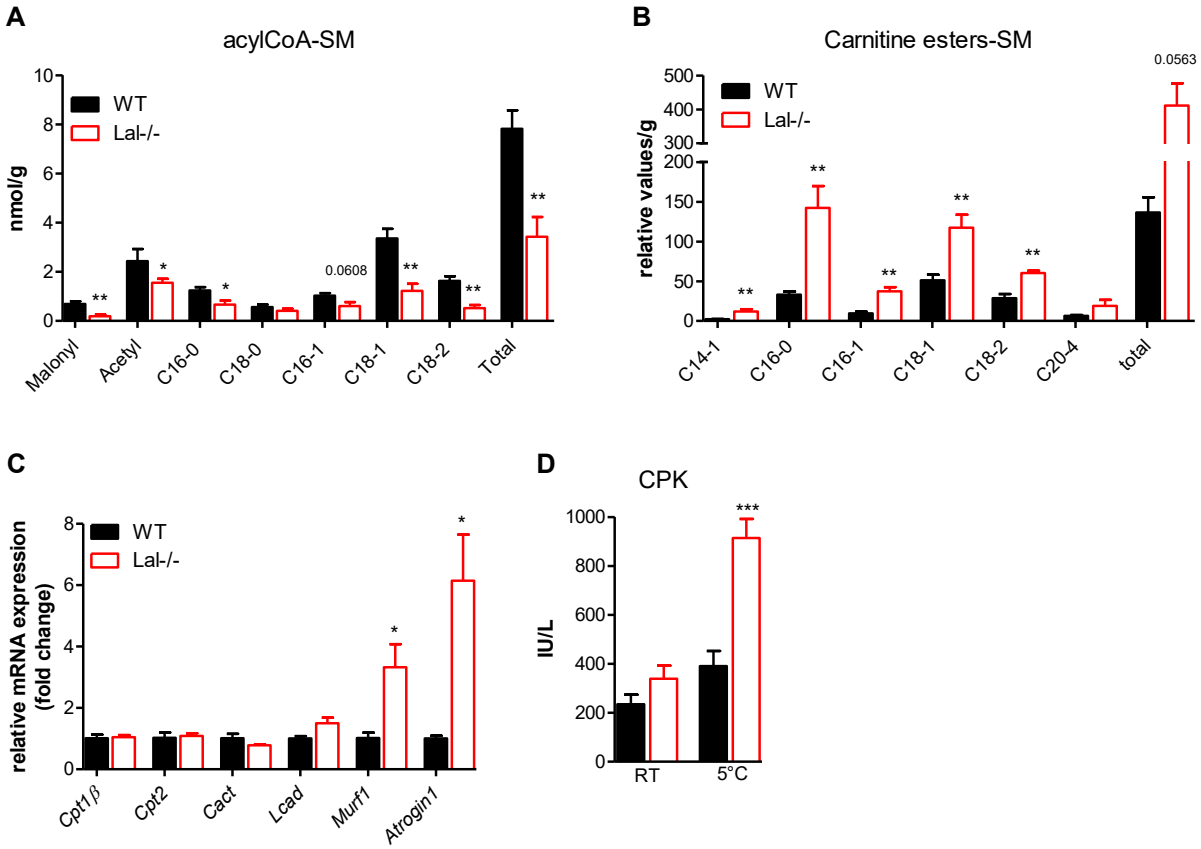

Figure 20: Proteolysis and shivering are intensified in Lal-/- mice during cold. (A) Long chain acyl-CoA and (B) carnitine ester concentrations in SM (n=3-5). (C) mRNA expression of genes involved in FA mitochondrial trafficking and oxidation and muscle damage, relative to cyclophilin A expression as reference gene. Expression profiles were determined using the $2^{-\Delta\Delta Ct}$ method (n=3). (D) Plasma creatine phosphokinase (CPK) activity. Data represent means + SEM; $p < 0.05$ (*), $p \leq 0.01$ (**), $p \leq 0.001$ (***). Student's unpaired t test (149). Requisite permission to use this figure was obtained (Appendix).

Lipid lowering by cold exposure is dependent on functional LAL

It was previously reported that cold exposure normalized dyslipidemia in rodents (137, 138). Moreover, our group showed that Lal-/- mice have increased plasma cholesterol and normal TG concentrations in the fed state (93). We therefore expected that cold might improve the observed hypercholesterolemia in Lal-/- mice. Unexpectedly, after cold exposure, cholesterol and TG concentrations were increased (Fig. 21A), whereas free glycerol was decreased in Lal-/- mice (Fig. 21B) suggesting a defect in lipid clearance. Lipoprotein profiling after fast protein liquid chromatography separation revealed disturbed lipoprotein distribution of

both TC and TG with increased LDL and decreased HDL fractions in pooled plasma of Lal-/- mice (Fig. 21C, D). Angiopoietin-like 4 protein is highly expressed in BAT and is a powerful LPL inhibitor, having a major role in the regulation of circulating TG during cold exposure (172). Although LPL mRNA expression was unchanged, Angptl4 transcript was 3-fold upregulated in BAT of Lal-/- mice (Fig. 21E). To assess if lipids are not taken up by BAT in Lal-/- mice, we gavaged cold-exposed mice with oil prior to organ collection and found impaired lipid uptake in BAT of Lal-/- mice (Fig. 21F). To quantify the extent to which lipid uptake is reduced in the BAT of cold-exposed Lal-/- mice, we performed the same experiment by gavaging the mice with [^{3}H]triolein. In accordance with the results from the micrographs, we found a profound reduction (85%) in radioactivity in the BAT of Lal-/- mice compared to controls (Fig. 21G). Thus, LAL deficiency in mice did not normalize, but further aggravated dyslipidemia upon cold exposure, indicating a possible role for LAL as a regulator of Angptl4 expression and, subsequently, LPL activity (149).

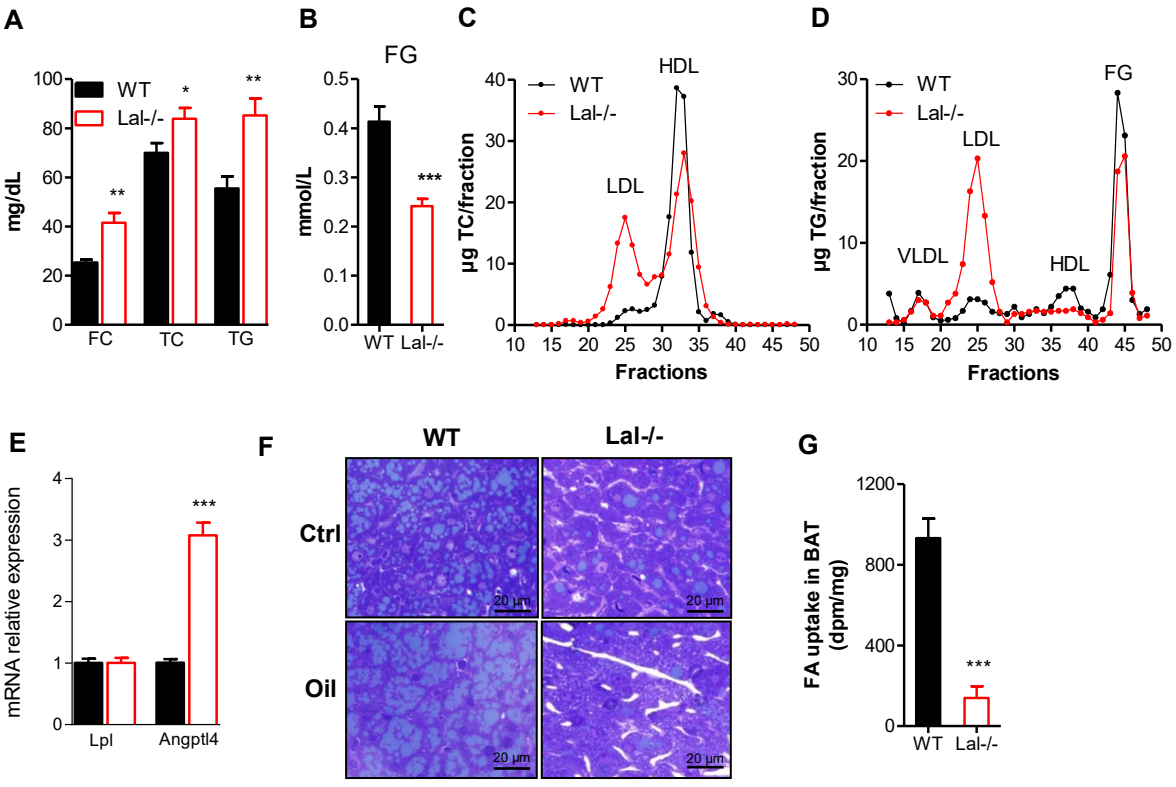

Figure 21: Cold exacerbates dyslipidemia in Lal-/- mice. (A) Plasma lipid parameters and (B) free glycerol concentrations after cold exposure (n=6-8). Lipoprotein profiles of (C) TC and (D) TG after separation by fast performance liquid chromatography of pooled plasma (n=6-8). (E) mRNA expression of lipoprotein lipase (Lpl) and angiopoietin-like 4 (Angptl4) in BAT, relative to cyclophilin

A expression as reference gene. Expression profiles were determined using the $2^{-\Delta\Delta Ct}$ method (n=3). (F) Chow diet-fed WT and Lal-/- female mice were exposed to cold with or without an additional corn oil gavage (100 µl). Representative micrographs of toluidine blue-stained BAT; magnification, 40x; scale bar, 20 µm. (G) FA uptake in BAT of cold-exposed female mice. Data represent means + SEM; $p < 0.05$ (*), $p \leq 0.01$ (**), $p \leq 0.001$ (***). Student's unpaired t test (149). Requisite permission to use this figure was obtained (Appendix).

Lal-/- mice have decreased oxidation of fat and carbohydrates during gradual cooling

Direct exposure to 5°C proved to be life threatening in the context of LAL deficiency, and additional stress by housing the mice in metabolic cages was impossible. We therefore decided to gradually decrease ambient temperature and monitored the mice in this setup. Although all mice survived 7 days, Lal-/- mice visibly deteriorated and two of them died shortly after day 7. Indirect calorimetry measurements showed a decrease in RER, indicating predominantly lipid usage and an obvious shift to the light-phase, while WT mice preserved normal RER and circadian-regulated rhythm (Fig. 22A). Detailed substrate oxidation revealed markedly decreased carbohydrate and lipid catabolism during the active night phase (Fig. 22B, C). Even striking was the decrease in energy expenditure of Lal-/- mice (Fig. 22D, E), accompanied by a more than 40% reduction in locomotor activity (Fig. 22F). Body temperature measured at day 3 and 7 of the cooling period was decreased (Fig. 22G). Unlike WT mice, which gained weight during the experiment, Lal-/- mice lost on average 1.5 grams BW(Fig. 22H) despite increased food intake (Fig. 22I) (149).

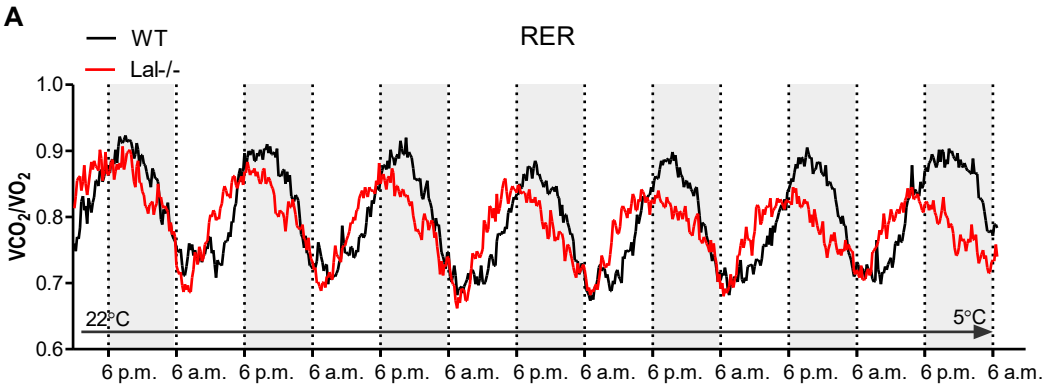

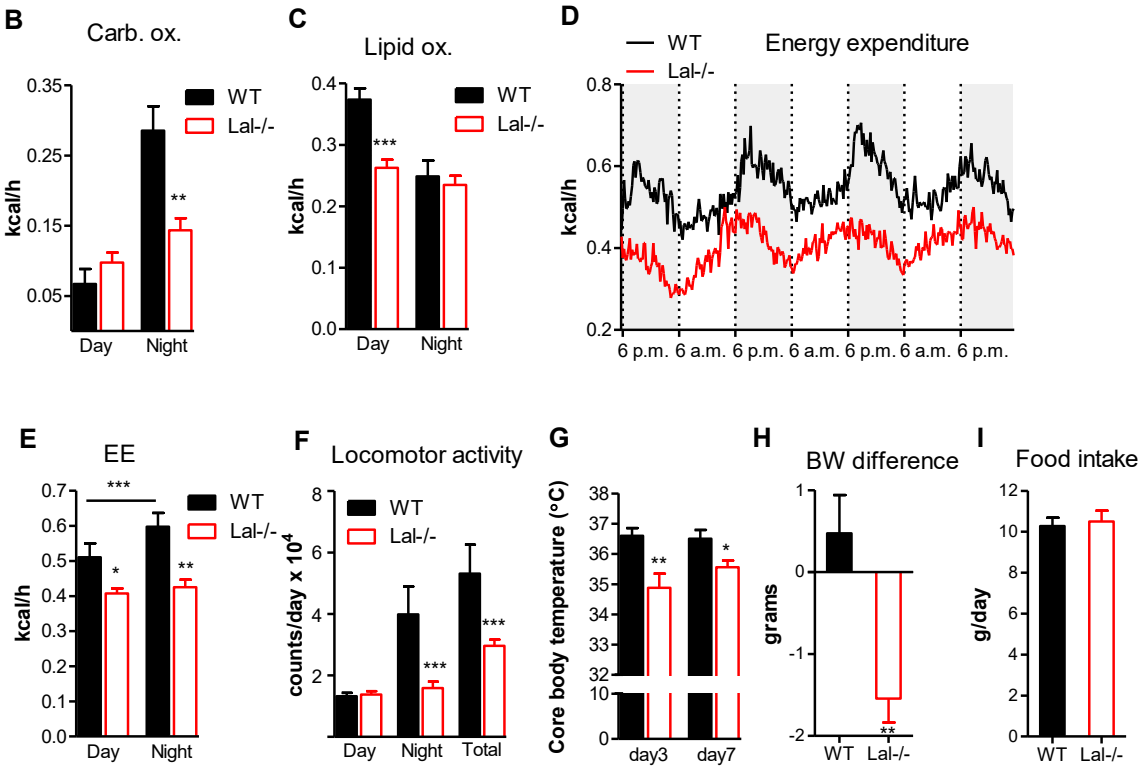

Figure 22: During gradual cooling, Lal-/- have decreased energy expenditure and substrate oxidation. Female WT and Lal-/- mice were housed in metabolic cages and ambient temperature was gradually decreased from RT to 5°C over a period of 7 days. (A) Respiratory exchange rate (RER). Gray-shaded areas represent dark phase (6 p.m. - 6 a.m.); non-shaded, light phase (6 a.m. - 6 p.m.). Quantification of (B) carbohydrate and (C) lipid oxidation. Energy expenditure (D) curves and (E) average values. (F) Daily locomotor activity. (G) Body temperature measured during the cooling period. (H) BWdifference and (I) daily food intake at the end of the cooling period (n=5-6). Data represent means + SEM; $p < 0.05$ (*), $p \leq 0.01$ (**), $p \leq 0.001$ (***). Student's unpaired t test; (E) Repeated measurements for same genotype, Student's paired t test (149). Requisite permission to use this figure was obtained (Appendix).

Age does not influence cold tolerance in Lal-/- mice

To rule out the age-dependent BAT dysfunction, we also analyzed BAT morphology in 6 weeks old mice and found milder differences when comparing Lal-/- and WT mice (Fig. 23A). Lal-/- mice had increased number of large LD (Fig. 23B) and total lipid surface (Fig. 23C). In addition, BAT already showed lysosomes accumulating lipids but mitochondria with a normal ultrastructure and cristae morphology. As Lal-/- mice have been described to have a progressive phenotype, we expected young mice to be less cold sensitive than aged mice. Surprisingly, 6 weeks old mice entered hypothermia after 3 h in cold (Fig. 23D), confirming that cold sensitivity is a constant feature of Lal-/- mice. Overall, our data prove that

lysosomal lipid hydrolysis provides crucial substrates for thermogenesis, irrespective of the cytosolic LD pool in BAT (149).

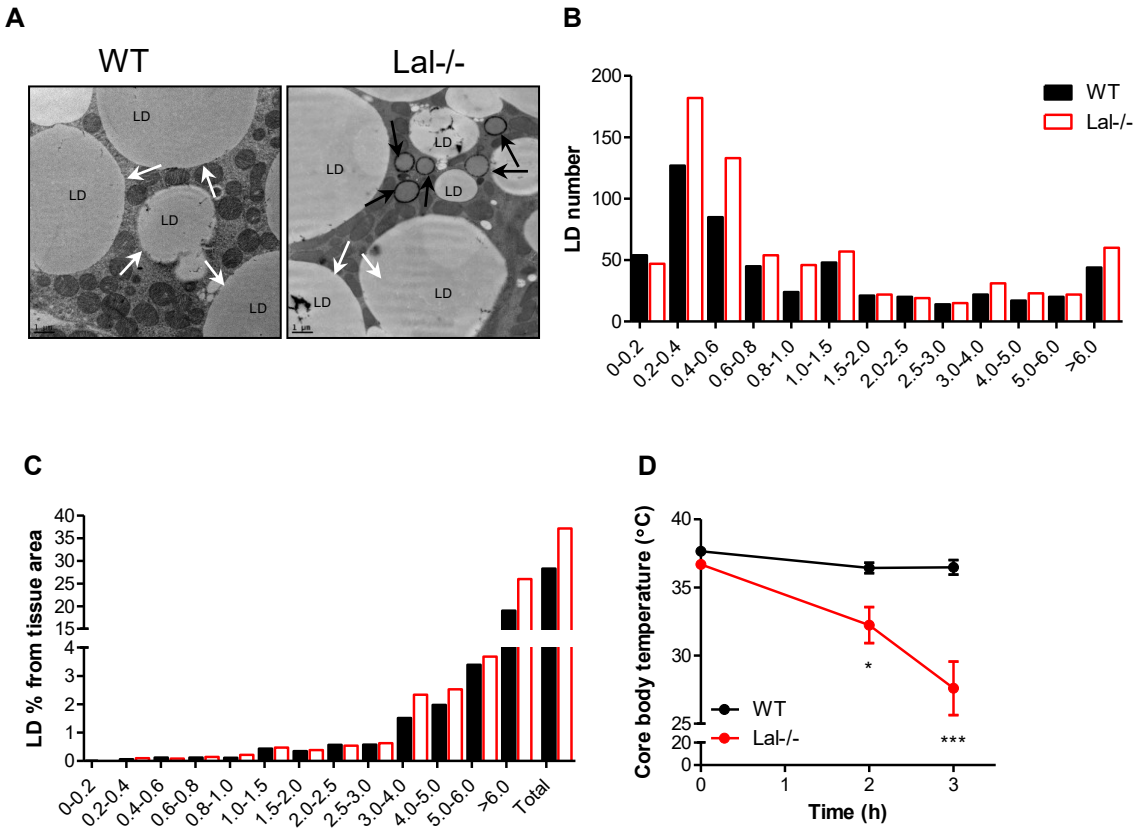

Figure 23: LAL deficiency causes modified BAT morphology in young mice. (A) Representative electron micrographs of BAT from 6 weeks old WT and Lal-/- mice housed RT; scale bar, 1 µm; White arrows indicate the phospholipid monolayer of cytosolic lipid droplets (LD), black arrows indicate electron-dense double membranes of lysosomes. (B) Cytosolic LD distribution and (C) surface in BAT of mice. (D) Body temperature curves of 6 weeks old WT and Lal-/- mice exposed to 5°C (n=5-6). Data represent means ± SEM; $p < 0.05$ (*), $p \leq 0.001$ (***). (D) ANOVA (149). Requisite permission to use this figure was obtained (Appendix).

3.3 Discussion

LAL is, to date, the only known enzyme to hydrolyze CE and TG within lysosomes to release FA and FC for catabolic, anabolic, and signaling purposes (1). LAL deficiency causes major metabolic disturbances in both humans and mice, which include hepatomegaly, shortened life span, and hypercholesterolemia (93). Thus, Lal-/- mice provide an intriguing opportunity to study the effects of LAL deficiency on the molecular level. The only targeted pharmacological treatment in LAL-D patients is the administration of recombinant LAL (82). However, the molecular complexities in these LAL-D patients including thermogenesis are still underexplored.

Lal-/- mice have been described to progressively lose WAT and BAT with aging (92). To our surprise, although WAT is decreased in Lal-/- mice, interscapular BAT as well as subscapular BAT depots were intact in our mice, at least until 20 weeks of age. A peculiarity observed in Lal-/- mice was decreased energy expenditure, reduced oxygen consumption and locomotor activity, but similar food intake. This metabolic discrepancy partly explains the regular drops in body temperature after the active phase observed in Lal-/- mice. In theory, these features should lead to increased fat/BW, which is, however, not the case, hinting toward an ineffective nutrient usage in Lal-/- mice. In line with our observations, massive lipid accumulations in liver, intestine, and spleen entrapping TG and CE have been reported in Lal-/- mice (92). Alterations in lipid metabolism seem to affect thermogenesis, as the ability of BAT to sustain thermogenesis is insufficient both at RT and cold conditions in Lal-/- mice. UCP1 expression was almost absent in Lal-/- mice housed at RT, supporting the idea that LAL hydrolysis products may play a role in UCP1 protein regulation independent of the β3 adrenergic stimulatory cascade. It was also reported that increased inflammation hampers UCP1 expression (167, 168) and it is well established that LAL deficiency causes a severe inflammatory status in mice (94) due to proliferation and infiltration of macrophages into various organs. Thus, more than one plausible explanation exists for the blunted UCP1 expression observed in BAT of Lal-/- mice. However, since UCP1 expression is restored in cold-exposed Lal-/- mice, inflammation might not be a causal factor of BAT dysfunction (149).

Lal-/- mice exhibit modified ultrastructural BAT morphology, but, during cold exposure, they can activate catabolic pathways necessary for heat production both from intracellular and external sources. UCP1 protein expression was normalized, several genes involved in BAT activation were upregulated, and concentrations of acyl-carnitines, acetyl-CoA and acyl-CoA, were altered in cold-exposed Lal-/- mice. FA trafficking to mitochondria was accelerated as shown by increased Cpt1b mRNA expression and its downstream product acyl-carnitine. On the other hand, acetyl-CoA, the end product of FA oxidation and an important fuel for mitochondrial respiration, was decreased in Lal-/- mice, which may hinder oxygen consumption in the BAT of cold-exposed Lal-/- mice. Furthermore, the reduced acyl-CoA concentrations may be caused by hypoglycemia and/or decreased FA availability and eventually lead to increased autophagy as indicated by the upregulation of autophagy markers in Lal-/- mice. In *ex vivo* studies, the use of supra-physiological levels of glucose in the high glucose concentration medium (450 mg/dl) normalized respiration in the BAT explant from Lal-/- mice. Interestingly, low glucose conditions (100 mg/dl) did not impair respiration in WT mice, confirming that (compared to physiological glucose levels) lipids are the preferred substrate for heat production in BAT. To determine if additional glucose can support thermogenesis *in vivo* in our mouse model, we administered the mice with 2 g/kg i.p. glucose in the presence of food. Lal-/- mice, however, were still severely hypothermic after 4 h in the cold. Although blood glucose levels rose in both groups, one can argue that *in vivo* glucose uptake itself is blunted, thereby affecting fuel availability in BAT from Lal-/- mice. However, this was not the case, as BAT incorporation of radioactively labeled glucose was increased in Lal-/- mice and increased mRNA expression of Glut1 and AKT phosphorylation. These data suggest a compensatory upregulation of glucose metabolism. Still, the thermogenesis under cold exposure remains impaired and the observed respiration defect might be a result of reduced FA availability in BAT. The uptake of the glucose radiotracer into SM was increased in Lal-/- mice, indicating an additional input for shivering thermogenesis. Indeed, reduced acyl-CoA concentrations together with elevated carnitine esters and proteolysis markers incriminated increased catabolic activity in the SM of Lal-/- mice. Pronounced shivering in Lal-/- mice was confirmed by more than 2-fold elevated plasma CPK activity compared to WT mice. Hence, it can be implied that under cold exposure,

Lal-/- mice suffer from severe depletion of lipids in BAT to maintain thermogenesis, which cannot be compensated by increased catabolic shivering in the muscles (149).

Hypercholesterolemia has been reported in Lal-/- mice housed at RT (93) and the prospect of reestablishing normal plasma cholesterol concentrations would be important for human patients affected by LAL-D, as they are predisposed to early atherosclerosis (82). Since BAT activation had beneficial effects in mice models of atherosclerosis and dyslipidemia (both on cholesterol and TG concentrations) (137, 138), we hypothesized that cold exposure might correct the increased plasma cholesterol concentration in Lal-/- mice. Nevertheless, cold exposure further aggravated dyslipidemia in Lal-/- mice by increasing circulating TG levels possibly due to a defect in vascular lipolysis and/or clearance of lipoprotein remnants by the liver. Activated BAT enhances the selective uptake of FA from TG-rich lipoproteins, while the cholesterol-enriched remnants are cleared by the liver (163). Angptl4 strongly inhibits LPL-mediated vascular TG hydrolysis and is normally suppressed in BAT after cold exposure to facilitate cellular lipid replenishment (172). The expression of Angptl4 in BAT of Lal-/- mice was markedly increased upon cold exposure together with blunted FA uptake in BAT from cold-exposed Lal-/- mice even after an oil gavage. These data indicate a possible influence of LAL on Angptl4 expression and consequently on LPL activity. Although lipid uptake in BAT was blunted causing increased plasma TG concentrations, we cannot exclude a possible defect in the liver clearance of cholesterol-rich remnants. It would be interesting to investigate if this is the case also in LAL-D patients, as their therapeutic options are rather limited, and statins proved to bring little benefit in ameliorating dyslipidemia (82). Furthermore BAT function in humans is positively correlated with metabolic health (122) thus, additional to increased Angptl4, UCP1 downregulation could contribute to the dyslipidemia observed in LAL-D patients (149).

As we confirmed Lalistat 2 specificity in inhibiting exclusively acid but not neutral lipolysis *in vitro*, it is highly probable that the reduced FA release in the basal state was caused by LAL-dependent hydrolysis in iBACs. These data stand for an important input of LAL-derived FA with regard to energy supply and possibly signaling. Our results suggest that LAL might provide FA from acid lipolysis as products to activate UCP1 assumption supported by the negative energy balance

observed in Lal-/- mice during gradual cooling. As these effects were independent of food intake, we assume a central role for LAL in substrate utilization and compartmentalization in BAT specifically during cold exposure (149).

In conclusion, we show for the first time that global loss of LAL in mice causes UCP1 downregulation in BAT from mice kept at RT. Cold challenge leads to severe energy imbalance in BAT and SM and immediate hypothermia in Lal-/- mice. Importantly, our data provide evidence that cold-dependent lipid clearance from the circulation relies, besides intact ApoE and LDL receptor, also on functional LAL (149). Our findings are summarized in Fig. 24.

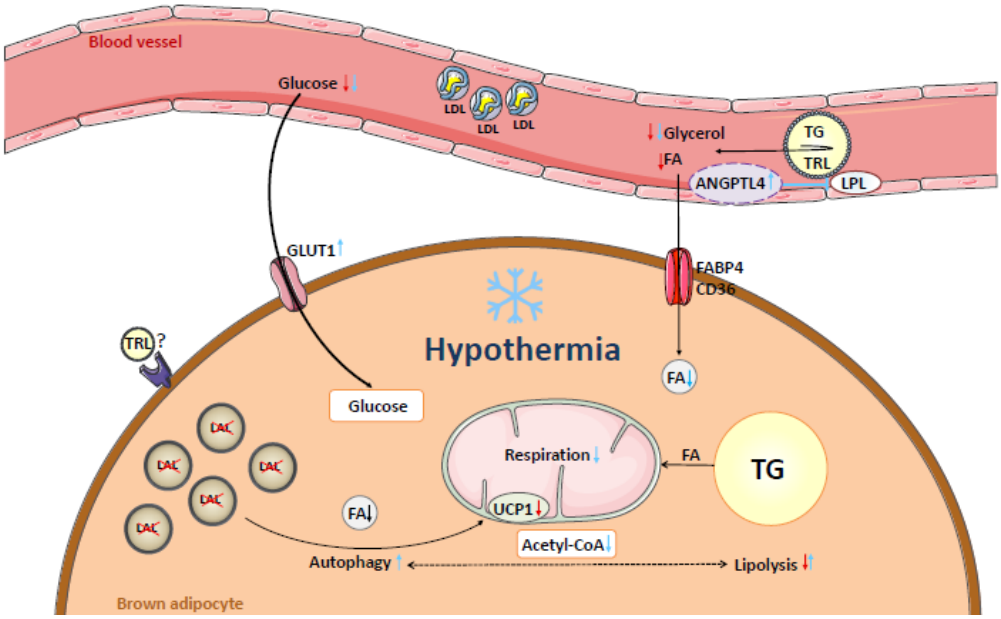

Figure 24: Lysosomal acid lipase regulates fatty acid channeling in brown adipose tissue to maintain thermogenesis. Lal-/- mice have accumulation of lipid-laden lysosomes in BAT and consequently decreased FA supply for mitochondrial respiration which is defective during cold exposure. LAL deficiency causes reduced UCP1 expression (at RT) and LD size in BAT. Lal-/- mice housed at RT have decreased neutral TG hydrolase activity which is enhanced in cold exposed Lal-/- mice. These mice have constant hypercholesterolemia and hypoglycemia. During cold challenge BAT glucose uptake is increased whereas LPL-mediated TRL hydrolysis and FA uptake in brown adipocytes is blunted. This effect is highly attributed to the upregulation of LPL inhibitor, ANGPTL4 (149). Requisite permission to use this figure was obtained (Appendix).

4. Consequences of adipose tissue LAL deficiency on energy metabolism

4.1 Introduction

WAT is the largest TG storage organ of the body being concomitantly a crucial player in energy metabolism and an endocrine hub through adipokines release (1). Excess fat accumulation leads to obesity, which is a pandemic condition and a principal cause of metabolic syndrome and related co-morbidities (173). On the other hand, lipodystrophy and lipoatrophy are equal threats to metabolic health as the buffer function of WAT is as well impaired (127).

WAT contains few mitochondria and has a minimal contribution to energy expenditure. Alternatively, BAT is abundant in mitochondria and, upon activation, can efficiently and extensively burn fat and glucose. This is achieved via the action of mitochondrial UCP1, which shifts the cellular respiration from ATP generation to heat production (134). In mice, dysfunctional BAT aggravates conditions such as dyslipidemia (149) and diet-induced obesity (174). Conversely, enhanced BAT function protects against atherosclerosis and improves metabolic parameters of obese and dyslipidemic animals (137, 138, 175). In humans, BAT activity is positively correlated with metabolic health and has an inverse relationship with body mass index (BMI) (122). Because of its power to alter energy expenditure, it is tempting to presume that BAT dysfunction can lead to an obesogenic phenotype. However, although defective BAT leads to cold intolerance in mice, its lack of function does not necessarily increase WAT depots at thermoneutrality (TN) conditions (176, 177).

LD are dynamic structures, serving as energy storage pools in both adipose and non-adipose cell types. Whereas the role of TG synthetizing enzymes and cytosolic TG hydrolases in LD plasticity is well described (178-180), acid lipolysis and its implication in fat turnover and energy metabolism is poorly understood. LAL is a unique hydrolase to break down autophagy and endocytosis-derived TG and CE. We recently showed that global LAL deficiency in mice causes severe cold intolerance and aggravates dyslipidemia due to blocked lipid uptake in BAT. Lal-/- mice have reduced WAT depots, despite preserved differentiation capacity of precursor cells into white adipocytes (149). Furthermore, our results showed

that, in certain conditions, Lal-/- SVC present increased differentiation capacity into white adipocytes, hinting that LAL may play a role in adipogenesis.

To discriminate between tissue-specific and global-induced effects, we generated mice lacking LAL in adipose tissue (atLal-/-). In the present study we demonstrate that global but not adipose tissue LAL loss is responsible for cold intolerance and WAT atrophy in mice. Moreover, Lal-/- mice present reduced weight gain during 7 weeks on WTD or 10 weeks glucose-supplemented water, unlike atLal-/- mice fed HF/HCD, which gained similar weight as WT controls on both RT and TN.

Our results indicate that LAL deficiency solely in adipose tissue does not impact lipid nor carbohydrate metabolism on both basal conditions and during dietary or cold challenges. However, the molecular adaptations to compensate the defective acid lipolysis remain to be investigated.

4.2 Results

Lal is expressed in different tissues and macrophages

In agreement with previous reports (24), LAL is expressed in multiple tissues and very abundant in macrophages. Additionally, we found moderate expression in BAT and low expression in spleen, SM, heart, and WAT. The lowest Lal expression of all tissues investigated was detected in the brain (Fig. 25).

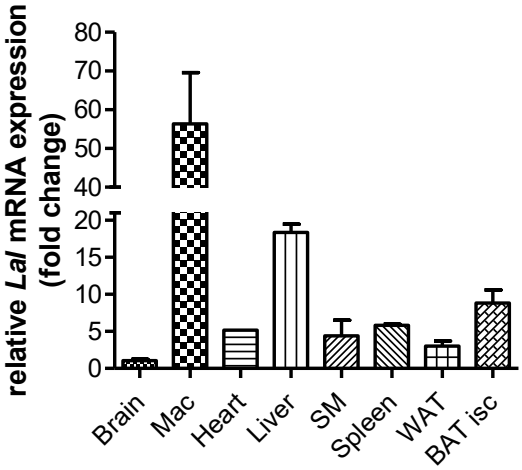

Figure 25: Lal is expressed in various tissues and macrophages

Lal mRNA expression in different tissues and macrophages, relative to cyclophilin A expression as reference gene. Expression profiles were determined using the 2-ΔΔCt method. Data represent means + SEM.

Lal-/- SVC have increased differentiation capacity to WAT compared to controls in the absence of rosiglitazone.

In the first chapter, we showed that SVC differentiation into white adipocytes is unaffected by LAL deficiency, indicating that Lal-/- mice lose WAT rather due to the impossibility to replenish the fat depots, as a consequence of defective energy metabolism. However, we also considered that the differentiation cocktail contains strong adipocyte differentiation inductors. Therefore, we also cultured SVC without rosiglitazone, a synthetic drug and potent PPARγ agonist. We found that Lal-/- SVC have increased differentiation capacity into white adipocytes, in the absence of rosiglitazone (Fig. 26A). Our results were consistent with upregulated gene expression of mature white adipocytes markers, such as Cebpα, Pparγ, Fabp4, and Cd36 in Lal-/- white adipocytes at day 7 of differentiation (Fig. 26B). Overall, these results indicated that LAL might be involved lipid storage regulation in WAT.

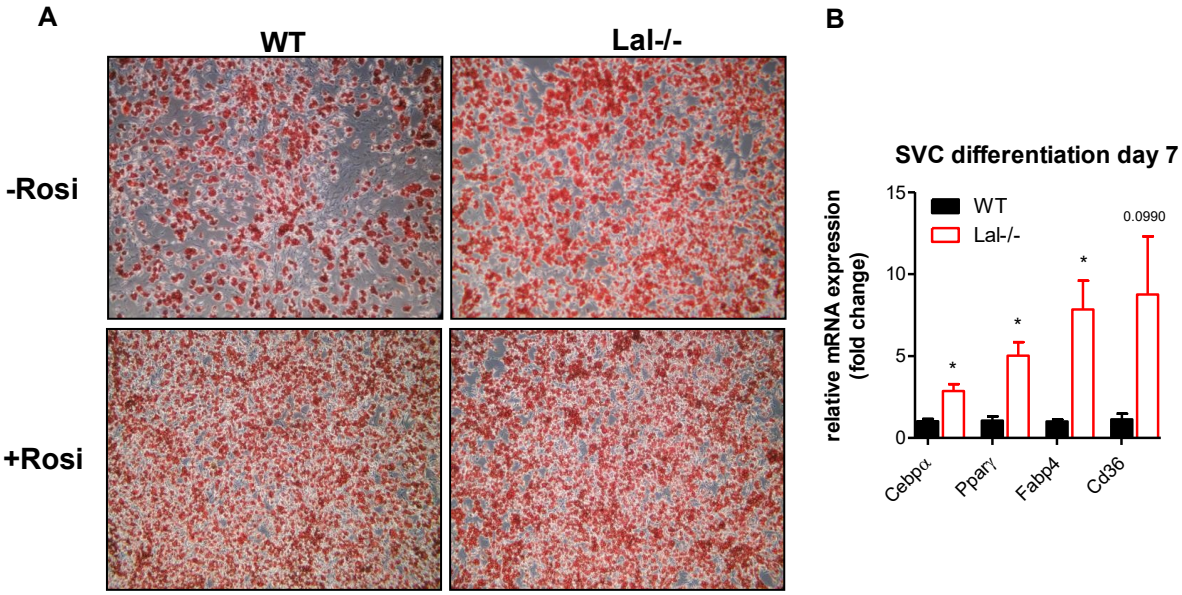

Figure 26: LAL deficiency promotes increased white adipocyte differentiation of SVC in the absence of rosiglitazone. (A) Representative oil red O stainings of white adipocytes to visualize neutral lipids (100x). (B) mRNA expression of white adipocytes markers at day 7 of SVC differentiation, in the absence of rosiglitazone in the differentiation medium, relative to cyclophilin A expression as reference gene. Expression profiles were determined using the $2^{-\Delta\Delta Ct}$ method. Data represent means + SEM; n=3; $p < 0.05$ (*). Student's unpaired t test.

Generation of mice with loss of LAL specifically in adipose tissue

We hypothesized that LAL deficiency specifically in adipose tissue may lead to increased fat mass and related adipose tissue hypertrophy and metabolic decompensation when challenged with HF/HCD.

We generated mice with a targeted deletion of LAL in white and brown adipose tissue by crossing $Lal^{flox/flox}$ mice and transgenic mice that express the Cre recombinase under the control of the murine adiponectin promoter (181). atLal-/- mice are viable and have normal appearance . Since we did not observe genotypic/phenotypic differences between genders, we used both males and females for our studies. We found markedly decreased Lal expression in BAT from both chow diet (Fig. 27A) and HF/HCD-fed (Fig. 27B) atLal-/- mice fasted for 12 h. Lal expression in perigonadal adipose tissue (PGAT) was less than 50% reduced in both feeding conditions (Fig. 27A, B). Liver Lal mRNA expression was unchanged in mice fed chow diet (Fig. 27A), confirming the conditional Lal gene deletion in adipose tissue. To see the LAL enzymatic function, we performed LAL activity assays at acidic pH, using the fluorogenic substrate 4-methyl-

umbelliferone. LAL activity was reduced by 60% in BAT (Fig. 27C) and only 22% in PGAT (Fig. 27D) from atLal-/- mice, compared to WT controls. We also found equivalent reduction in BAT of global Lal-/- mice but more pronounced differences in LAL activity in PGAT compared to WT mice (Fig. 27D). These results indicate that non-adipocytes substantially contribute to LAL activity in PGAT, which is, however not the case in BAT, at least in the tested conditions.

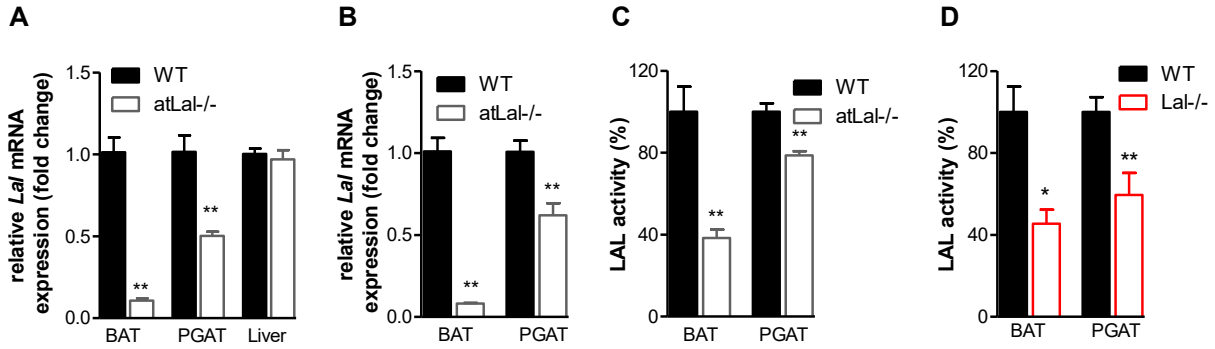

Figure 27: LAL mRNA expression and activity in adipose tissue-specific Lal-/- (atLal-/-) mice. *Lal* mRNA expression in tissues of 15 weeks old female mice fed (A) chow diet or on (B) HF/HCD, relative to cyclophilin A expression as reference gene. Expression profiles were determined using the $2^{-\Delta\Delta Ct}$ method. (C) LAL activity in BAT and WAT of 15 weeks old female WT and atLal-/- mice fed chow diet. (D) LAL activity in BAT and WAT of Lal-/- mice fed chow diet. Data represent means + SEM; n=4-5; $p \leq 0.01$ (**). Student's unpaired t test.

Global but not adipose tissue LAL deficiency causes reduced adiposity and BW gain in mice fed chow diet

Lal-/- mice fed chow diet have reduced BW and BW gain with aging (Fig. 28A) in 80% of all cohorts . At the age of 20 weeks, the livers of Lal-/- mice are on average 3-fold heavier compared to WT controls. Additionally, Lal-/ mice have reduced WAT but not BAT weights (Fig. 28B) in the fed state. Already at the age of 8 weeks Lal-/- mice have increased TC and FC but decreased circulating TG concentrations (Fig. 28C), after 12 h of fasting. In addition, they have reduced blood glucose levels in the fed state (Fig. 28D).

Unlike Lal-/- mice, which have shortened life span (92), atLal-/- mice fed chow diet have normal growth and weight gain at least up to 50 weeks of age (Fig. 28E). In the fasted state (12 h) atLal-/- mice have increased ingWAT weight (Fig. 28F), while BAT, liver, spleen, and kidney weights were comparable between the genotypes. Plasma FC, TC, and TG concentrations were similar in atLal-/- and WT mice fasted for 12 h (Fig. 28G).

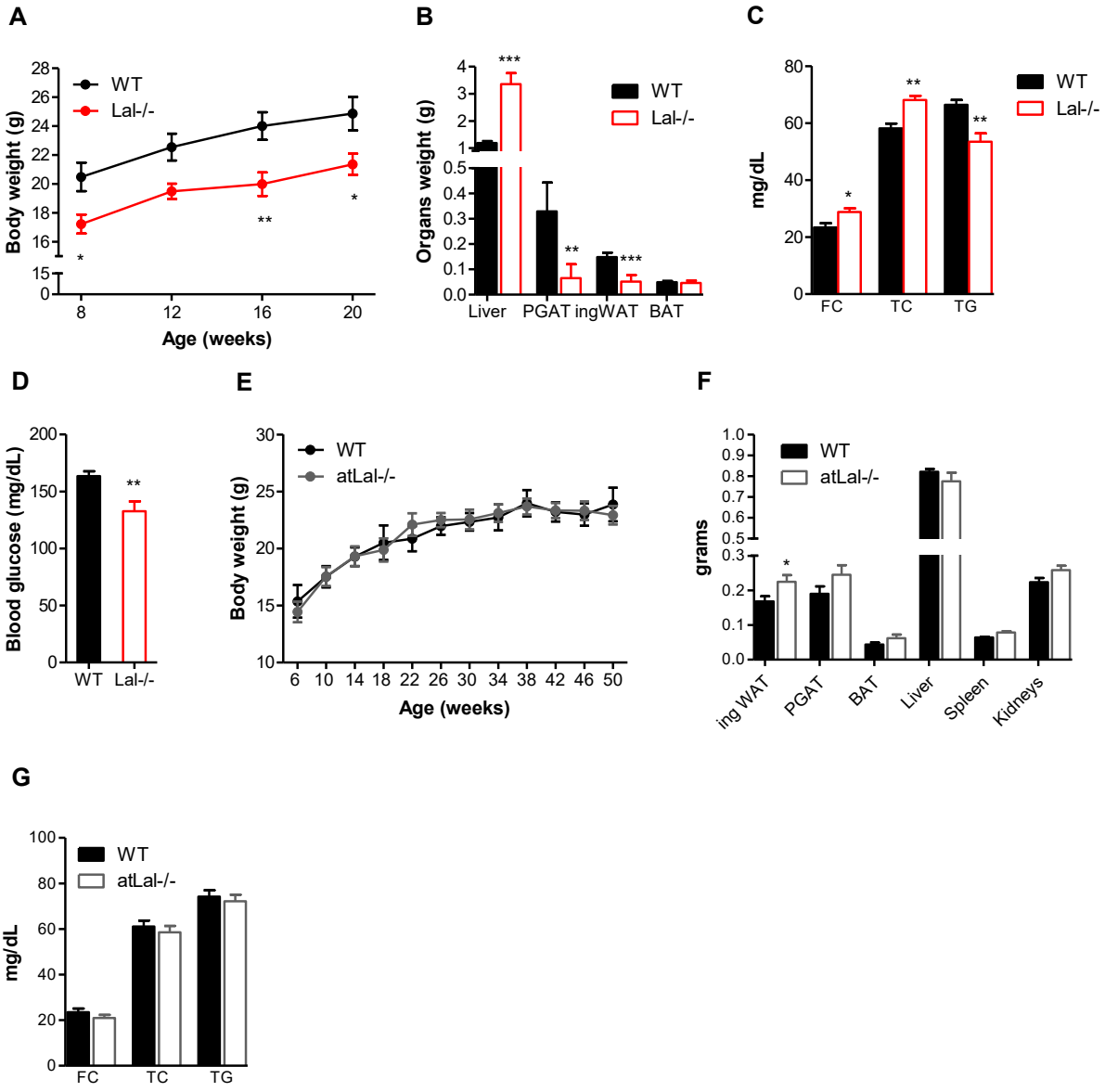

Figure 28: Global but not adipose tissue LAL deficiency causes reduced adiposity and BW gain and in mice fed chow diet. (A) BW curves and (B) organs weights of 20 weeks old female WT and Lal-/- mice. (C) Plasma free cholesterol (FC), total cholesterol (TC), triglycerides (TG) in 12 h-fasted condition, and (D) blood glucose of 8 weeks old female mice (fed state). (E) BW curves. (F) Organ weights and (G) plasma FC, TC, and TG concentrations of 16 weeks old female WT and atLal-/- mice fasted for 12 h. Data represent means ± SEM; n=5-7; $p < 0.05$ (*), $p \leq 0.01$ (**), $p \leq 0.001$ (***). (B-D, F, G) Student's unpaired t test; (A, E) ANOVA.

LAL deletion in adipose tissue does not influence VLDL secretion in mice fed chow diet

In the fasted state, adipose tissue is the main source of FA directly shuttled to organs or budded into TG-rich VLDL particles by the liver and secreted into the blood stream (164, 165). We found reduced circulating FA concentrations in atLal-

/- mice after 12 h of fasting and similar values between genotypes in the refed state (Fig. 29A). Plasma free glycerol concentrations did not differ significantly in any of the feeding conditions (Fig. 29B). To see the impact of decreased plasma FA on liver VLDL production, we administered the mice (subsequent to a 12 h fasting period) tyloxapol to inhibit vascular lipolysis. The resulting plasma TG concentrations were identical in WT and atLal-/- mice, indicating unaffected VLDL secretion in mice lacking LAL in adipose tissue (Fig. 29C). Additionally, we investigated the TC and TG distributions in the lipoproteins of fasted mice by fast performance liquid chromatography of pooled plasma and found comparable lipoproteins profiles (Fig 29D, E). These data indicate that LAL deficiency in adipose tissue does not impact liver TG production in mice fed chow diet, despite reduced fasted FA plasma concentrations.

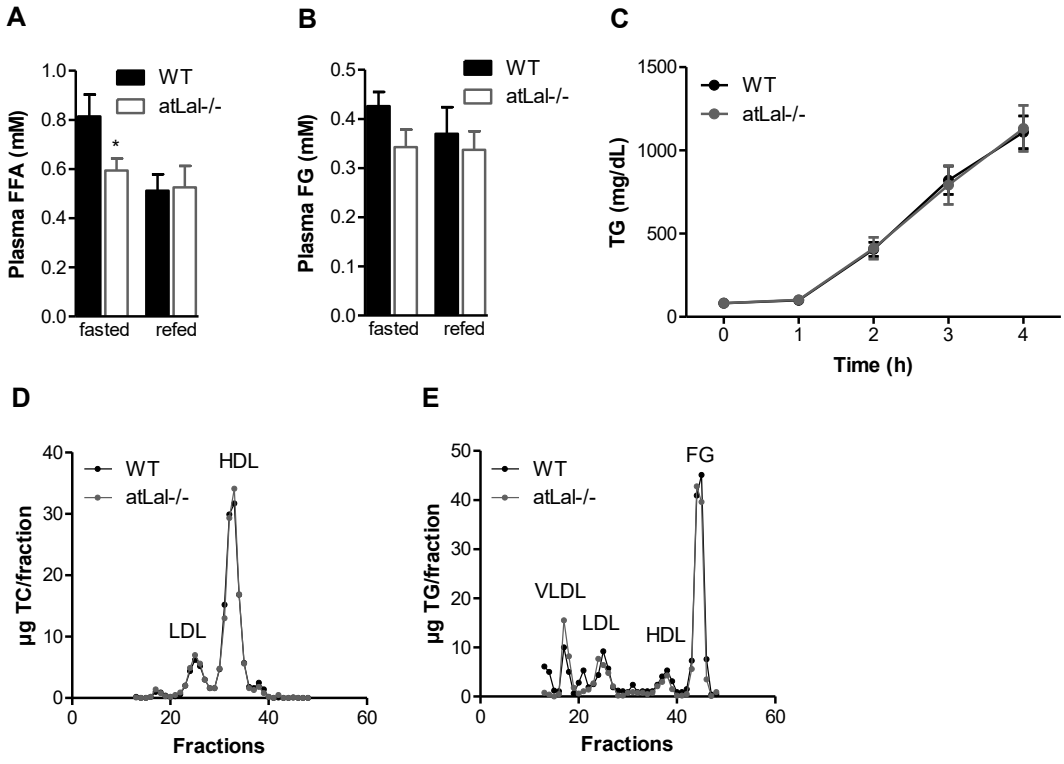

Figure 29: atLal-/- and WT mice fed chow diet have comparable lipoprotein profiles and VLDL secretion. Plasma (A) free fatty acids (FFA) and (B) free glycerol (FG) concentrations of 45 weeks old WT and atLal-/- male mice fasted for 12 h and refed for 2 h. (C) VLDL secretion of 12 h-fasted female mice (16 weeks old) following tyloxapol injection. Lipoprotein distribution of (D) TC and (E) TG after separation by fast performance liquid chromatography of pooled plasma of female mice aged 12 weeks. Data represent means ± SEM; n=5-7; (A, B) Student's unpaired t test; (C) ANOVA.

atLal-/- and WT mice fed chow diet have comparable glucose metabolism and energy expenditure

Since global LAL deficiency in mice causes increased glucose tolerance and insulin sensitivity (93), we sought to investigate the implications of adipose tissue LAL deletion on glucose metabolism. For this purpose we used mice fed chow diet. In line with similar blood glucose concentrations in both 12 h-fasted and refed conditions (Fig. 31A), atLal-/- mice showed comparable glucose tolerance as WT controls (Fig. 31B). Detailed metabolic analyses were performed using fully automated metabolic cages for indirect calorimetry measurements. Both genotypes have equivalent substrate oxidation, as shown by comparable RER curves (Fig. 31C) and energy expenditure (Fig. 31D) in fed and fasted states. In line, we found similar food intake (Fig. 31E) and locomotory activity (Fig. 31F) in WT and atLal-/ mice.

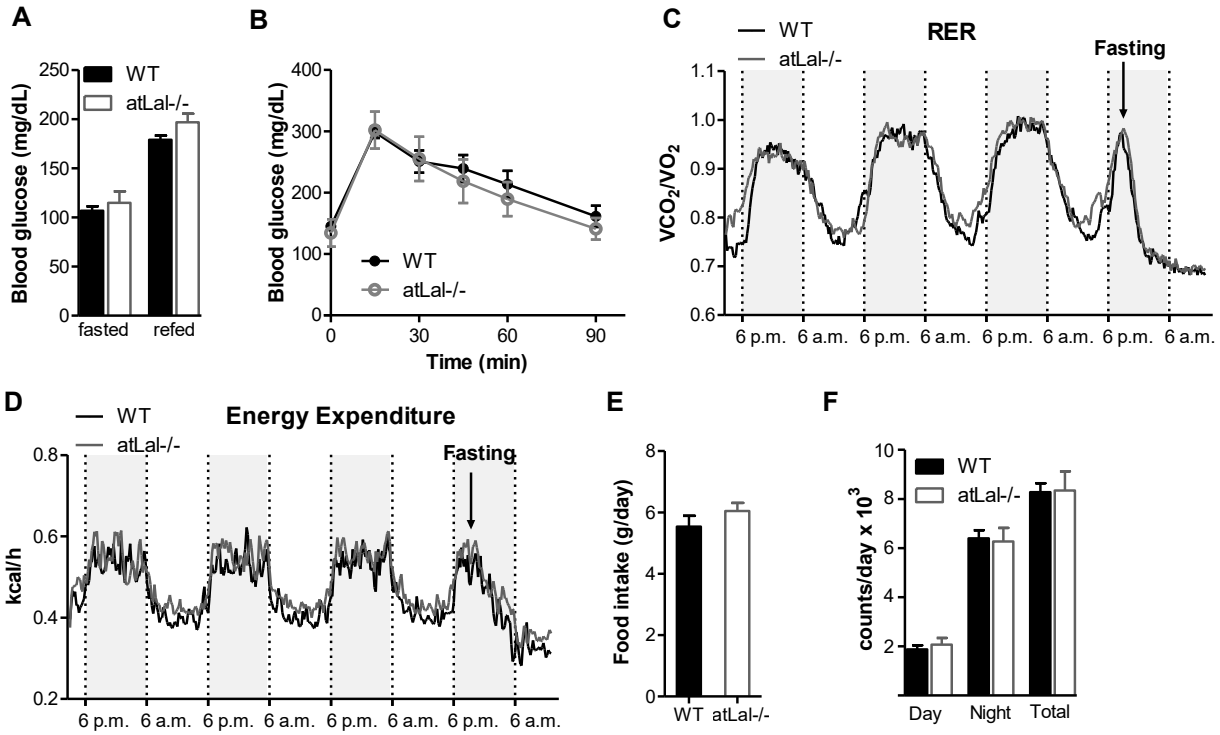

Figure 30: atLal-/- and WT mice fed chow diet have comparable metabolic parameters

WT and atLal-/- (45 weeks old) male mice were fasted for 12 h and refed chow diet for 2 h. (A) Blood glucose concentrations in fasted and refed states and (B) glucose tolerance test. (C) Respiratory exchange rate (RER) and (D) energy expenditure measured by indirect gas calorimetry in WT (black line) and atLal-/- mice (grey line). Gray-shaded areas represent dark phase (6 p.m. - 6 a.m.); non-shaded, light phase (6 a.m. - 6 p.m.). (E) Food intake and (F) locomotory activity. Data represent means ± SEM; n=5-7; $p < 0.05$ (*). (A-E), G, H) Student's unpaired t test; (F) ANOVA.

Lal-/- mice but not atLal-/- have decreased BW gain during high fat diet or glucose feeding

Since Lal-/- mice have reduced weight gain on chow diet but Lal-/- SVC have increased differentiation capacity, we increased caloric intake by supplementing chow diet with 10% glucose water or by feeding the mice WTD. Contrarily to our expectations, Lal-/- mice do not gain weight during WTD (Fig. 31A) or glucose water (Fig. 31D) feeding, with differences in BW of >10 grams at the end of the experiments. Accordingly, RER curves of mice fed glucose water confirmed that, although Lal-/- mice use carbohydrates as catabolic substrate, they fail to undergo lipogenesis as their RER is ≤ 1 at all time points. Conversely, and in line with BWgain, WT mice undergo *de novo* lipogenesis and have RER ≥ 1 (182, 183) during the might phase (Fig. 31B). In Lal-/- mice energy expenditure was constantly below WT values (Fig. 31C). Next, we challenged WT and atLal-/- mice with HF/HCD to see if an increase in lipid-rich food caused an effect in atLal-/- mice with regard to BW and metabolic parameters. Throughout the 8 weeks of feeding, WT and atLal-/- mice gained weight comparatively (Fig. 31E) and had similar blood glucose concentrations in the fasted state (Fig. 31F). Consistently, both genotypes had equivalent plasma FC, TC, and TG (Fig. 31G) concentrations and lipoprotein cholesterol (Fig. 31H) and TG (Fig. 31I) profiles. We also fed female mice HF/HCD for 8 weeks and observed similar BW gain in atLal-/- and control mice.

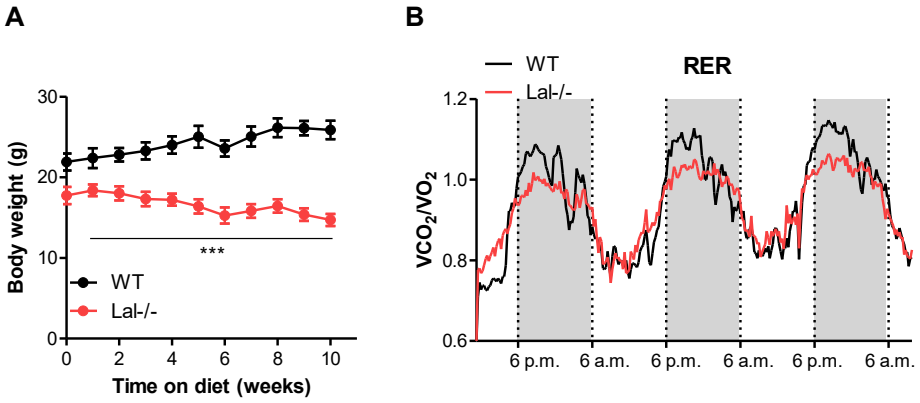

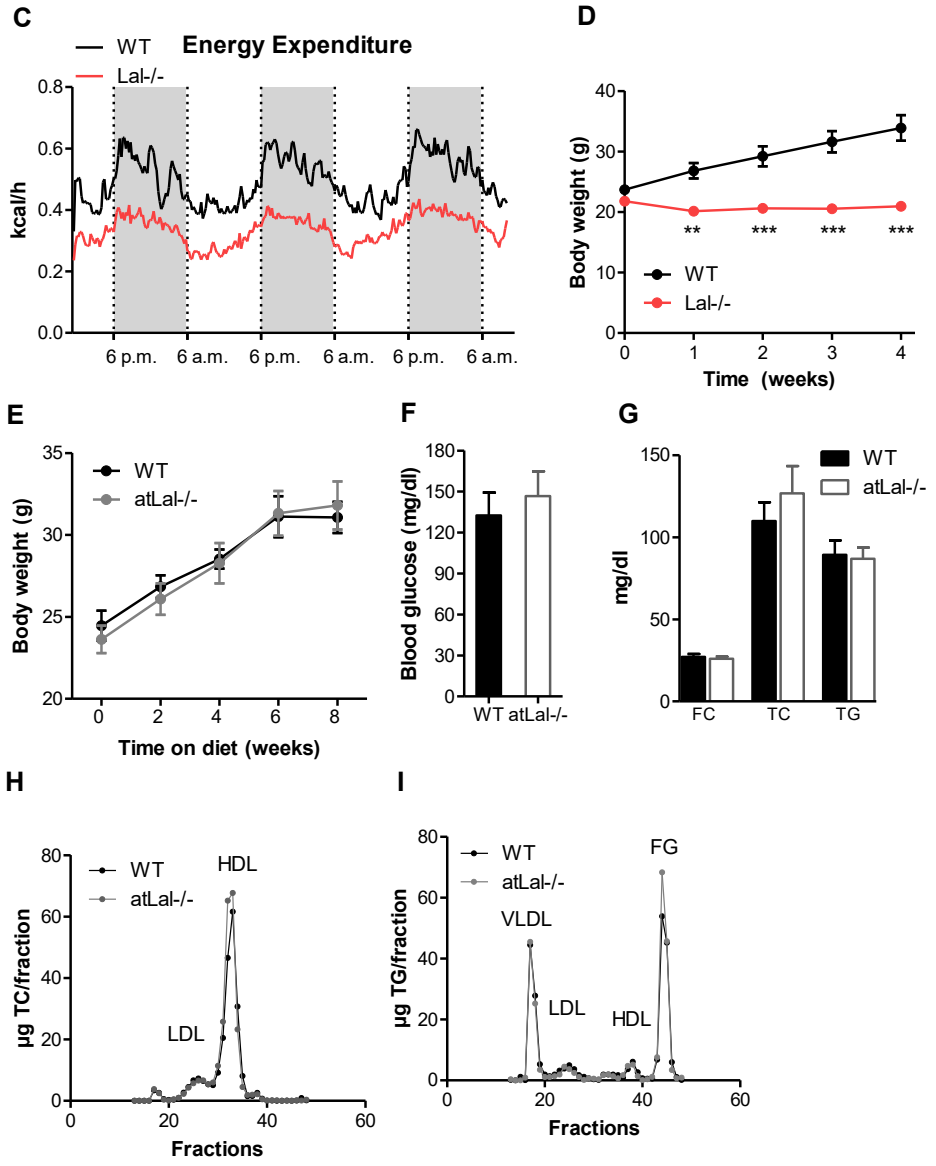

Figure 31: Lal-/- mice have decreased BW gain during high fat diet or glucose feeding

BW curves of (A) female mice fed chow diet and 10% glucose water for 10 weeks. (B) Respiratory exchange rate (RER) and (C) energy expenditure measured by indirect gas calorimetry in WT (black line) and Lal-/- mice (red line) (n=4-5). Gray-shaded areas represent dark phase (6 p.m. - 6 a.m.); non-shaded, light phase (6 a.m. - 6 p.m.). (D) BW curves of male mice fed WTD for 4 weeks (n=6). WT and atLal-/- male mice were fed HF/HCD for 8 weeks. (E) BW curves and (F) blood glucose concentrations (12 h-fasted state; n=7-9). (G) Plasma lipid parameters and lipoprotein profiles of (H) TC and (I) TG after separation by fast performance liquid chromatography of pooled plasma from overnight fasted mice (n = 4-5). Data represent means ± SEM; $p \leq 0.001$ (***). (F, G) Student's unpaired t test; (A, D, E) ANOVA.

To elucidate whether LAL deficiency in adipose tissue leads to altered lipid distribution we analyzed HE-stained tissues from female mice fed HF/HCD for 8 weeks and fasted for 12 h. Although BAT morphology was visibly affected by the

feeding experiment with increased lipid accumulation, this feature was comparable between WT and atLal-/- mice. Liver and WAT architecture was preserved in both genotypes, mirroring the modest effect of HF/HCD in female mice (Fig. 32).

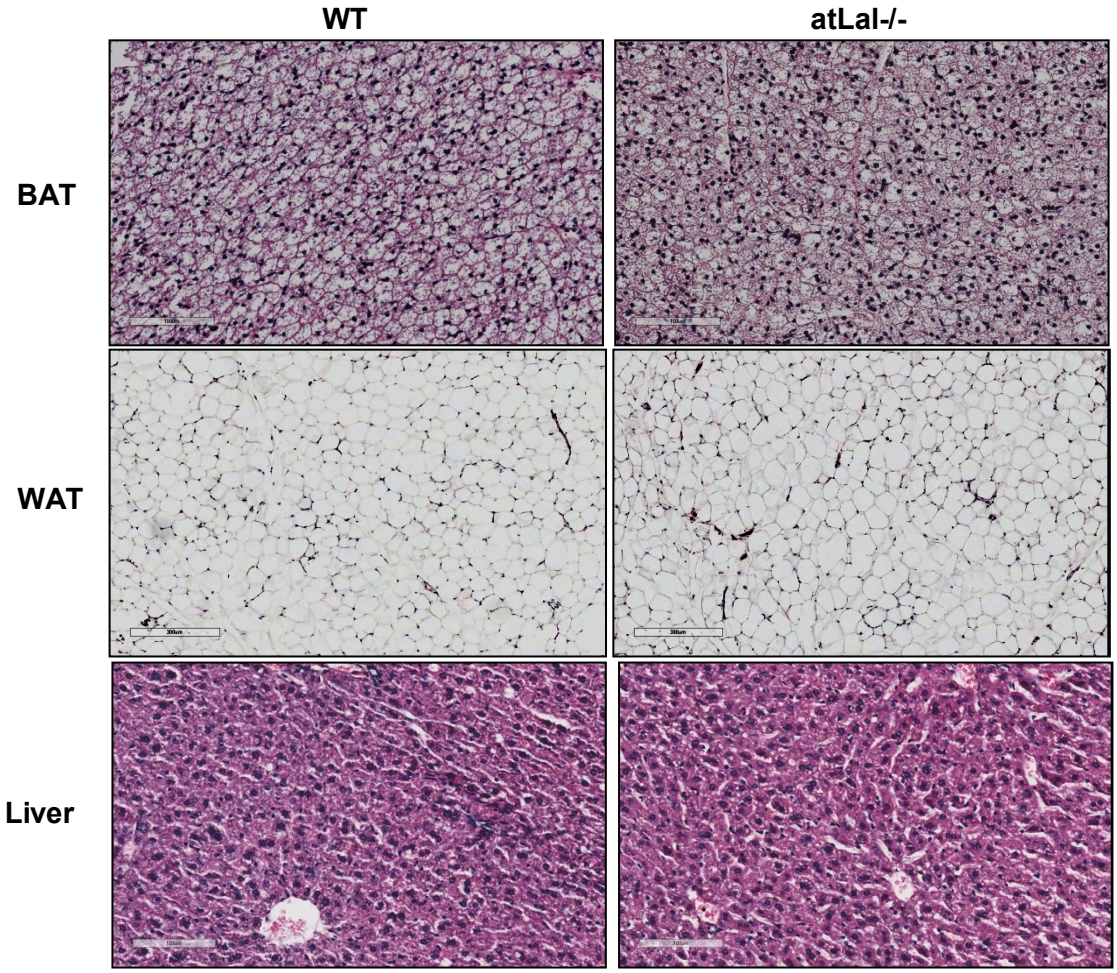

Figure 32: Adipose tissue LAL deficiency does not affect BAT, Liver and WAT tissue morphology in mice fed HF/HCD. Hematoxylin and eosin staining of BAT, WAT and liver isolated from 12 h-fasted female mice fed 10 weeks HF/HCD.

Global but not adipose LAL deficiency causes cold intolerance in mice fed chow diet

As shown in Chapter 3, global Lal-/- mice undergo severe hypothermia within few h of cold exposure at both 6 and 20 weeks of age (149). Accordingly, 12 weeks old Lal-/- mice reach a sharp decrease in their body temperature after only 6 h at 5°C (Fig. 33A) and loose more weight than WT mice (Fig. 33B, C). Lal-/- mice have decreased blood glucose at both RT and in cold (Fig. 33D) and BAT sections stained with hematoxylin and eosin depicted reduced lipids depots in the cold-exposed Lal-/- mice (Fig. 33E).

To investigate if deletion of adipose tissue LAL affects cold tolerance, we also exposed atLal-/- mice to 5°C and observed that they were able to maintain their temperature homeostasis throughout 48 h in cold (Fig. 33F). Although BW were not significantly different at the beginning or at the end of the experiment (Fig. 33G), atLal-/- mice lost more weight than their WT controls (Fig. 33H) despite comparable food intake (Fig. 33I). We did not see significant changes in the circulating cholesterol, TG, FFA, FG or glucose concentrations (Fig. 33J- L), respectively.

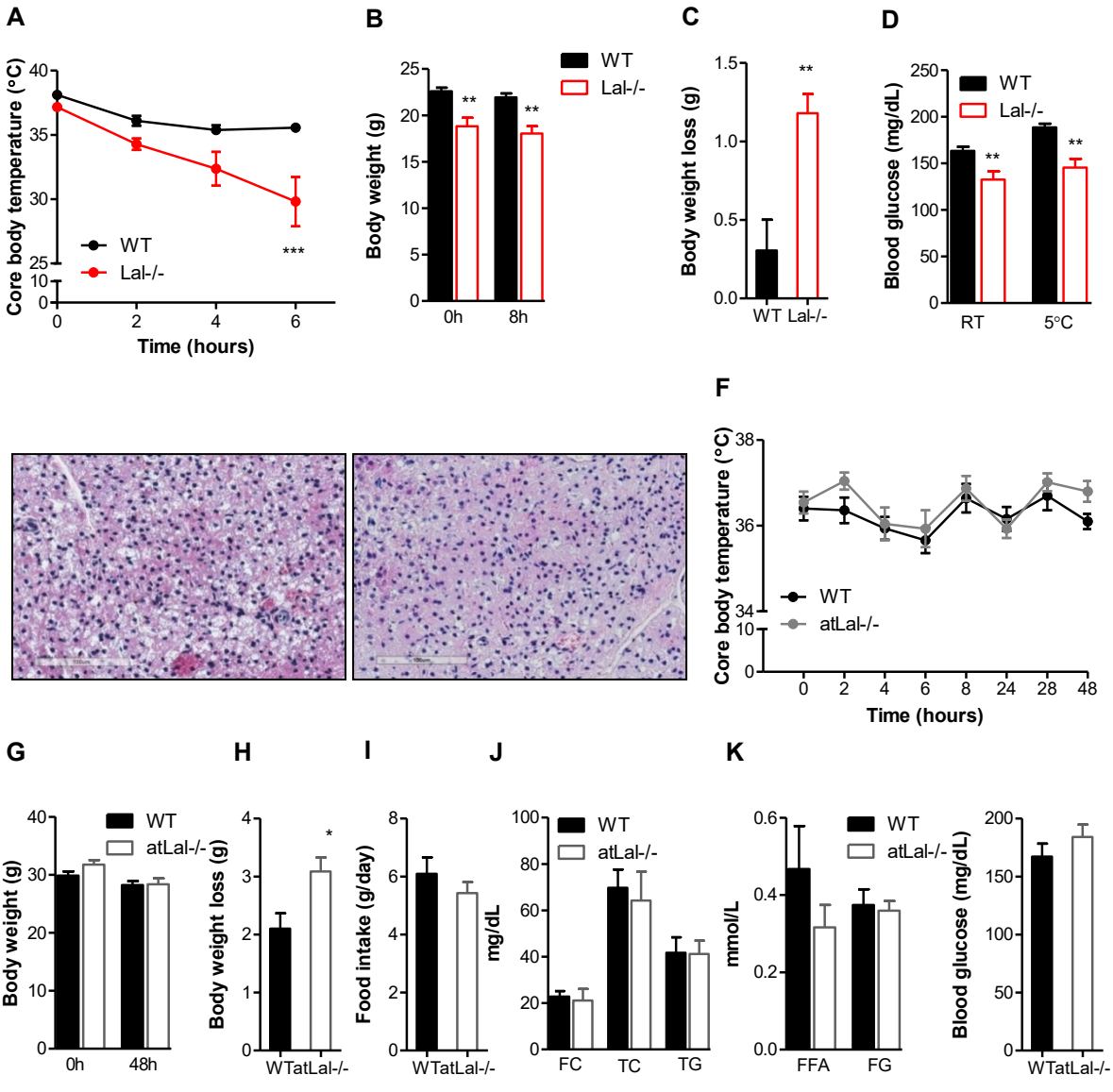

Figure 33: Global but not adipose LAL deficiency causes cold intolerance in mice fed chow diet. (A) Body temperature curves, (B) BW, (C) BW loss and (D) blood glucose concentrations of female WT and Lal-/- mice aged 12 weeks during 6 h cold exposure (n=6). (E) Hematoxilin and eosin staining of BAT from 12 weeks old WT and Lal-/- mice exposed to cold for 6 h. (F) Body

temperature curves, (G) BW, (H) BW loss, (I) food intake, (J) FC, TC , and TG, (K) free fatty acids (FFA), and (L) blood glucose of 48 h cold exposed WT and atLal-/- male mice aged 55 weeks. Data represent means ±SEM; n=5-7; $p < 0.05$ (*), $p \leq 0.01$ (**). (B-D, G-L) Student's unpaired t test; (A, F) ANOVA.

Next, we performed a glucose uptake experiment using WT and atLal-/- mice exposed to cold and injected i.p with [^{3}H]2-deoxi-glucose. Radioactivity in plasma was similar between genotypes (Fig. 34A) whereas we observed a trend to decreased glucose uptake in BAT and liver (Fig. 34B).

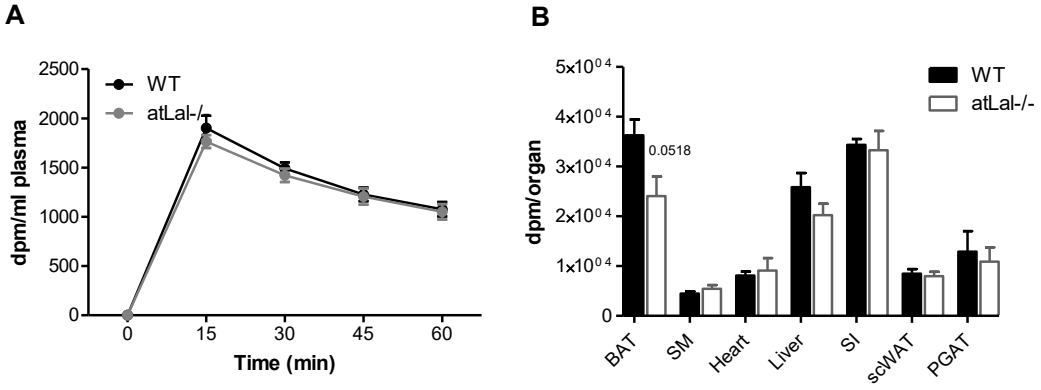

Figure 34: Chow-fed atLal-/- mice have comparable BAT glucose uptake in cold

Fifty five weeks old female mice were exposed to cold for 2 h before [^{3}H]2-deoxi-glucose i.p injection. (A) Radioactivity in plasma, following [^{3}H]2-deoxi-glucose injection. (B) Tissue radioactivity 60 min after injection. Data represent means ± SEM; n=4. (B) Student's unpaired t test; (A) ANOVA.

Fasting does not impact cold tolerance in atLal-/- mice fed chow or HF/HCD

We next wanted to exclusively investigate the WAT efficiency to supply cold-activated brown adipocytes by subjecting WT, Lal-/-, and atLal-/- mice to nutrient restriction in cold. We observed a dramatic drop in body temperature of Lal-/- mice immediately after cold exposure (Fig. 35A). Even though atLal-/- showed an initial trend to maintain core body temperature, they eventually entered hypothermia after 6 h in cold (Fig. 35B), similarly to WT controls. BW (Fig. 35C), BW loss (Fig. 35D), and organs weight (Fig. 35E) were comparable between genotypes. Furthermore, plasma lipid parameters and blood glucose concentrations were comparable in atLal-/- and WT mice (Fig. 35F, G).

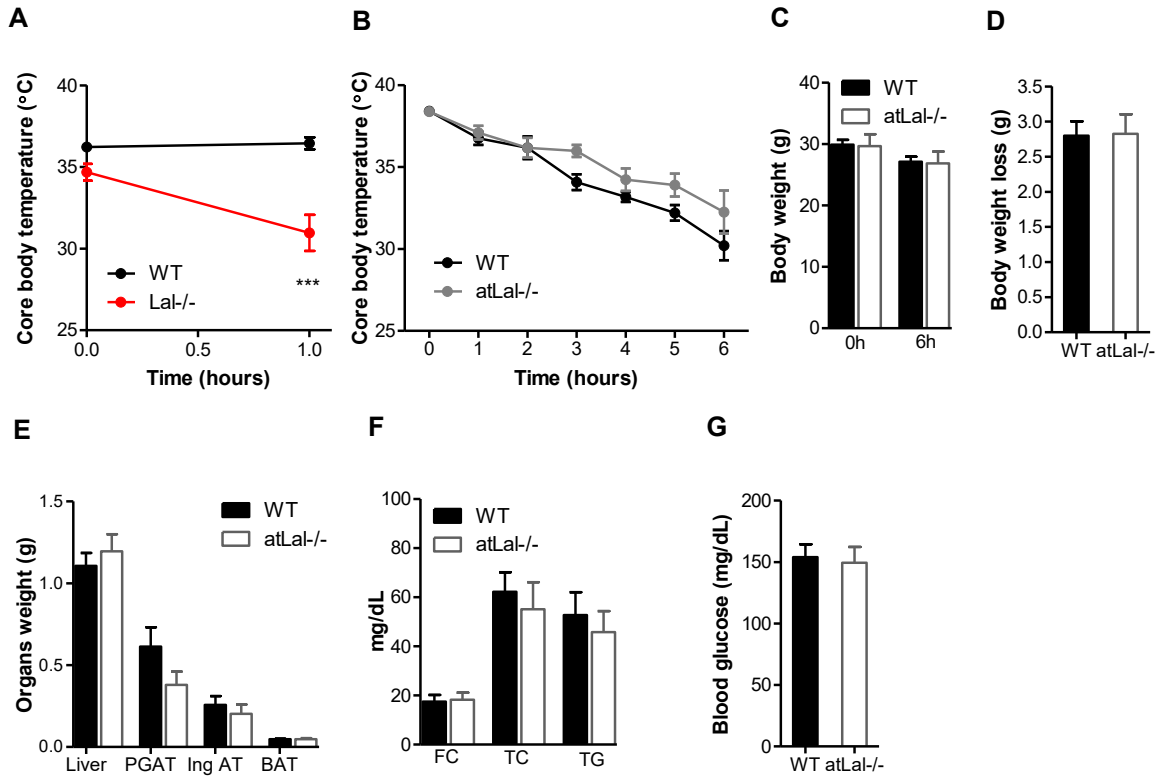

Figure 35: Fasting does not impact cold tolerance in atLal-/- mice fed chow diet. Male WT, Lal-/-, and atLal-/- mice aged 20 weeks were exposed to cold without access to food. (A) body temperature curves of Lal-/- mice. (B) Body temperature curves, (C) BW, (D) BW loss, (E) organ weights, (F) plasma lipid parameters and (G) blood glucose concentrations of atLal-/- mice after 6 h of cold exposure. Data represent means ± SEM; n=4. (C-G) Student's unpaired t test; (A, B) ANOVA.

A similar experimental approach as shown in Fig. 34 and 35 was performed using WT and atLal-/- mice fed HF/HCD. In the fed and fasted states, both genotypes showed equal capacity to use diet- or WAT-derived FA (Fig. 36).

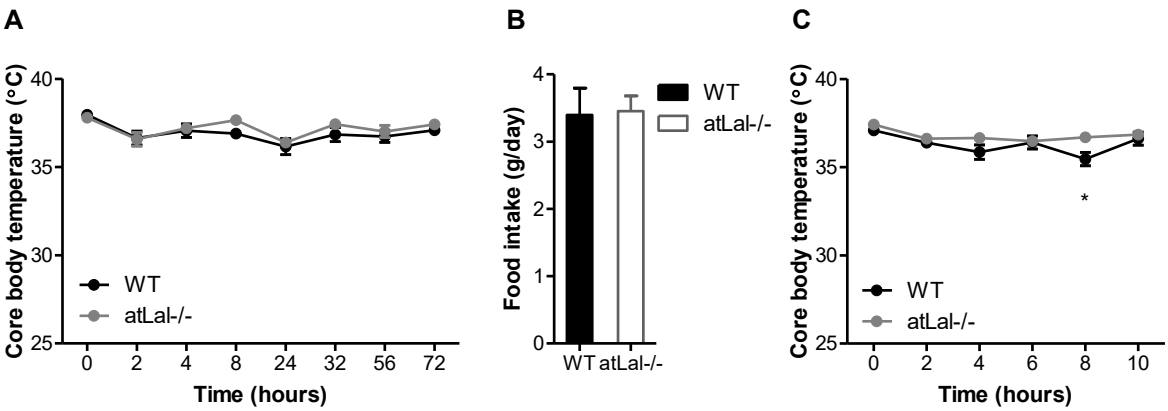

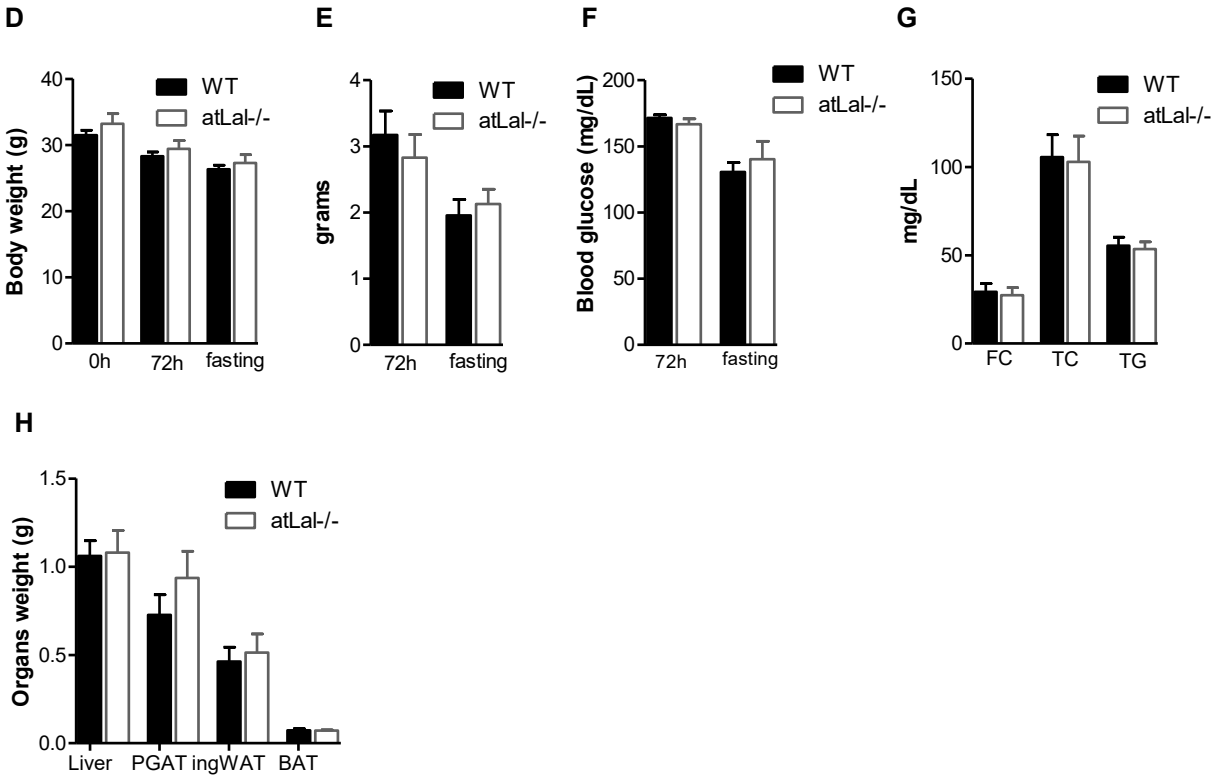

Figure 36: HF/HCD-fed atLal-/- mice show comparable metabolic parameters to controls during cold exposure. WT and atLal-/- male mice (20 weeks old) were fed HF/HCD for 10 weeks, acutely exposed to cold for 72 h and, thereafter, food was removed for 10 h. (A) Body temperature curves and (B) food intake of mice kept in cold with unlimited access to food. (C) Body temperature of mice fasted in cold. (D) BW, (E) BW loss and (F) blood glucose during the entire experiment. (G) Plasma lipid parameters and (H) organs weight of mice fasted in cold. Data represent means ± SEM; n=7; $p < 0.05$ (*). (B, (D-H) Student's unpaired t test; (A, C) ANOVA.

Comparable BW gain in WT and atLal-/- kept at TN fed chow diet or HF/HCD

To eliminate any thermic discomfort created by the RT housing conditions (22°C), we housed WT and atLal-/- mice fed chow diet at TN (30°C). Two weeks later, using fully automated climate-regulated metabolic cages we performed indirect calorimetry measurements before and after a single dose of 1 mg/kg i.p. injection of the β3 adrenergic agonist CL316,243 (CL). Both genotypes showed preserved circadian rhythm, as showed by increased RER and EE curves during the dark phase and decreased values during the light phase. CL injection induced similar responses in WT and atLal-/-, with a drastic drop in RER and peak values of EE immediately after CL administration (Fig. 37A, B). While BW and body volumes were comparable (Fig. 37C, D), we found a trend toward increased fat volume and

fat/body volume ratio in atLal-/- mice, which however did not reach statistical significance (Fig. 37E, F).

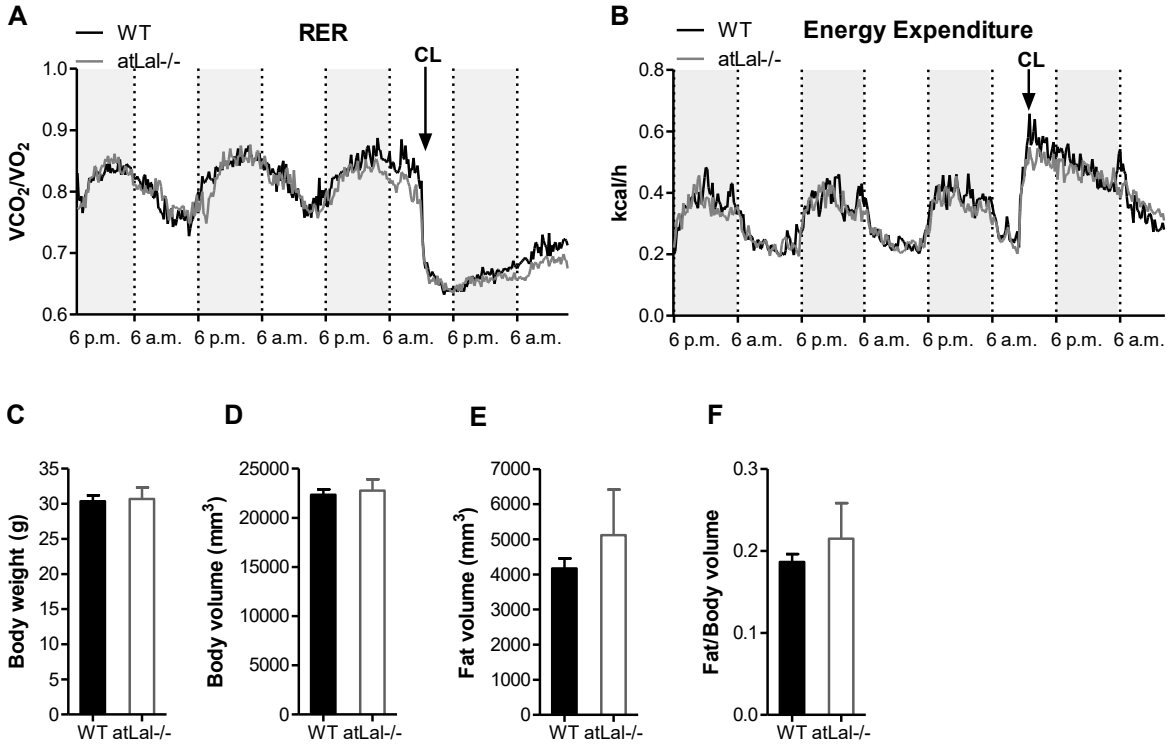

Figure 37: Unchanged metabolism and body fat in chow diet-fed atLal-/- when housed at TN
Mice aged 20 weeks and fed chow diet were housed at TN for 2 weeks. (A) Respiratory exchange rate (RER) and (B) energy expenditure. (C) BW, (D) total body volume, (E) fat volume and (F) fat/body volume ratio. Data represent means ±SEM; n=6. (C-F) Student's unpaired t test.

We further challenged the mice on HF/HCD for 6 weeks and kept them at TN for the entire time. RER and EE curves showed comparable values in WT and atLal-/- mice in basal conditions and after β3-AR agonist (CL) injection (Fig. 38A, B). Although all mice gained weight during the feeding period, we found no differences in BW and food intake between genotypes (Fig. 38C, D). In line with our previous results, LAL deletion in adipose tissue did not impact plasma cholesterol, TG, FFA and blood glucose concentrations, with only a slight increase in plasma free glycerol in atLal-/- mice under fed-state conditions (Fig. 38E- G).

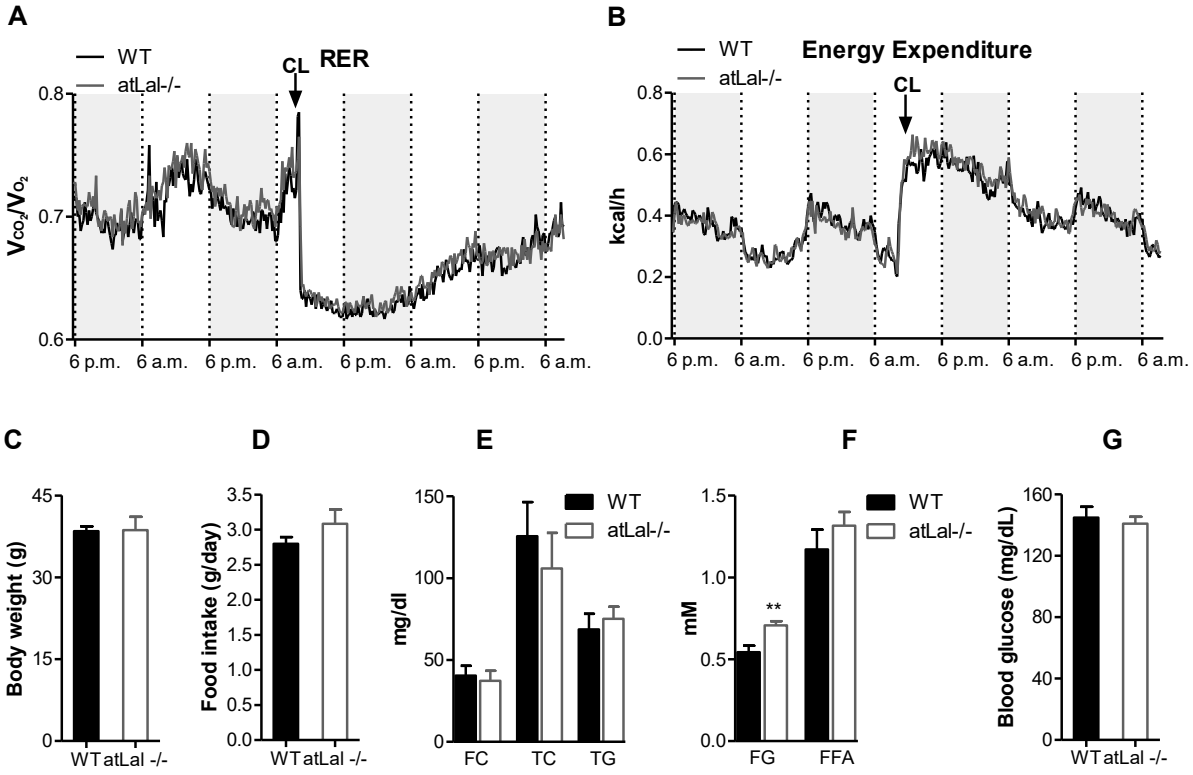

Figure 38: Comparable combined effect of TN and HF/HCD feeding in atLal-/- mice

WT and atLal-/- mice were fed HF/HCD for 6 weeks at TN. (A) Respiratory exchange rate (RER) and (B) energy expenditure. (C) BW, (D) food intake, (E) plasma lipid parameters, (F) free glycerol, free fatty acids and (G) blood glucose measured in the fed state. Data represent means ± SEM. n=6; $p \leq 0.01$ (**). (C-G) Student's unpaired t test.

4.3 Discussion

LAL plays a unique role to catalyze the hydrolysis of CE and TG inside the lysosome. LAL deficiency in humans and mice results in marked hepatomegaly, dyslipidemia and shortened life span (57, 91-93). Lal-/- mice present progressive lipoatrophy, despite normal *in vitro* differentiation of LAL-deficient SVC into white adipocytes and LAL-inhibited iBACs and severe cold intolerance due to BAT dysfunction (149).

By modulating the differentiation cocktail, we found that in the absence of rosiglitazone Lal-/- SVC have increased lipid accumulation and upregulated white adipocyte markers compared to WT cells. These preliminary data hinted that, beyond the dramatic phenotype driven by total LAL deficiency, LAL regulates metabolism in a cell-specific manner. To discriminate between global and adipose tissue-targeted effects of LAL deficiency, we generated mice lacking LAL in the WAT and BAT. atLal-/- mice appear healthy at birth and throughout their life and have normal weight gain, WAT depots and circulating cholesterol and TG concentrations. However, this is not the case in global Lal-/- mice, which present growth retardation already at young age and further loose WAT and have decreased fasting TG concentrations. This feature can be likely caused by the long-term reduced FA supply from WAT and probably limited LD stores in the liver of Lal-/- mice (93). Although we found decreased circulating FA levels in fasted atLal-/- mice, this did not affect liver VLDL production, indicating that a sufficient threshold FA supply is fulfilling liver demand to synthetize TG and to secrete them as VLDL. Interestingly, we found increased WAT weights in fasted atLal-/- mice. This finding is in agreement with previous studies showing that LAL contributes to FA release from adipocytes via autophagy and buffers the energy gap during nutrient restriction (39). However indirect calorimetry measurements revealed no changes in energy expenditure and RER, indicative of unaltered substrate oxidation in alLal-/- mice fed chow diet. These features were opposite to Lal-/- mice, which presented decreased energy expenditure (149) despite reduced weight gain on chow diet. To investigate if calories supplementation improved weight gain in Lal-/- mice, we fed the animals WTD or chow diet and 10% glucose water. While WT mice gained weight on both diets, Lal-/- mice lost BW on WTD and even when they received chow diet supplemented with 10% glucose in

drinking water. On the other hand atLal-/- mice fed HF/HCD had comparable weight gain to controls and similar BAT, WAT, and liver tissue morphology indicating that, unlike Lal-/- mice, LAL deficiency solely in adipose tissue does not impair weight gain and fat depots.

Acute cold exposure is a challenge to both BAT and WAT due to an increased energy demand to maintain metabolic and thermic homeostasis in organisms not adapted to the low temperatures of the environment. Upon cold exposure, Lal-/- mice became hypothermic within h, lost more weight, and virtually lacked LD in BAT, despite unlimited access to food. This is, however, not the case for atLal-/- mice, which were normothermic for at least 48 h in cold although they lost more weight. Moreover, in the absence of food, Lal-/- mice were viable for only 1 h, whereas atLal-/- mice resisted the challenge for as long as 6 h.

Decreases in BAT activity causally relates to obesity and consequent poor thermogenesis translated in low energy expenditure and relative resistance to weight loss (184-186). To elucidate if adipose tissue-derived LAL additionally influenced BAT function in mice fed HF/HCD we exposed the animals to cold with or without access to food. WT and atLal-/- mice had comparable body temperatures as well as BW loss, plasma lipid, and blood glucose concentrations. This finding indicates that, during extreme metabolic challenges the neutral lipases fully compensate for LAL deficiency and fulfill the FA demand of BAT to sustain thermogenesis and maintain temperature homeostasis.

While extreme differences in adiposity are easily measurable as BW variations, milder changes in WAT mass may be overseen when routinely measuring animals' weight. We tested if our *in vitro* observations regarding the increased ability of Lal-/- SVC to differentiate into white fat cells were recapitulated in atLal-/- mice. To exclude the thermic stress due to standard housing temperature (at 22°C) (120, 157), we kept WT and atLal-/- mice fed chow diet at TN for 2 weeks before measuring body fat. We found, however, no changes in fat volumes between genotypes, in accordance with comparable BW. Accordingly, HF/HCD and TN housing for 6 weeks led to similar weight gain in WT and atLal-/- mice. We also tested BAT thermogenic capacity after CL injection and observed equivalent responses in WT and atLal-/- mice housed at TN on chow and HF/HCD, confirming that LAL-dependent lipolysis is not influenced by the β3-adrenergic signaling cascade.

Altogether, our data brings important clarifications on the role of lysosomal lipid hydrolysis in adipose tissue during different metabolic states. atLal-/- mice had unaltered lipid metabolism in the fed state when housed at 5°C, RT or TN, confirming that LAL does not contribute to lipid synthesis in adipose tissue. In the fasted state, atLal-/- mice on chow diet had decreased plasma FA levels and slightly increased adipose tissue mass, suggesting a role of lipophagy in complementing neutral lipolysis in adipocytes. Additionally, our findings confirm that upon extreme stimuli, as cold exposure and fasting in cold, the canonical lipolytic pathways regulate the FA supply from WAT. This is not the case in Lal-/- mice, arguing for a combined metabolic effect of global LAL deficiency on circulating lipoprotein clearance as previously demonstrated (149).

5. Role of macrophage LAL in lipid and carbohydrate metabolism

5.1 Introduction

Macrophages are components of innate immunity and influence the metabolism of other cells metabolism by secreting a wide variety of cytokines. Cells of the monocyte-macrophage lineage are characterized by remarkable plasticity and they regulate tissue remodeling and homeostatsis, host defense and tumor progression (187). Whether macrophages metabolize glucose or FA has a clear consequence on polarization and thus their ability to induce particular effects (188). Interestingly, acid lipolysis delivers FA necessary for alternative polarization of differentiated macrophages, beneficially involved in wound healing, anti-inflammatory and anti-tumoral responses(189). In Lal-/- mice, myeloid precursors fail to differentiate to mature macrophages and become myeloid-derived suppressive cells (MDSC), first described as tumor-associated macrophages. Indeed, Lal-/- mice have increased inflammation and tumor metastasis susceptibility and increased circulating myeloid cells (97, 190). Macrophages have a crucial function in clearing apoptotic cells and thus preventing consequential inflammatory responses in a process called efferocytosis (191). Our recent research proved that LAL -derived cholesterol signaling is crucial for efferocytosis and macrophage LAL deficiency hampers immune homeostasis and blocks liver and spleen reactions in repairing physiological cellular debris (99).

LAL deficiency causes severe hepatosplenomegaly, and liver resident macrophages (Kupffer cells) play a central role in the pathology evolution as they become hyperplasic and hypertrophic, which is indicative of a crucial role for LAL in modulating macrophage function. Lal-/- mice present a gradual shift in lipid accumulation from hepatocytes to Kupffer cells with cholesterol crystal formation (92, 93), suggesting an important role of Kupffer cells in liver cholesterol metabolism. Restoring LAL in macrophages of Lal-/- mice and Wolman Disease patients (74, 94) improved the pathological manifestations caused by LAL deficiency, at the same time proving the crucial role of macrophage LAL in energy metabolism and immune system homeostasis. To precisely determine the role of macrophage LAL in global energy metabolism, we generated myeloid-specific

LAL-deficient mice (macLal-/-). Surprisingly, our data show that LAL is dispensable for macrophage function in the context of LAL deletion only cells of myeloid lineage. macLal-/- mice lack the expected metabolic effects on chow and HF/HCD, and, unlike Lal-/- mice, have normal growth. Macrophage and inflammation markers in the liver and intestine of macLal-/- mice were comparable to controls. We speculate that either the observed residual LAL activity is sufficient for TG and CE acid hydrolysis or macrophages undergo functional adaptations to compensate for LAL deficiency. The latter hypothesis remains to be clarified in future studies.

5.2 Results

LAL is efficiently knocked out in macrophages of macLal-/- mice

Lal-/- mice have an overall increased inflammatory profile mainly due to macrophage infiltration in multiple organs like lungs, liver, and intestine (92, 95). To discriminate between global and cell-specific effects triggered by LAL deletion, we generated macLal-/- mice. For this purpose, we used a Cre/loxP recombination system and crossed mice carrying both floxed Lal alleles with mice expressing a Cre-recombinase under the Lysozyme M gene promoter, present in myeloid cells, including macrophages (192). To verify the efficient deletion of LAL, we performed a series of experiments using thioglycollate-elicited mouse peritoneal macrophages. macLal-/- mice hax markedly decreased Lal mRNA and virtually no protein expression in macrophages cultured for 24 h after harvest (Fig. 39A, B). We found no differences between WT and macLal-/- mice in liver and intestinal Lal mRNA expression (Fig. 39A), two of the most affected organs by global LAL deficiency. These results indicate no effect of macrophage LAL deletion on liver and intestinal Lal expression. Next, we measured LAL activity in peritoneal macrophages cultured over a period of 74 h after harvesting. Previous reports showed reduced Lal expression in M1 polarized (hence inflammatory) macrophages (189). Accordingly, we observed a decrease in LAL activity in WT cells cultured for 2 h compared to 24, 48 and 72 h cultured macrophages confirming that LAL activity is decreased due to the inflammatory effect of thioglycollate (Fig. 39C). Compared to WT cells, macrophages from macLal-/- mice had decreased but still more LAL activity than the cells harvested from Lal-/- mice (Fig. 39C). To determine the exact residual activity preserved in the macLal-/- macrophages, we incubated cell lysates from WT, macLal-/-, and Lal-/- mice with or without Lalistat2. Indeed, macrophages from macLal-/- mice had on average 2-fold higher activity than the cells isolated from Lal-/- mice. This activity which could be inhibited by Lalistat2 (Fig. 39D).

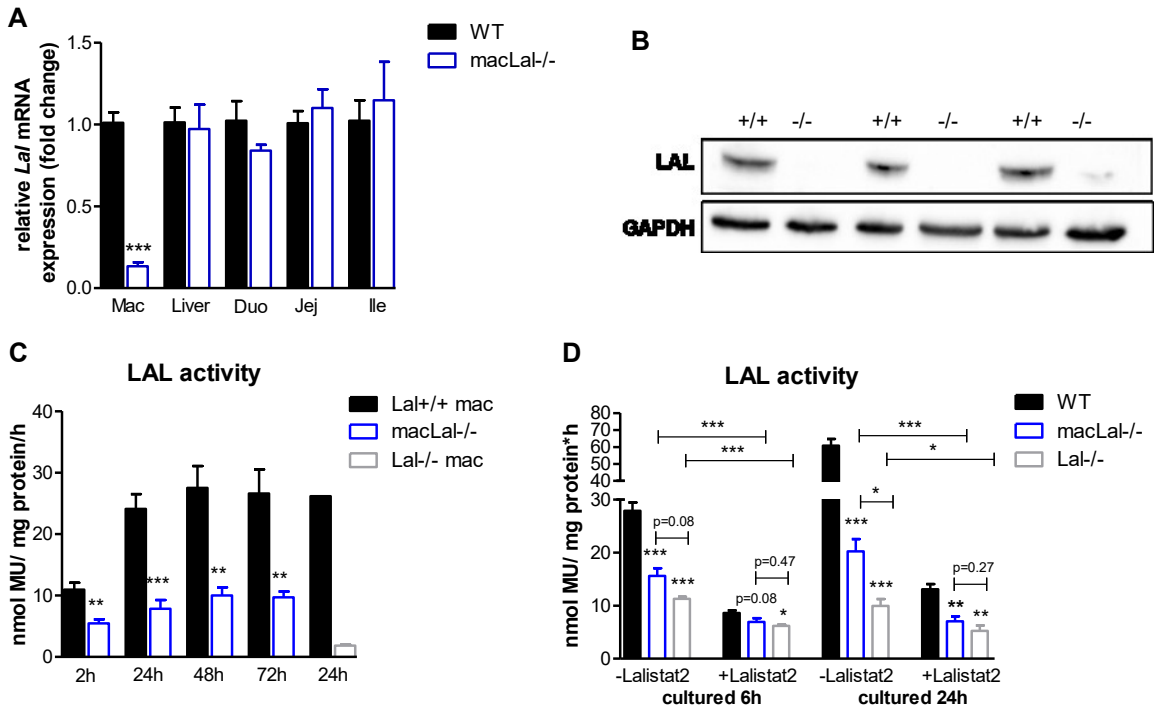

Figure 39: macLal-/- mice have no LAL protein expression in macrophages, but present residual LAL activity

(A) Lal mRNA expression in macrophages, liver, and small intestine. (B) Immunoblotting against LAL in macrophages using GAPDH as loading control. (C) LAL activity over 72 h of culture after harvesting and (D) LAL activity in macrophages cultured 6 h or 24 h after harvesting in the absence or presence of Lalistat 2. Data represent means ± SEM; n=3-9; $p < 0.05$ (*), $p \leq 0.01$ (**), $p \leq 0.001$ (***). Student's unpaired t test.

LAL deficiency in macrophages does neither impact weight gain nor lipid and glucose metabolism in chow diet-fed macLal-/- mice

macLal-/- mice are viable with no apparent changes in health status and have comparable BW gain on chow diet (Fig. 40A). Moreover, both males and females are phenotypically identical and therefore we used both genders for our studies. Previous studies showed that restoring LAL expression only in macrophages from Lal-/- mice markedly reduced lysosomal lipids accumulation and inflammation (94), indicating that functional macrophage LAL is essential for lipid metabolism homeostasis. However, in mice fed chow diet, macrophage LAL deletion showed no effect on plasma parameters in fed (Fig. 40B) or fasted (Fig. 40C) conditions or on lipoprotein distribution of cholesterol (Fig. 40D) and TG (Fig. 40E). Lal-/- mice have impaired liver VLDL secretion, decreased blood glucose concentrations and improved glucose tolerance (93) yet macLal-/- mice lacked these effects (Fig. 40F-H). Organs weights (Fig. 40I) and glucose tolerance test were similar between

both genotypes in 60 weeks old mice. These data indicate that unlike global Lal-/- mice, LAL deficiency in myeloid cells does neither cause a pathological phenotype, nor progressive organ modifications in mice fed chow diet.

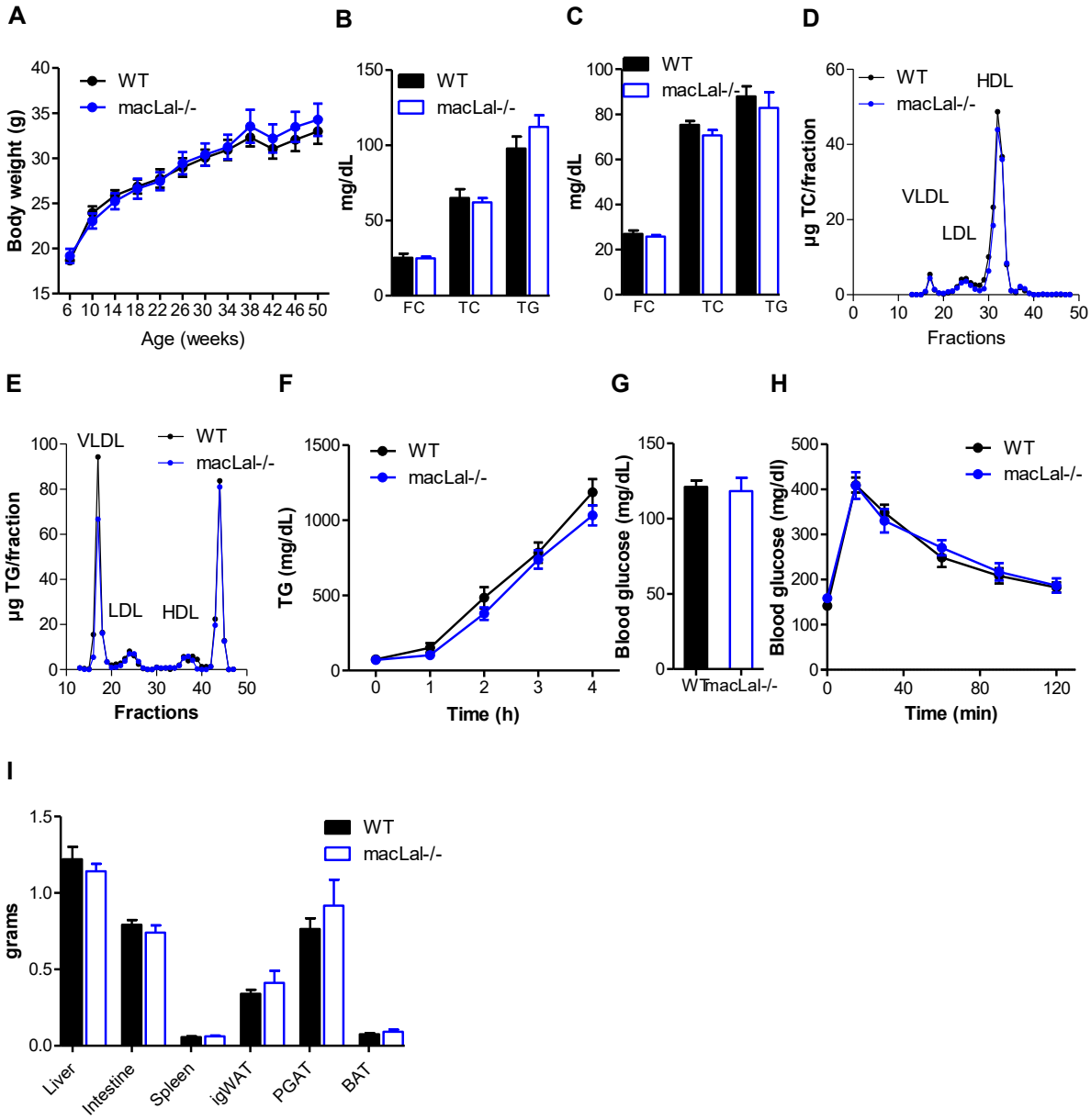

Figure 40: LAL deficiency in macrophages does not impact weight gain, lipid and glucose metabolism in chow fed macLal-/- mice. (A) BW curves of male mice fed chow diet. Plasma lipid parameters of 8 weeks old mice in the (B) fed and (C) 15 weeks old mice fasted overnight. Lipoprotein profiles of (D) TC and (E) TG after separation by fast performance liquid chromatography of pooled plasma. (F) VLDL secretion of 12 h-fasted mice (20 weeks old) after tyloxapol injection. (G) Blood glucose concentrations of 12 h fasted mice (15 weeks old) and (H) glucose tolerance test (14 weeks old). (I) Organ weights of mice aged 60 weeks. Data represent means ± SEM; n=5-7. (B, C, G, I) Student's unpaired t test; (A, F, H) ANOVA.

WT and macLal-/- mice have comparable BW gain, lipid and carbohydrate metabolism on HF/HCD

To check if any of the effects observed in Lal-/- mice are caused by the lack of the enzyme in macrophages, we challenged the mice with HF/HCD for 10 weeks. Over the entire feeding period, macLal-/- mice gained weight to the same extent as their WT controls (Fig. 41A). We measured plasma parameters in both fed and fasted states and found no effect on circulating FC, TC, and TG concentrations (Fig. 41B, C). Lipoprotein distribution of TC and TG were similar between genotypes. After 7 weeks on HF/HCD, macLal-/- mice had comparable blood glucose concentrations in the fasted state (Fig. 41E) and glucose tolerance (Fig. 41F). Serum transaminase concentrations and liver lipid levels were similar between the genotypes (Fig. 41G, H). Lal-/- mice have abundant macrophage accumulation in livers and intestines as shown in previous studies, in immunohistochemistry and H&E-stained tissue sections (92, 94). We measured mRNA gene expression of inflammatory markers in liver and intestines of WT and Lal-/- fed WTD for 6 weeks and WT and macLal-/- mice fed HF/HCD for 10 weeks. We found increased Emr1 gene expression (macrophage marker) in the livers and jejunum of Lal-/- mice and no difference in hepatic and intestinal Emr1 transcripts in macLal-/- mice. Lal-/- mice had markedly increased Tnfα mRNA expression in both liver and intestine, whereas macLal-/- mice exhibited only a slight increase in TNFα in duodenum (Fig. 41J). Il1β was increased in the livers of Lal-/- mice (Fig. 41K). Overall our data show no effect of HF/HCD BW gain, plasma cholesterol, TG, glucose metabolism, liver lipids, hepatic and intestinal inflammation in macLal-/- compared to WT mice.

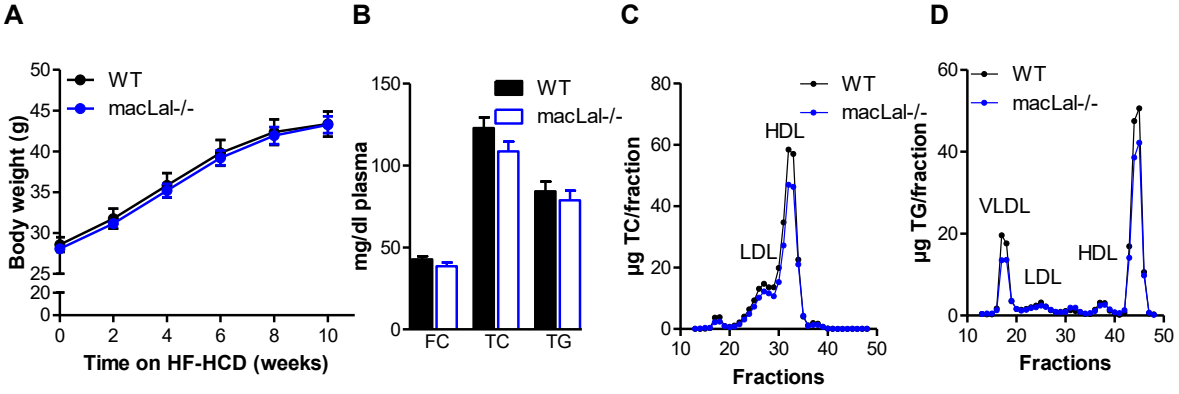

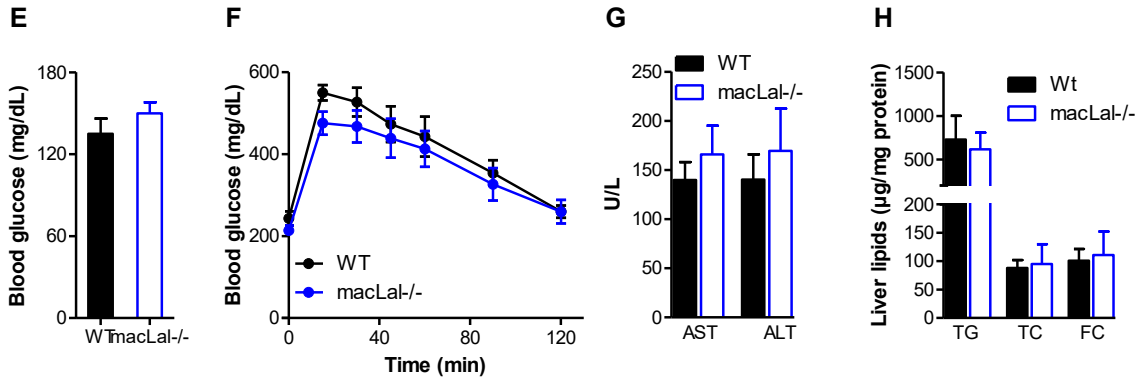

Figure 41: WT and macLal-/- mice have comparable BW gain, lipid and carbohydrate metabolism on HF/HCD. (A) BW curves of male mice fed HF/HCD. (B) Plasma lipid parameters of mice after 6 weeks on HF/HCD fasted overnight. Lipoprotein profiles of (C) TC and (D) TG after separation by fast performance liquid chromatography of pooled plasma. (E) Overnight fasted blood glucose and (F) glucose tolerance test in mice after 6 weeks on HF/HCD; n=9-11. (G) Concentrations of serum transaminases of 10 weeks HF/HCD fed and overnight fasted mice and (H) biochemical quantification of TG, TC, and FC in liver (n=4-6); mRNA expression of (I) *Emr1*, (J) *Tnfα* and (K) *Il1β* in liver and intestine from WT (Lal+/+) Lal-/- mice fed for 6 weeks WTD and fasted overnight or WT (macLal+/+) and macLal-/- mice fed for 10 weeks HF/HCD and fasted overnight, relative to cyclophilin A expression as reference gene. Expression profiles were determined using the $2^{-\Delta\Delta Ct}$ method. Data represent means + SEM; n=4; $p < 0.05$ (*), $p \leq 0.01$ (**), $p \leq 0.001$ (***). Data represent means ±SEM; (B), (E), (G), (H), (I), (J), (K) Student's unpaired t test; (A), (F) ANOVA.

5.3 Discussion

LAL deficiency in mice and humans leads to marked liver lipid accumulation, increased circulating transaminases concentrations, and elevated plasma cholesterol in the LDL fraction accompanied by decreased HDL cholesterol. Additionally, Lal-/- mice have reduced body fat, improved glucose tolerance, and reduced blood glucose in both fed and fasted states. (57, 92, 93, 96). The pathological manifestations are highlighted by abundant infiltration of foamy macrophages in multiple organs like thymus, lungs, liver, spleen and intestine (92, 95, 193). Restoring LAL only in the macrophages of Lal-/- mice improved the pathogenic phenotype, suggesting that macrophages play a central role in the pathogenic phenotype of Lal-/- mice (94). However, also hepatocyte (169) and lung epithelial cell (194) LAL re-expression in Lal-/- mice improved the phenotype. Bone marrow and liver transplantations in LAL-D patients were only partly successful and often followed by severe complications (74, 75).

To decipher the contribution of macrophage LAL on lipid and carbohydrate metabolism, we generated macLal-/- mice. Although LAL was effectively knocked-out in macrophages with virtually no protein expression, we were able to detect some residual enzyme activity. macLal-/- mice had normal growth at least until 50 weeks of age, with no modification in liver VLDL production, glucose tolerance, and organs weight compared to WT animals. Conversely, global Lal-/- mice present growth retardation already at young age and further loose WAT but accumulate unhydrolyzed lipids in other organs and cells i.e. their liver weight reached 3-fold increase in size compared to WT mice by the age of 20 weeks. This lack of metabolic changes in macLal-/- mice was in strong contrast to Lal-/- mice, indicating that LAL deficiency in macrophages results in a metabolic decompensation only in a multi-factorial environment. Among contributing factors, additional stress induced by diets enriched in calories and cholesterol may reveal macrophage-dependent CE and TG recycling. Therefore we hypothesized that, by challenging macLal-/- mice with HF/HCD we would detect global effects caused by blunted macrophage lysosomal neutral lipid hydrolysis. Although we observed the feeding consequence in BW gain, glucose and lipid metabolism, both WT and macLal-/- mice fed HF/HCD were phenotypically similar. Hepatic lipid quantification showed no additional fat accumulation in the macLal-/- mice and

serum transaminases revealed similar values to WT controls. Opposite to macLal-/- mice, Lal-/- mice have increased macrophage accumulation and inflammation in liver and intestine. These data are rather intriguing given that decreases in LAL activity were reported in patients with NAFLD and NASH (195). Nevertheless it unclear to date if this modification is a causal factor or a consequence of the liver injury present in such conditions. Our results show that LAL deficiency only in myeloid cells does not impact lipid and carbohydrate metabolism and that hepatic and intestinal inflammation are not affected by a HF/HCD challenge in macLal-/- mice. LAL is a secreted enzyme and can be taken up via mannose receptors (23, 27, 28). Therefore, it is quite likely that in macLal-/- mice, macrophages have sufficient exogenous enzyme supply to sustain metabolic homeostasis. It is thus likely that the observed residual LAL activity is sufficient for TG and CE acid hydrolysis in macrophages. Furthermore future studies exploring macrophage LAL contribution to highly inflammatory conditions like atherosclerosis and infection will elucidate the questions not addressed by the current study.

6. References

1. Zechner R, Madeo F, Kratky D. Cytosolic lipolysis and lipophagy: two sides of the same coin. Nat Rev Mol Cell Biol. 2017 Nov;18(11):671-84. PubMed PMID: 28852221.

2. Brown MS, Goldstein JL. Receptor-mediated control of cholesterol metabolism. Science. 1976 Jan 16;191(4223):150-4. PubMed PMID: 174194.

3. Schneider WJ, Beisiegel U, Goldstein JL, Brown MS. Purification of the low density lipoprotein receptor, an acidic glycoprotein of 164,000 molecular weight. The Journal of biological chemistry. 1982 Mar 10;257(5):2664-73. PubMed PMID: 6277909.

4. Goldstein JL, Dana SE, Faust JR, Beaudet AL, Brown MS. Role of lysosomal acid lipase in the metabolism of plasma low density lipoprotein. Observations in cultured fibroblasts from a patient with cholesteryl ester storage disease. The Journal of biological chemistry. 1975 Nov 10;250(21):8487-95. PubMed PMID: 172501.

5. Goldstein JL, Brunschede GY, Brown MS. Inhibition of proteolytic degradation of low density lipoprotein in human fibroblasts by chloroquine, concanavalin A, and Triton WR 1339. The Journal of biological chemistry. 1975 Oct 10;250(19):7854-62. PubMed PMID: 170273.

6. Brown MS, Goldstein JL. Receptor-mediated endocytosis: insights from the lipoprotein receptor system. Proceedings of the National Academy of Sciences of the United States of America. 1979 Jul;76(7):3330-7. PubMed PMID: 226968. Pubmed Central PMCID: 383819.

7. Goldstein JL, Brown MS. The LDL receptor. Arteriosclerosis, thrombosis, and vascular biology. 2009 Apr;29(4):431-8. PubMed PMID: 19299327. Pubmed Central PMCID: 2740366.

8. Ouimet M, Franklin V, Mak E, Liao X, Tabas I, Marcel YL. Autophagy regulates cholesterol efflux from macrophage foam cells via lysosomal acid lipase. Cell metabolism. 2011 Jun 8;13(6):655-67. PubMed PMID: 21641547. Pubmed Central PMCID: 3257518.

9. Singh R, Cuervo AM. Lipophagy: connecting autophagy and lipid metabolism. International journal of cell biology. 2012;2012:282041. PubMed PMID: 22536247. Pubmed Central PMCID: 3320019.

10. Singh R, Kaushik S, Wang Y, Xiang Y, Novak I, Komatsu M, et al. Autophagy regulates lipid metabolism. Nature. 2009 Apr 30;458(7242):1131-5. PubMed PMID: 19339967. Pubmed Central PMCID: 2676208.
11. Kaushik S, Cuervo AM. Degradation of lipid droplet-associated proteins by chaperone-mediated autophagy facilitates lipolysis. Nature cell biology. 2015 Jun;17(6):759-70. PubMed PMID: 25961502. Pubmed Central PMCID: 4449813.
12. Martinez-Lopez N, Garcia-Macia M, Sahu S, Athonvarangkul D, Liebling E, Merlo P, et al. Autophagy in the CNS and Periphery Coordinate Lipophagy and Lipolysis in the Brown Adipose Tissue and Liver. Cell metabolism. 2016 Jan 12;23(1):113-27. PubMed PMID: 26698918. Pubmed Central PMCID: 4715637.
13. Jeong SJ, Lee MN, Oh GT. The Role of Macrophage Lipophagy in Reverse Cholesterol Transport. Endocrinology and metabolism. 2017 Mar;32(1):41-6. PubMed PMID: 28345315. Pubmed Central PMCID: 5368120.
14. Moore KJ, Sheedy FJ, Fisher EA. Macrophages in atherosclerosis: a dynamic balance. Nature reviews Immunology. 2013 Oct;13(10):709-21. PubMed PMID: 23995626. Pubmed Central PMCID: 4357520.
15. Ikonen E. Cellular cholesterol trafficking and compartmentalization. Nat Rev Mol Cell Biol. 2008 Feb;9(2):125-38. PubMed PMID: 18216769.
16. Grumet L, Eichmann TO, Taschler U, Zierler KA, Leopold C, Moustafa T, et al. Lysosomal Acid Lipase Hydrolyzes Retinyl Ester and Affects Retinoid Turnover. The Journal of biological chemistry. 2016 Aug 19;291(34):17977-87. PubMed PMID: 27354281. Pubmed Central PMCID: 5016185.
17. Warner TG, Dambach LM, Shin JH, O'Brien JS. Purification of the lysosomal acid lipase from human liver and its role in lysosomal lipid hydrolysis. The Journal of biological chemistry. 1981 Mar 25;256(6):2952-7. PubMed PMID: 7204383.
18. Hayase K, Tappel AL. Specificity and other properties of lysosomal lipase of rat liver. The Journal of biological chemistry. 1970 Jan 10;245(1):169-75. PubMed PMID: 5413966.
19. Anderson RA, Sando GN. Cloning and expression of cDNA encoding human lysosomal acid lipase/cholesteryl ester hydrolase. Similarities to gastric and lingual lipases. The Journal of biological chemistry. 1991 Nov 25;266(33):22479-84. PubMed PMID: 1718995.

20. Anderson RA, Rao N, Byrum RS, Rothschild CB, Bowden DW, Hayworth R, et al. In situ localization of the genetic locus encoding the lysosomal acid lipase/cholesteryl esterase (LIPA) deficient in Wolman disease to chromosome 10q23.2-q23.3. Genomics. 1993 Jan;15(1):245-7. PubMed PMID: 8432549.

21. Anderson RA, Byrum RS, Coates PM, Sando GN. Mutations at the lysosomal acid cholesteryl ester hydrolase gene locus in Wolman disease. Proceedings of the National Academy of Sciences of the United States of America. 1994 Mar 29;91(7):2718-22. PubMed PMID: 8146180. Pubmed Central PMCID: 43441.

22. Ameis D, Merkel M, Eckerskorn C, Greten H. Purification, characterization and molecular cloning of human hepatic lysosomal acid lipase. European journal of biochemistry. 1994 Feb 1;219(3):905-14. PubMed PMID: 8112342.

23. Sando GN, Rosenbaum LM. Human lysosomal acid lipase/cholesteryl ester hydrolase. Purification and properties of the form secreted by fibroblasts in microcarrier culture. The Journal of biological chemistry. 1985 Dec 5;260(28):15186-93. PubMed PMID: 4066668.

24. Du H, Witte DP, Grabowski GA. Tissue and cellular specific expression of murine lysosomal acid lipase mRNA and protein. J Lipid Res. 1996 May;37(5):937-49. PubMed PMID: 8725147.

25. Sheriff S, Du H, Grabowski GA. Characterization of lysosomal acid lipase by site-directed mutagenesis and heterologous expression. The Journal of biological chemistry. 1995 Nov 17;270(46):27766-72. PubMed PMID: 7499245.

26. Ullrich K, Mersmann G, Weber E, Von Figura K. Evidence for lysosomal enzyme recognition by human fibroblasts via a phosphorylated carbohydrate moiety. The Biochemical journal. 1978 Mar 15;170(3):643-50. PubMed PMID: 646806. Pubmed Central PMCID: 1183943.

27. Sando GN, Henke VL. Recognition and receptor-mediated endocytosis of the lysosomal acid lipase secreted by cultured human fibroblasts. J Lipid Res. 1982 Jan;23(1):114-23. PubMed PMID: 7057100.

28. Sando GN, Ma GP, Lindsley KA, Wei YP. Intercellular transport of lysosomal acid lipase mediates lipoprotein cholesteryl ester metabolism in a human vascular endothelial cell-fibroblast coculture system. Cell regulation. 1990 Aug;1(9):661-74. PubMed PMID: 2150334. Pubmed Central PMCID: 361630.

29. Du H, Levine M, Ganesa C, Witte DP, Cole ES, Grabowski GA. The role of mannosylated enzyme and the mannose receptor in enzyme replacement therapy. American journal of human genetics. 2005 Dec;77(6):1061-74. PubMed PMID: 16380916. Pubmed Central PMCID: 1285163.

30. Koch G, Lalley PA, McAvoy M, Shows TB. Assignment of LIPA, associated with human acid lipase deficiency, to human chromosome 10 and comparative assignment to mouse chromosome 19. Somatic cell genetics. 1981 May;7(3):345-58. PubMed PMID: 7292252.

31. Du H, Duanmu M, Rosa LR. Mouse lysosomal acid lipase: characterization of the gene and analysis of promoter activity. Gene. 1998 Feb 27;208(2):285-95. PubMed PMID: 9524282.

32. Roczniak-Ferguson A, Petit CS, Froehlich F, Qian S, Ky J, Angarola B, et al. The transcription factor TFEB links mTORC1 signaling to transcriptional control of lysosome homeostasis. Science signaling. 2012 Jun 12;5(228):ra42. PubMed PMID: 22692423. Pubmed Central PMCID: 3437338.

33. Laplante M, Sabatini DM. Regulation of mTORC1 and its impact on gene expression at a glance. Journal of cell science. 2013 Apr 15;126(Pt 8):1713-9. PubMed PMID: 23641065. Pubmed Central PMCID: 3678406.

34. Martina JA, Chen Y, Gucek M, Puertollano R. MTORC1 functions as a transcriptional regulator of autophagy by preventing nuclear transport of TFEB. Autophagy. 2012 Jun;8(6):903-14. PubMed PMID: 22576015. Pubmed Central PMCID: 3427256.

35. Emanuel R, Sergin I, Bhattacharya S, Turner J, Epelman S, Settembre C, et al. Induction of lysosomal biogenesis in atherosclerotic macrophages can rescue lipid-induced lysosomal dysfunction and downstream sequelae. Arteriosclerosis, thrombosis, and vascular biology. 2014 Sep;34(9):1942-52. PubMed PMID: 25060788. Pubmed Central PMCID: 4140993.

36. Settembre C, De Cegli R, Mansueto G, Saha PK, Vetrini F, Visvikis O, et al. TFEB controls cellular lipid metabolism through a starvation-induced autoregulatory loop. Nature cell biology. 2013 Jun;15(6):647-58. PubMed PMID: 23604321. Pubmed Central PMCID: 3699877.

37. Dubland JA, Francis GA. Lysosomal acid lipase: at the crossroads of normal and atherogenic cholesterol metabolism. Frontiers in cell and

developmental biology. 2015;3:3. PubMed PMID: 25699256. Pubmed Central PMCID: 4313778.

38. Chakrabarti P, English T, Karki S, Qiang L, Tao R, Kim J, et al. SIRT1 controls lipolysis in adipocytes via FOXO1-mediated expression of ATGL. J Lipid Res. 2011 Sep;52(9):1693-701. PubMed PMID: 21743036. Pubmed Central PMCID: 3151689.

39. Lettieri Barbato D, Tatulli G, Aquilano K, Ciriolo MR. FoxO1 controls lysosomal acid lipase in adipocytes: implication of lipophagy during nutrient restriction and metformin treatment. Cell death & disease. 2013 Oct 17;4:e861. PubMed PMID: 24136225. Pubmed Central PMCID: 3920962.

40. Cox BE, Griffin EE, Ullery JC, Jerome WG. Effects of cellular cholesterol loading on macrophage foam cell lysosome acidification. J Lipid Res. 2007 May;48(5):1012-21. PubMed PMID: 17308299.

41. Li W, Yuan XM, Olsson AG, Brunk UT. Uptake of oxidized LDL by macrophages results in partial lysosomal enzyme inactivation and relocation. Arteriosclerosis, thrombosis, and vascular biology. 1998 Feb;18(2):177-84. PubMed PMID: 9484981.

42. Griffin EE, Ullery JC, Cox BE, Jerome WG. Aggregated LDL and lipid dispersions induce lysosomal cholesteryl ester accumulation in macrophage foam cells. J Lipid Res. 2005 Oct;46(10):2052-60. PubMed PMID: 16024919.

43. Lukacs Z, Barr M, Hamilton J. Best practice in the measurement and interpretation of lysosomal acid lipase in dried blood spots using the inhibitor Lalistat 2. Clinica chimica acta; international journal of clinical chemistry. 2017 Aug;471:201-5. PubMed PMID: 28532785.

44. Brown WJ, Sgoutas DS. Purification of rat liver lysosomal cholesteryl ester hydrolase. Biochimica et biophysica acta. 1980 Feb 22;617(2):305-17. PubMed PMID: 7357021.

45. Mahadevan S, Tappel AL. Lysosomal lipases of rat liver and kidney. The Journal of biological chemistry. 1968 Jun 10;243(11):2849-54. PubMed PMID: 5653176.

46. Stokke KT. Subcellular distribution and kinetics of the acid cholesterol esterase in liver. Biochimica et biophysica acta. 1972 Oct 5;280(2):329-35. PubMed PMID: 4345144.

47. Imanaka T, Amanuma-Muto K, Ohkuma S, Takano T. Effects of phospholipids on lysosomal acid lipase purified from rabbit liver. Journal of biochemistry. 1983 Jun;93(6):1517-21. PubMed PMID: 6885736.

48. Klemets R, Lundberg B. Substrate specificity of lysosomal cholesteryl ester hydrolase isolated from rat liver. Lipids. 1986 Aug;21(8):481-5. PubMed PMID: 3762320.

49. Villamil Giraldo AM, Appelqvist H, Ederth T, Ollinger K. Lysosomotropic agents: impact on lysosomal membrane permeabilization and cell death. Biochem Soc Trans. 2014 Oct;42(5):1460-4. PubMed PMID: 25233432.

50. Hamilton J, Jones I, Srivastava R, Galloway P. A new method for the measurement of lysosomal acid lipase in dried blood spots using the inhibitor Lalistat 2. Clinica chimica acta; international journal of clinical chemistry. 2012 Aug 16;413(15-16):1207-10. PubMed PMID: 22483793.

51. Rosenbaum AI, Cosner CC, Mariani CJ, Maxfield FR, Wiest O, Helquist P. Thiadiazole carbamates: potent inhibitors of lysosomal acid lipase and potential Niemann-Pick type C disease therapeutics. Journal of medicinal chemistry. 2010 Jul 22;53(14):5281-9. PubMed PMID: 20557099. Pubmed Central PMCID: 2912405.

52. Rosenbaum AI, Rujoi M, Huang AY, Du H, Grabowski GA, Maxfield FR. Chemical screen to reduce sterol accumulation in Niemann-Pick C disease cells identifies novel lysosomal acid lipase inhibitors. Biochimica et biophysica acta. 2009 Dec;1791(12):1155-65. PubMed PMID: 19699313. Pubmed Central PMCID: 2783675.

53. Schlager S, Vujic N, Korbelius M, Duta-Mare M, Dorow J, Leopold C, et al. Lysosomal lipid hydrolysis provides substrates for lipid mediator synthesis in murine macrophages. Oncotarget. 2017 Jun 20;8(25):40037-51. PubMed PMID: 28402950. Pubmed Central PMCID: 5522325.

54. Rosenbaum AI, Maxfield FR. Niemann-Pick type C disease: molecular mechanisms and potential therapeutic approaches. Journal of neurochemistry. 2011 Mar;116(5):789-95. PubMed PMID: 20807315. Pubmed Central PMCID: 3008286.

55. Gandarias JM, Lacort M, Martinez MJ, De Nicolas MA, Ochoa B. Cholesteryl ester hydrolysis in rat liver lysosomes: different response to female

sex hormones. Biochemical medicine and metabolic biology. 1986 Aug;36(1):14-24. PubMed PMID: 3741699.

56. Imanaka T, Moriyama Y, Ecsedi GG, Aoyagi T, Amanuma-Muto K, Ohkuma S, et al. Esterastin: a potent inhibitor of lysosomal acid lipase. Journal of biochemistry. 1983 Sep;94(3):1017-20. PubMed PMID: 6643414.

57. Bernstein DL, Hulkova H, Bialer MG, Desnick RJ. Cholesteryl ester storage disease: review of the findings in 135 reported patients with an underdiagnosed disease. Journal of hepatology. 2013 Jun;58(6):1230-43. PubMed PMID: 23485521.

58. Aguisanda F, Thorne N, Zheng W. Targeting Wolman Disease and Cholesteryl Ester Storage Disease: Disease Pathogenesis and Therapeutic Development. Current chemical genomics and translational medicine. 2017;11:1-18. PubMed PMID: 28401034. Pubmed Central PMCID: 5362971.

59. Abramov A, Schorr S, Wolman M. Generalized xanthomatosis with calcified adrenals. AMA journal of diseases of children. 1956 Mar;91(3):282-6. PubMed PMID: 13301142.

60. Boldrini R, Devito R, Biselli R, Filocamo M, Bosman C. Wolman disease and cholesteryl ester storage disease diagnosed by histological and ultrastructural examination of intestinal and liver biopsy. Pathology, research and practice. 2004;200(3):231-40. PubMed PMID: 15200275.

61. Grabowski GA, Du H, Charnas L. Lysosomal Acid Lipase Deficiencies: The Wolman Disease/Cholesteryl Ester Storage Disease Spectrum. Metabolic and molecular bases of inherited disease – OMMBID 2012

62. Patrick AD, Lake BD. Deficiency of an acid lipase in Wolman's disease. Nature. 1969 Jun 14;222(5198):1067-8. PubMed PMID: 5787090.

63. Pericleous M, Kelly C, Wang T, Livingstone C, Ala A. Wolman's disease and cholesteryl ester storage disorder: the phenotypic spectrum of lysosomal acid lipase deficiency. The lancet Gastroenterology & hepatology. 2017 Sep;2(9):670-9. PubMed PMID: 28786388.

64. vom Dahl S, Harzer K, Rolfs A, Albrecht B, Niederau C, Vogt C, et al. Hepatosplenomegalic lipidosis: what unless Gaucher? Adult cholesteryl ester storage disease (CESD) with anemia, mesenteric lipodystrophy, increased plasma chitotriosidase activity and a homozygous lysosomal acid lipase -1 exon 8 splice

junction mutation. Journal of hepatology. 1999 Oct;31(4):741-6. PubMed PMID: 10551400.
65. Fouchier SW, Defesche JC. Lysosomal acid lipase A and the hypercholesterolaemic phenotype. Current opinion in lipidology. 2013 Aug;24(4):332-8. PubMed PMID: 23652569.
66. Zhang B, Porto AF. Cholesteryl ester storage disease: protean presentations of lysosomal acid lipase deficiency. Journal of pediatric gastroenterology and nutrition. 2013 Jun;56(6):682-5. PubMed PMID: 23403440.
67. Kostner GM, Hadorn B, Roscher A, Zechner R. Plasma lipids and lipoproteins of a patient with cholesteryl ester storage disease. Journal of inherited metabolic disease. 1985;8(1):9-12. PubMed PMID: 3921762.
68. Valayannopoulos V, Mengel E, Brassier A, Grabowski G. Lysosomal acid lipase deficiency: Expanding differential diagnosis. Molecular genetics and metabolism. 2017 Jan - Feb;120(1-2):62-6. PubMed PMID: 27876313.
69. Reiner Z, Guardamagna O, Nair D, Soran H, Hovingh K, Bertolini S, et al. Lysosomal acid lipase deficiency--an under-recognized cause of dyslipidaemia and liver dysfunction. Atherosclerosis. 2014 Jul;235(1):21-30. PubMed PMID: 24792990.
70. Beaudet AL, Ferry GD, Nichols BL, Jr., Rosenberg HS. Cholesterol ester storage disease: clinical, biochemical, and pathological studies. The Journal of pediatrics. 1977 Jun;90(6):910-4. PubMed PMID: 859064.
71. HH AK. Lysosomal acid lipase deficiency: a form of non-obese fatty liver disease (NOFLD). Expert review of gastroenterology & hepatology. 2017 Oct;11(10):911-24. PubMed PMID: 28612634.
72. Maciejko JJ. Managing Cardiovascular Risk in Lysosomal Acid Lipase Deficiency. American journal of cardiovascular drugs : drugs, devices, and other interventions. 2017 Jun;17(3):217-31. PubMed PMID: 28197978.
73. Dairaku T, Iwamoto T, Nishimura M, Endo M, Ohashi T, Eto Y. A practical fluorometric assay method to measure lysosomal acid lipase activity in dried blood spots for the screening of cholesteryl ester storage disease and Wolman disease. Molecular genetics and metabolism. 2014 Feb;111(2):193-6. PubMed PMID: 24295952.

74. Krivit W, Peters C, Dusenbery K, Ben-Yoseph Y, Ramsay NK, Wagner JE, et al. Wolman disease successfully treated by bone marrow transplantation. Bone marrow transplantation. 2000 Sep;26(5):567-70. PubMed PMID: 11019848.
75. Bernstein DL, Lobritto S, Iuga A, Remotti H, Schiano T, Fiel MI, et al. Lysosomal acid lipase deficiency allograft recurrence and liver failure- clinical outcomes of 18 liver transplantation patients. Molecular genetics and metabolism. 2018 Mar 27. PubMed PMID: 29655841.
76. Su K, Donaldson E, Sharma R. Novel treatment options for lysosomal acid lipase deficiency: critical appraisal of sebelipase alfa. The application of clinical genetics. 2016;9:157-67. PubMed PMID: 27799810. Pubmed Central PMCID: 5074735.
77. Du H, Schiavi S, Levine M, Mishra J, Heur M, Grabowski GA. Enzyme therapy for lysosomal acid lipase deficiency in the mouse. Human molecular genetics. 2001 Aug 1;10(16):1639-48. PubMed PMID: 11487567.
78. Sun Y, Xu YH, Du H, Quinn B, Liou B, Stanton L, et al. Reversal of advanced disease in lysosomal acid lipase deficient mice: a model for lysosomal acid lipase deficiency disease. Molecular genetics and metabolism. 2014 Jul;112(3):229-41. PubMed PMID: 24837159.
79. Quinn A, Leavitt M, Hu W, Harvey A, Chen M, Nagy T, et al. SBC-102, a recombinant enzyme replacement therapy corrects clinically relevant phenotypic abnormalities in a rat model of lysosomal acid lipase deficiency. Molecular genetics and metabolism. 2011;102(2):S37.
80. Burton BK, Balwani M, Feillet F, Baric I, Burrow TA, Camarena Grande C, et al. A Phase 3 Trial of Sebelipase Alfa in Lysosomal Acid Lipase Deficiency. The New England journal of medicine. 2015 Sep 10;373(11):1010-20. PubMed PMID: 26352813.
81. Jones SA, Rojas-Caro S, Quinn AG, Friedman M, Marulkar S, Ezgu F, et al. Survival in infants treated with sebelipase Alfa for lysosomal acid lipase deficiency: an open-label, multicenter, dose-escalation study. Orphanet journal of rare diseases. 2017 Feb 8;12(1):25. PubMed PMID: 28179030. Pubmed Central PMCID: 5299659.
82. Valayannopoulos V, Malinova V, Honzik T, Balwani M, Breen C, Deegan PB, et al. Sebelipase alfa over 52 weeks reduces serum transaminases, liver volume and improves serum lipids in patients with lysosomal acid lipase

deficiency. Journal of hepatology. 2014 Nov;61(5):1135-42. PubMed PMID: 24993530. Pubmed Central PMCID: 4203712.

83. Wilson DP, Friedman M, Marulkar S, Hamby T, Bruckert E. Sebelipase alfa improves atherogenic biomarkers in adults and children with lysosomal acid lipase deficiency. Journal of clinical lipidology. 2018 Mar 9. PubMed PMID: 29628368.

84. Balwani M, Breen C, Enns GM, Deegan PB, Honzik T, Jones S, et al. Clinical effect and safety profile of recombinant human lysosomal acid lipase in patients with cholesteryl ester storage disease. Hepatology. 2013 Sep;58(3):950-7. PubMed PMID: 23348766. Pubmed Central PMCID: 3728169.

85. Kanuma - FULL PRESCRIBING INFORMATION. FDA- Food and Drug Adminstration 2015.

86. Kanuma - Report on the Deliberation Results PMDA- Pharmacetuticals and Medical Devices Agency- JAPAN. 2016.

87. Kanuma - Summary of Product Characteristics. European Medicines Agency. 2017.

88. NICE. Evaluation consultation document: Sebelipase alfa for treating lysosomal acid lipase deficiency. NATIONAL INSTITUTE FOR HEALTH AND CARE EXCELLENCE. 2016.

89. Yoshida H, Kuriyama M. Genetic lipid storage disease with lysosomal acid lipase deficiency in rats. Laboratory animal science. 1990 Sep;40(5):486-9. PubMed PMID: 2170747.

90. Kuriyama M, Yoshida H, Suzuki M, Fujiyama J, Igata A. Lysosomal acid lipase deficiency in rats: lipid analyses and lipase activities in liver and spleen. J Lipid Res. 1990 Sep;31(9):1605-12. PubMed PMID: 2246613.

91. Du H, Duanmu M, Witte D, Grabowski GA. Targeted disruption of the mouse lysosomal acid lipase gene: long-term survival with massive cholesteryl ester and triglyceride storage. Human molecular genetics. 1998 Sep;7(9):1347-54. PubMed PMID: 9700186.

92. Du H, Heur M, Duanmu M, Grabowski GA, Hui DY, Witte DP, et al. Lysosomal acid lipase-deficient mice: depletion of white and brown fat, severe hepatosplenomegaly, and shortened life span. J Lipid Res. 2001 Apr;42(4):489-500. PubMed PMID: 11290820.

93. Radovic B, Vujic N, Leopold C, Schlager S, Goeritzer M, Patankar JV, et al. Lysosomal acid lipase regulates VLDL synthesis and insulin sensitivity in mice. Diabetologia. 2016 May 6. PubMed PMID: 27153842.
94. Yan C, Lian X, Li Y, Dai Y, White A, Qin Y, et al. Macrophage-specific expression of human lysosomal acid lipase corrects inflammation and pathogenic phenotypes in lal-/- mice. Am J Pathol. 2006 Sep;169(3):916-26. PubMed PMID: 16936266. Pubmed Central PMCID: 1698822.
95. Lian X, Yan C, Yang L, Xu Y, Du H. Lysosomal acid lipase deficiency causes respiratory inflammation and destruction in the lung. American journal of physiology Lung cellular and molecular physiology. 2004 Apr;286(4):L801-7. PubMed PMID: 14644759.
96. Aqul A, Lopez AM, Posey KS, Taylor AM, Repa JJ, Burns DK, et al. Hepatic entrapment of esterified cholesterol drives continual expansion of whole body sterol pool in lysosomal acid lipase-deficient mice. American journal of physiology Gastrointestinal and liver physiology. 2014 Oct 15;307(8):G836-47. PubMed PMID: 25147230. Pubmed Central PMCID: 4200320.
97. Yan C, Zhao T, Du H. Lysosomal acid lipase in cancer. Oncoscience. 2015;2(9):727-8. PubMed PMID: 26501068. Pubmed Central PMCID: 4605996.
98. Bowden KL, Dubland JA, Chan T, Xu YH, Grabowski GA, Du H, et al. LAL (Lysosomal Acid Lipase) Promotes Reverse Cholesterol Transport In Vitro and In Vivo. Arteriosclerosis, thrombosis, and vascular biology. 2018 May;38(5):1191-201. PubMed PMID: 29599133. Pubmed Central PMCID: 5920716.
99. Viaud M, Ivanov S, Vujic N, Duta-Mare M, Aira LE, Barouillet T, et al. Lysosomal Cholesterol Hydrolysis Couples Efferocytosis to Anti-Inflammatory Oxysterol Production. Circulation research. 2018 Mar 9. PubMed PMID: 29523554.
100. Kaur J. A comprehensive review on metabolic syndrome. Cardiology research and practice. 2014;2014:943162. PubMed PMID: 24711954. Pubmed Central PMCID: 3966331.
101. Aggoun Y. Obesity, metabolic syndrome, and cardiovascular disease. Pediatric research. 2007 Jun;61(6):653-9. PubMed PMID: 17426660.
102. WHO. Definition, diagnosis and classification of diabetes mellitus and its complications : report of a WHO consultation. Wold Health Organisation. 1999.

103. Shaw JE, Chisholm DJ. 1: Epidemiology and prevention of type 2 diabetes and the metabolic syndrome. The Medical journal of Australia. 2003 Oct 6;179(7):379-83. PubMed PMID: 14503906.

104. Alberti KG, Eckel RH, Grundy SM, Zimmet PZ, Cleeman JI, Donato KA, et al. Harmonizing the metabolic syndrome: a joint interim statement of the International Diabetes Federation Task Force on Epidemiology and Prevention; National Heart, Lung, and Blood Institute; American Heart Association; World Heart Federation; International Atherosclerosis Society; and International Association for the Study of Obesity. Circulation. 2009 Oct 20;120(16):1640-5. PubMed PMID: 19805654.

105. Xiao C, Dash S, Morgantini C, Hegele RA, Lewis GF. Pharmacological Targeting of the Atherogenic Dyslipidemia Complex: The Next Frontier in CVD Prevention Beyond Lowering LDL Cholesterol. Diabetes. 2016 Jul;65(7):1767-78. PubMed PMID: 27329952.

106. Boudreau DM, Malone DC, Raebel MA, Fishman PA, Nichols GA, Feldstein AC, et al. Health care utilization and costs by metabolic syndrome risk factors. Metabolic syndrome and related disorders. 2009 Aug;7(4):305-14. PubMed PMID: 19558267.

107. Curtis LH, Hammill BG, Bethel MA, Anstrom KJ, Gottdiener JS, Schulman KA. Costs of the metabolic syndrome in elderly individuals: findings from the Cardiovascular Health Study. Diabetes care. 2007 Oct;30(10):2553-8. PubMed PMID: 17623825.

108. Chan RS, Woo J. Prevention of overweight and obesity: how effective is the current public health approach. International journal of environmental research and public health. 2010 Mar;7(3):765-83. PubMed PMID: 20617002. Pubmed Central PMCID: 2872299.

109. Picot J, Jones J, Colquitt JL, Gospodarevskaya E, Loveman E, Baxter L, et al. The clinical effectiveness and cost-effectiveness of bariatric (weight loss) surgery for obesity: a systematic review and economic evaluation. Health technology assessment. 2009 Sep;13(41):1-190, 215-357, iii-iv. PubMed PMID: 19726018.

110. Batsis JA, Romero-Corral A, Collazo-Clavell ML, Sarr MG, Somers VK, Lopez-Jimenez F. Effect of bariatric surgery on the metabolic syndrome: a

population-based, long-term controlled study. Mayo Clinic proceedings. 2008 Aug;83(8):897-907. PubMed PMID: 18674474. Pubmed Central PMCID: 2714704.
111. Martin KA, Mani MV, Mani A. New targets to treat obesity and the metabolic syndrome. European journal of pharmacology. 2015 Sep 15;763(Pt A):64-74. PubMed PMID: 26001373. Pubmed Central PMCID: 4573317.
112. Wing RR, Lang W, Wadden TA, Safford M, Knowler WC, Bertoni AG, et al. Benefits of modest weight loss in improving cardiovascular risk factors in overweight and obese individuals with type 2 diabetes. Diabetes care. 2011 Jul;34(7):1481-6. PubMed PMID: 21593294. Pubmed Central PMCID: 3120182.
113. Hamdy O, Mottalib A, Morsi A, El-Sayed N, Goebel-Fabbri A, Arathuzik G, et al. Long-term effect of intensive lifestyle intervention on cardiovascular risk factors in patients with diabetes in real-world clinical practice: a 5-year longitudinal study. BMJ open diabetes research & care. 2017;5(1):e000259. PubMed PMID: 28090332. Pubmed Central PMCID: 5223646.
114. Brown JD, Buscemi J, Milsom V, Malcolm R, O'Neil PM. Effects on cardiovascular risk factors of weight losses limited to 5-10. Translational behavioral medicine. 2016 Sep;6(3):339-46. PubMed PMID: 27528523. Pubmed Central PMCID: 4987606.
115. Stevens VJ, Obarzanek E, Cook NR, Lee IM, Appel LJ, Smith West D, et al. Long-term weight loss and changes in blood pressure: results of the Trials of Hypertension Prevention, phase II. Annals of internal medicine. 2001 Jan 2;134(1):1-11. PubMed PMID: 11187414.
116. Look ARG, Wing RR. Long-term effects of a lifestyle intervention on weight and cardiovascular risk factors in individuals with type 2 diabetes mellitus: four-year results of the Look AHEAD trial. Archives of internal medicine. 2010 Sep 27;170(17):1566-75. PubMed PMID: 20876408. Pubmed Central PMCID: 3084497.
117. Nedergaard J, Bengtsson T, Cannon B. Unexpected evidence for active brown adipose tissue in adult humans. American journal of physiology Endocrinology and metabolism. 2007 Aug;293(2):E444-52. PubMed PMID: 17473055.
118. Merklin RJ. Growth and distribution of human fetal brown fat. The Anatomical record. 1974 Mar;178(3):637-45. PubMed PMID: 4856126.

119. Houstek J, Vizek K, Pavelka S, Kopecky J, Krejcova E, Hermanska J, et al. Type II iodothyronine 5'-deiodinase and uncoupling protein in brown adipose tissue of human newborns. The Journal of clinical endocrinology and metabolism. 1993 Aug;77(2):382-7. PubMed PMID: 8393883.
120. Cannon B, Nedergaard J. Nonshivering thermogenesis and its adequate measurement in metabolic studies. The Journal of experimental biology. 2011 Jan 15;214(Pt 2):242-53. PubMed PMID: 21177944.
121. Nedergaard J, Bengtsson T, Cannon B. New powers of brown fat: fighting the metabolic syndrome. Cell metabolism. 2011 Mar 2;13(3):238-40. PubMed PMID: 21356513.
122. Betz MJ, Enerback S. Human Brown Adipose Tissue: What We Have Learned So Far. Diabetes. 2015 Jul;64(7):2352-60. PubMed PMID: 26050667.
123. Cypess AM, Lehman S, Williams G, Tal I, Rodman D, Goldfine AB, et al. Identification and importance of brown adipose tissue in adult humans. The New England journal of medicine. 2009 Apr 9;360(15):1509-17. PubMed PMID: 19357406. Pubmed Central PMCID: 2859951.
124. Scheele C, Nielsen S. Metabolic regulation and the anti-obesity perspectives of human brown fat. Redox biology. 2017 Aug;12:770-5. PubMed PMID: 28431377. Pubmed Central PMCID: 5397125.
125. Chondronikola M, Volpi E, Borsheim E, Porter C, Saraf MK, Annamalai P, et al. Brown Adipose Tissue Activation Is Linked to Distinct Systemic Effects on Lipid Metabolism in Humans. Cell metabolism. 2016 Jun 14;23(6):1200-6. PubMed PMID: 27238638. Pubmed Central PMCID: 4967557.
126. Saito M. Brown adipose tissue as a regulator of energy expenditure and body fat in humans. Diabetes & metabolism journal. 2013 Feb;37(1):22-9. PubMed PMID: 23441053. Pubmed Central PMCID: 3579148.
127. Rosen ED, Spiegelman BM. What we talk about when we talk about fat. Cell. 2014 Jan 16;156(1-2):20-44. PubMed PMID: 24439368. Pubmed Central PMCID: 3934003.
128. Bartelt A, Heeren J. Adipose tissue browning and metabolic health. Nature reviews Endocrinology. 2014 Jan;10(1):24-36. PubMed PMID: 24146030.
129. Seale P, Bjork B, Yang W, Kajimura S, Chin S, Kuang S, et al. PRDM16 controls a brown fat/skeletal muscle switch. Nature. 2008 Aug 21;454(7207):961-7. PubMed PMID: 18719582. Pubmed Central PMCID: 2583329.

130. Schulz TJ, Tseng YH. Brown adipose tissue: development, metabolism and beyond. The Biochemical journal. 2013 Jul 15;453(2):167-78. PubMed PMID: 23805974. Pubmed Central PMCID: 3887508.

131. Nedergaard J, Golozoubova V, Matthias A, Asadi A, Jacobsson A, Cannon B. UCP1: the only protein able to mediate adaptive non-shivering thermogenesis and metabolic inefficiency. Biochimica et biophysica acta. 2001 Mar 1;1504(1):82-106. PubMed PMID: 11239487.

132. Golozoubova V, Hohtola E, Matthias A, Jacobsson A, Cannon B, Nedergaard J. Only UCP1 can mediate adaptive nonshivering thermogenesis in the cold. FASEB J. 2001 Sep;15(11):2048-50. PubMed PMID: 11511509.

133. Heeren J, Munzberg H. Novel aspects of brown adipose tissue biology. Endocrinology and metabolism clinics of North America. 2013 Mar;42(1):89-107. PubMed PMID: 23391242. Pubmed Central PMCID: 3568264.

134. Harms M, Seale P. Brown and beige fat: development, function and therapeutic potential. Nature medicine. 2013 Oct;19(10):1252-63. PubMed PMID: 24100998.

135. Scheja L, Heeren J. Metabolic interplay between white, beige, brown adipocytes and the liver. Journal of hepatology. 2016 May;64(5):1176-86. PubMed PMID: 26829204.

136. Peng XR, Gennemark P, O'Mahony G, Bartesaghi S. Unlock the Thermogenic Potential of Adipose Tissue: Pharmacological Modulation and Implications for Treatment of Diabetes and Obesity. Frontiers in endocrinology. 2015;6:174. PubMed PMID: 26635723. Pubmed Central PMCID: 4657528.

137. Berbee JF, Boon MR, Khedoe PP, Bartelt A, Schlein C, Worthmann A, et al. Brown fat activation reduces hypercholesterolaemia and protects from atherosclerosis development. Nature communications. 2015;6:6356. PubMed PMID: 25754609. Pubmed Central PMCID: 4366535.

138. Bartelt A, Bruns OT, Reimer R, Hohenberg H, Ittrich H, Peldschus K, et al. Brown adipose tissue activity controls triglyceride clearance. Nature medicine. 2011 Feb;17(2):200-5. PubMed PMID: 21258337.

139. Stanford KI, Middelbeek RJ, Townsend KL, An D, Nygaard EB, Hitchcox KM, et al. Brown adipose tissue regulates glucose homeostasis and insulin sensitivity. The Journal of clinical investigation. 2013 Jan;123(1):215-23. PubMed PMID: 23221344. Pubmed Central PMCID: PMC3533266.

140. Dallner OS, Chernogubova E, Brolinson KA, Bengtsson T. Beta3-adrenergic receptors stimulate glucose uptake in brown adipocytes by two mechanisms independently of glucose transporter 4 translocation. Endocrinology. 2006 Dec;147(12):5730-9. PubMed PMID: 16959848.

141. Chernogubova E, Cannon B, Bengtsson T. Norepinephrine increases glucose transport in brown adipocytes via beta3-adrenoceptors through a cAMP, PKA, and PI3-kinase-dependent pathway stimulating conventional and novel PKCs. Endocrinology. 2004 Jan;145(1):269-80. PubMed PMID: 14551227.

142. Bostrom P, Wu J, Jedrychowski MP, Korde A, Ye L, Lo JC, et al. A PGC1-alpha-dependent myokine that drives brown-fat-like development of white fat and thermogenesis. Nature. 2012 Jan 11;481(7382):463-8. PubMed PMID: 22237023. Pubmed Central PMCID: 3522098.

143. Handschin C, Spiegelman BM. Peroxisome proliferator-activated receptor gamma coactivator 1 coactivators, energy homeostasis, and metabolism. Endocrine reviews. 2006 Dec;27(7):728-35. PubMed PMID: 17018837.

144. Nielsen TS, Jessen N, Jorgensen JO, Moller N, Lund S. Dissecting adipose tissue lipolysis: molecular regulation and implications for metabolic disease. Journal of molecular endocrinology. 2014 Jun;52(3):R199-222. PubMed PMID: 24577718.

145. Grimpo K, Volker MN, Heppe EN, Braun S, Heverhagen JT, Heldmaier G. Brown adipose tissue dynamics in wild-type and UCP1-knockout mice: in vivo insights with magnetic resonance. J Lipid Res. 2014 Mar;55(3):398-409. PubMed PMID: 24343897. Pubmed Central PMCID: 3934725.

146. Hoeke G, Kooijman S, Boon MR, Rensen PC, Berbee JF. Role of Brown Fat in Lipoprotein Metabolism and Atherosclerosis. Circulation research. 2016 Jan 8;118(1):173-82. PubMed PMID: 26837747.

147. Khedoe PP, Hoeke G, Kooijman S, Dijk W, Buijs JT, Kersten S, et al. Brown adipose tissue takes up plasma triglycerides mostly after lipolysis. J Lipid Res. 2015 Jan;56(1):51-9. PubMed PMID: 25351615. Pubmed Central PMCID: 4274071.

148. Ferrannini E. The theoretical bases of indirect calorimetry: a review. Metabolism: clinical and experimental. 1988 Mar;37(3):287-301. PubMed PMID: 3278194.

149. Duta-Mare M, Sachdev V, Leopold C, Kolb D, Vujic N, Korbelius M, et al. Lysosomal acid lipase regulates fatty acid channeling in brown adipose tissue to maintain thermogenesis. Biochimica et biophysica acta. 2018 Jan 31;1863(4):467-78. PubMed PMID: 29374543.

150. Sachdev V, Leopold C, Bauer R, Patankar JV, Iqbal J, Obrowsky S, et al. Novel role of a triglyceride-synthesizing enzyme: DGAT1 at the crossroad between triglyceride and cholesterol metabolism. Biochimica et biophysica acta. 2016 Sep;1861(9 Pt A):1132-41. PubMed PMID: 27344248. Pubmed Central PMCID: 4948681.

151. Prokesch A, Pelzmann HJ, Pessentheiner AR, Huber K, Madreiter-Sokolowski CT, Drougard A, et al. N-acetylaspartate catabolism determines cytosolic acetyl-CoA levels and histone acetylation in brown adipocytes. Scientific reports. 2016 Apr 05;6:23723. PubMed PMID: 27045997. Pubmed Central PMCID: 4820693.

152. Chandak PG, Radovic B, Aflaki E, Kolb D, Buchebner M, Frohlich E, et al. Efficient phagocytosis requires triacylglycerol hydrolysis by adipose triglyceride lipase. The Journal of biological chemistry. 2010 Jun 25;285(26):20192-201. PubMed PMID: 20424161. Pubmed Central PMCID: 2888432.

153. Vujic N, Korbelius M, Leopold C, Duta-Mare M, Rainer S, Schlager S, et al. Monoglyceride lipase deficiency affects hepatic cholesterol metabolism and lipid-dependent gut transit in ApoE-/- mice. Oncotarget. 2017 May 16;8(20):33122-36. PubMed PMID: 28380440. Pubmed Central PMCID: 5464855.

154. Livak KJ, Schmittgen TD. Analysis of relative gene expression data using real-time quantitative PCR and the 2(-Delta Delta C(T)) Method. Methods. 2001 Dec;25(4):402-8. PubMed PMID: 11846609.

155. Aune UL, Ruiz L, Kajimura S. Isolation and differentiation of stromal vascular cells to beige/brite cells. Journal of visualized experiments : JoVE. 2013 Mar 28(73). PubMed PMID: 23568137. Pubmed Central PMCID: 3641667.

156. Sloan HR, Fredrickson DS. Enzyme deficiency in cholesteryl ester storage idisease. The Journal of clinical investigation. 1972 Jul;51(7):1923-6. PubMed PMID: 5032533. Pubmed Central PMCID: 292343.

157. Cannon B, Nedergaard J. Brown adipose tissue: function and physiological significance. Physiological reviews. 2004 Jan;84(1):277-359. PubMed PMID: 14715917.

158. Marzetti E, D'Angelo E, Savera G, Leeuwenburgh C, Calvani R. Integrated control of brown adipose tissue. Heart Metab. 2016 Mar;69:9-14. PubMed PMID: 27524955. Pubmed Central PMCID: PMC4980093.

159. Nedergaard J, Golozoubova V, Matthias A, Shabalina I, Ohba K, Ohlson K, et al. Life without UCP1: mitochondrial, cellular and organismal characteristics of the UCP1-ablated mice. Biochem Soc Trans. 2001 Nov;29(Pt 6):756-63. PubMed PMID: 11709070.

160. Christoffolete MA, Linardi CC, de Jesus L, Ebina KN, Carvalho SD, Ribeiro MO, et al. Mice with targeted disruption of the Dio2 gene have cold-induced overexpression of the uncoupling protein 1 gene but fail to increase brown adipose tissue lipogenesis and adaptive thermogenesis. Diabetes. 2004 Mar;53(3):577-84. PubMed PMID: 14988240.

161. Zimmermann R, Strauss JG, Haemmerle G, Schoiswohl G, Birner-Gruenberger R, Riederer M, et al. Fat mobilization in adipose tissue is promoted by adipose triglyceride lipase. Science. 2004 Nov 19;306(5700):1383-6. PubMed PMID: 15550674.

162. van der Stelt I, Hoevenaars F, Siroka J, de Ronde L, Friedecky D, Keijer J, et al. Metabolic Response of Visceral White Adipose Tissue of Obese Mice Exposed for 5 Days to Human Room Temperature Compared to Mouse Thermoneutrality. Frontiers in physiology. 2017;8:179. PubMed PMID: 28386236. Pubmed Central PMCID: 5362617.

163. Scheja L, Heeren J. Metabolic interplay between white, beige, brown adipocytes and the liver. Journal of hepatology. 2016 May;64(5):1176-86. PubMed PMID: 26829204.

164. Rui L. Energy metabolism in the liver. Comprehensive Physiology. 2014 Jan;4(1):177-97. PubMed PMID: 24692138. Pubmed Central PMCID: 4050641.

165. Ramasamy I. Recent advances in physiological lipoprotein metabolism. Clinical chemistry and laboratory medicine. 2014 Dec;52(12):1695-727. PubMed PMID: 23940067.

166. Tiwari S, Siddiqi SA. Intracellular trafficking and secretion of VLDL. Arteriosclerosis, thrombosis, and vascular biology. 2012 May;32(5):1079-86. PubMed PMID: 22517366. Pubmed Central PMCID: 3334296.

167. Nohr MK, Bobba N, Richelsen B, Lund S, Pedersen SB. Inflammation Downregulates UCP1 Expression in Brown Adipocytes Potentially via SIRT1 and

DBC1 Interaction. Int J Mol Sci. 2017 May 8;18(5). PubMed PMID: 28481291. Pubmed Central PMCID: 5454919.

168. Sakamoto T, Takahashi N, Sawaragi Y, Naknukool S, Yu R, Goto T, et al. Inflammation induced by RAW macrophages suppresses UCP1 mRNA induction via ERK activation in 10T1/2 adipocytes. American journal of physiology Cell physiology. 2013 Apr 15;304(8):C729-38. PubMed PMID: 23302779. Pubmed Central PMCID: 3625802.

169. Du H, Zhao T, Ding X, Yan C. Hepatocyte-Specific Expression of Human Lysosome Acid Lipase Corrects Liver Inflammation and Tumor Metastasis in lal(-/-) Mice. Am J Pathol. 2015 Sep;185(9):2379-89. PubMed PMID: 26212911. Pubmed Central PMCID: 4597280.

170. Shabalina IG, Backlund EC, Bar-Tana J, Cannon B, Nedergaard J. Within brown-fat cells, UCP1-mediated fatty acid-induced uncoupling is independent of fatty acid metabolism. Biochimica et biophysica acta. 2008 Jul-Aug;1777(7-8):642-50. PubMed PMID: 18489899.

171. Haemmerle G, Moustafa T, Woelkart G, Buttner S, Schmidt A, van de Weijer T, et al. ATGL-mediated fat catabolism regulates cardiac mitochondrial function via PPAR-alpha and PGC-1. Nat Med. 2011 Aug 21;17(9):1076-85. PubMed PMID: 21857651. Pubmed Central PMCID: PMC3244833.

172. Dijk W, Heine M, Vergnes L, Boon MR, Schaart G, Hesselink MK, et al. ANGPTL4 mediates shuttling of lipid fuel to brown adipose tissue during sustained cold exposure. eLife. 2015 Oct 17;4. PubMed PMID: 26476336. Pubmed Central PMCID: 4709329.

173. Han TS, Lean ME. A clinical perspective of obesity, metabolic syndrome and cardiovascular disease. JRSM cardiovascular disease. 2016 Jan-Dec;5:2048004016633371. PubMed PMID: 26998259. Pubmed Central PMCID: 4780070.

174. Feldmann HM, Golozoubova V, Cannon B, Nedergaard J. UCP1 ablation induces obesity and abolishes diet-induced thermogenesis in mice exempt from thermal stress by living at thermoneutrality. Cell metabolism. 2009 Feb;9(2):203-9. PubMed PMID: 19187776.

175. Bartelt A, John C, Schaltenberg N, Berbee JFP, Worthmann A, Cherradi ML, et al. Thermogenic adipocytes promote HDL turnover and reverse cholesterol

transport. Nature communications. 2017 Apr 19;8:15010. PubMed PMID: 28422089. Pubmed Central PMCID: 5399294.

176. Mahdaviani K, Benador IY, Su S, Gharakhanian RA, Stiles L, Trudeau KM, et al. Mfn2 deletion in brown adipose tissue protects from insulin resistance and impairs thermogenesis. EMBO reports. 2017 Jul;18(7):1123-38. PubMed PMID: 28539390. Pubmed Central PMCID: 5887905.

177. Lee J, Choi J, Aja S, Scafidi S, Wolfgang MJ. Loss of Adipose Fatty Acid Oxidation Does Not Potentiate Obesity at Thermoneutrality. Cell reports. 2016 Feb 16;14(6):1308-16. PubMed PMID: 26854223. Pubmed Central PMCID: 4758873.

178. Irshad Z, Dimitri F, Christian M, Zammit VA. Diacylglycerol acyltransferase 2 links glucose utilization to fatty acid oxidation in the brown adipocytes. J Lipid Res. 2017 Jan;58(1):15-30. PubMed PMID: 27836993. Pubmed Central PMCID: 5234708.

179. Harris CA, Haas JT, Streeper RS, Stone SJ, Kumari M, Yang K, et al. DGAT enzymes are required for triacylglycerol synthesis and lipid droplets in adipocytes. J Lipid Res. 2011 Apr;52(4):657-67. PubMed PMID: 21317108. Pubmed Central PMCID: 3284159.

180. Schweiger M, Romauch M, Schreiber R, Grabner GF, Hutter S, Kotzbeck P, et al. Pharmacological inhibition of adipose triglyceride lipase corrects high-fat diet-induced insulin resistance and hepatosteatosis in mice. Nature communications. 2017 Mar 22;8:14859. PubMed PMID: 28327588. Pubmed Central PMCID: 5364409.

181. Wang ZV, Deng Y, Wang QA, Sun K, Scherer PE. Identification and characterization of a promoter cassette conferring adipocyte-specific gene expression. Endocrinology. 2010 Jun;151(6):2933-9. PubMed PMID: 20363877. Pubmed Central PMCID: 2875825.

182. Schutz Y. Concept of fat balance in human obesity revisited with particular reference to de novo lipogenesis. International journal of obesity and related metabolic disorders : journal of the International Association for the Study of Obesity. 2004 Dec;28 Suppl 4:S3-S11. PubMed PMID: 15592484.

183. Bruss MD, Khambatta CF, Ruby MA, Aggarwal I, Hellerstein MK. Calorie restriction increases fatty acid synthesis and whole body fat oxidation rates. American journal of physiology Endocrinology and metabolism. 2010

Jan;298(1):E108-16. PubMed PMID: 19887594. Pubmed Central PMCID: 4056782.

184. Trayhurn P, James WP. Thermoregulation and non-shivering thermogenesis in the genetically obese (ob/ob) mouse. Pflugers Archiv : European journal of physiology. 1978 Feb 22;373(2):189-93. PubMed PMID: 565045.

185. Jung RT, Shetty PS, James WP, Barrand MA, Callingham BA. Reduced thermogenesis in obesity. Nature. 1979 May 24;279(5711):322-3. PubMed PMID: 450084.

186. Valente A, Jamurtas AZ, Koutedakis Y, Flouris AD. Molecular pathways linking non-shivering thermogenesis and obesity: focusing on brown adipose tissue development. Biological reviews of the Cambridge Philosophical Society. 2015 Feb;90(1):77-88. PubMed PMID: 24708171.

187. Sica A, Mantovani A. Macrophage plasticity and polarization: in vivo veritas. The Journal of clinical investigation. 2012 Mar;122(3):787-95. PubMed PMID: 22378047. Pubmed Central PMCID: 3287223.

188. Galvan-Pena S, O'Neill LA. Metabolic reprograming in macrophage polarization. Frontiers in immunology. 2014;5:420. PubMed PMID: 25228902. Pubmed Central PMCID: 4151090.

189. Huang SC, Everts B, Ivanova Y, O'Sullivan D, Nascimento M, Smith AM, et al. Cell-intrinsic lysosomal lipolysis is essential for alternative activation of macrophages. Nature immunology. 2014 Sep;15(9):846-55. PubMed PMID: 25086775. Pubmed Central PMCID: 4139419.

190. Qu P, Shelley WC, Yoder MC, Wu L, Du H, Yan C. Critical roles of lysosomal acid lipase in myelopoiesis. Am J Pathol. 2010 May;176(5):2394-404. PubMed PMID: 20348241. Pubmed Central PMCID: 2861104.

191. Elliott MR, Koster KM, Murphy PS. Efferocytosis Signaling in the Regulation of Macrophage Inflammatory Responses. Journal of immunology. 2017 Feb 15;198(4):1387-94. PubMed PMID: 28167649. Pubmed Central PMCID: 5301545.

192. Clausen BE, Burkhardt C, Reith W, Renkawitz R, Forster I. Conditional gene targeting in macrophages and granulocytes using LysMcre mice. Transgenic research. 1999 Aug;8(4):265-77. PubMed PMID: 10621974.

193. Qu P, Du H, Wilkes DS, Yan C. Critical roles of lysosomal acid lipase in T cell development and function. Am J Pathol. 2009 Mar;174(3):944-56. PubMed PMID: 19179613. Pubmed Central PMCID: 2665754.

194. Zhao T, Ding X, Du H, Yan C. Lung Epithelial Cell-Specific Expression of Human Lysosomal Acid Lipase Ameliorates Lung Inflammation and Tumor Metastasis in Lipa(-/-) Mice. Am J Pathol. 2016 Aug;186(8):2183-92. PubMed PMID: 27461363. Pubmed Central PMCID: 4973654.

195. Baratta F, Pastori D, Del Ben M, Polimeni L, Labbadia G, Di Santo S, et al. Reduced Lysosomal Acid Lipase Activity in Adult Patients With Non-alcoholic Fatty Liver Disease. EBioMedicine. 2015 Jul;2(7):750-4. PubMed PMID: 26288848. Pubmed Central PMCID: 4534687.

Appendix

Permissions granted by the publishers to use their figures in this doctoral thesis

Figure or Table number	**Licensed content publisher and granted license number**
Figure 1	Springer Nature; 4353751477348
Figure 2	Springer Nature; 4353760121246
Figure 3	Professional Group McGraw-Hill Education; permission granted by email
Figure 4	Elsevier; permission not required
Figure 5	The American Society for Biochemistry and Molecular Biology; permission not required
Figure 6	Professional Group McGraw-Hill Education; permission granted by email
Figure 7	The American Physiological Society; permission not required
Figure 8	Front. Endocrinol.; open-access journal
Figure 9	Wolters Kluwer Health, Inc.; 4353780210345
Figures 10-15; 17-24	Elsevier; permission not required

Note: Detailed PDF copies of the license documents will be provided upon request.